2014

A Treatment Planning Comparison of Volumetric Modulated Arc Therapy and Proton Therapy for a Sample of Breast Cancer Patients Treated with Post-Mastectomy Radiotherapy

Margaret Hernandez
Louisiana State University and Agricultural and Mechanical College

A TREATMENT PLANNING COMPARISON OF VOLUMETRIC MODULATED ARC THERAPY AND PROTON THERAPY FOR A SAMPLE OF BREAST CANCER PATIENTS TREATED WITH POST-MASTECTOMY RADIOTHERAPY

A Thesis

Submitted to the Graduate Faculty of the
Louisiana State University and
Agricultural and Mechanical College
in partial fulfilment of the
requirements for the degree of
Master of Science

in

The Department of Physics and Astronomy

by
Margaret Olivia Hernandez
B.S., Oregon State University, 2011
August 2014

This work is dedicated to my mother,
Callie,
for always believing in me

Acknowledgements

I would like to thank my advisor, Dr. Rui Zhang, for his patience and guidance on this project. It has been a great pleasure being one of your first graduate students. I would also like to express my deepest gratitude to the other members of my graduate committee: Drs. Wayne Newhauser, Oleg Vassiliev, Mary Ella Sanders, and Mette Gaarde. Their assistance and feedback was of great importance for the completion of this project. I would also like to thank Frank Apollo, Eddie Singleton, and Chad Dunn for sharing their expertise in radiotherapy treatment planning and dosimetry.

I would like to thank Ms. Susan Hammond for making sure all paperwork was in order, and for always helping me schedule meetings despite everyone's busy schedules.

A huge thank you to my classmates for their support, friendship, and laughs. I will always look back on my experience at LSU with great fondness. To my roommate and classmate Melissa Lamberto who was always there to listen to me and calm me down when research obstacles arose. I would also like to thank Derek Freund, whose research was very similar to mine, for all his input and peer editing.

I would like to acknowledge my family for their endless support in my educational endeavors even when it moves me 1,500 miles away from them. I love them more than they know and would not be the woman I am today without them.

Finally, I would like to thank the remaining medical physics staff at LSU and Mary Bird Perkins Cancer Center for all they have taught me. Their wisdom has been immeasurable to my growth as a medical physicist.

Table of Contents

List of Tables

List of Figures

Abstract

Purpose: The delivery of post-mastectomy radiotherapy (PMRT) can be challenging for patients with left-sided breast cancer due to the planning target volume (PTV) size and proximity to critical organs. This study investigates the use of protons, both passively scattered (PS) and intensity modulated proton therapy (IMPT), for PMRT in a clinically-representative cohort of patients, and quantitatively compares the predicted outcomes of volumetric modulated photon arc therapy (VMAT) to those of proton therapy to develop an evidence-based rationale for selecting a treatment modality for PMRT patients.

Methods: Eight left-sided PMRT patients previously treated at our clinic with VMAT were included in this study. PTVs included the chest wall and regional lymph nodes. PS and IMPT plans were constructed using a commercial proton treatment planning system. The resulting plans were compared to the corresponding VMAT plans on the basis of PTV coverage; dose homogeneity index (DHI) and conformity index (CI); dose to organs at risk (OAR); tumor control probability (TCP), normal tissue complication probability (NTCP) and secondary cancer complication probability (SCCP). The impact of range, set-up errors, and sensitivity of dose-response models was also evaluated. Statistical significance between VMAT and each proton modality was tested using the paired Student's t-test ($p<0.05$).

Results: All modalities produced clinically acceptable PMRT plans with nearly 100% TCP. The proton treatment plans provided significantly lower NTCP values for the heart and the lung while maintaining significantly better CI and DHI values. At a prescribed dose of 50.4 Gy (RBE) in the PTV, the mean NTCP value for the patients decreased from 0.83%±0.67% to <0.05%±0.05% for the whole heart (cardiac mortality) and from 2.05%±0.23% to <1% for the lungs (radiation pneumonitis) for VMAT and proton plans, respectively. Proton therapy NTCP and SCCP values

were consistently lower than those of VMAT regardless of biological parameter values. Target coverage for VMAT and IMPT plans was most sensitive to positional uncertainties.

Conclusions: All three techniques (VMAT, PS, and IMPT) provide acceptable PMRT treatment plans for each patient in this study. However, proton therapy showed significant advantages in terms of sparing OARs and lower complication risks when compared to VMAT.

Chapter 1 Introduction

1.1 Background

According to the Surveillance Epidemiology and End Results database (2013), breast cancer is the most common cancer, other than non-melanoma skin cancer, among women in the United States, with 1 in 8 women diagnosed in their lifetime. Breast cancer is the second leading cause of cancer deaths among women. The majority of women will be diagnosed with invasive breast cancer and there are about 2.8 million breast cancer survivors in the United States. Women between the ages of 55 and 64 have the highest incidence rate of breast cancer.

The female breast is made up mainly of lobules, ducts, and stroma. The majority of breast cancers, 50% to 75%, begin in the milk ducts, with the most common ductal cancers being ductal carcinoma in situ or DCIS. This type of cancer happens when abnormal cells grow inside the ducts, but have not spread to nearby tissue or beyond. DCIS is also referred to as a non-invasive cancer. If the abnormal or cancer cells have spread to nearby tissues outside of the ducts then it is called an invasive or infiltrating ductal carcinoma. DCIS, if left untreated, will likely become invasive. In fact, 80% of invasive cancers are invasive ductal carcinomas. The remaining percentage of breast cancers are mainly lobular cancers and may be invasive or non-invasive (Dillon *et al.*, 2010).

Due to the high incidence and morbidity rates of breast cancer, great strides have been made in the early detection and treatment of breast cancer. Treatment of breast cancer includes any combination of surgery, radiation therapy, and chemotherapy. According to the National Comprehensive Cancer Network (NCCN, 2014), most breast cancer patients will have surgery, e.g. a lumpectomy or a mastectomy. A mastectomy can be a radical mastectomy, modified radical mastectomy, or simple mastectomy. The most common type is a modified radical

mastectomy which removes the entire breast and all of the axillary lymph nodes, but the pectoralis muscles remain intact. A mastectomy is highly recommended (NCCN, 2014), if the following qualities describe the patient: signs of cancer throughout the breast and regional lymph nodes, tumors larger than 5 cm that cannot be reduced by neoadjuvant therapy, or previous history of radiation therapy to the breast.

1.2 Post-Mastectomy Radiotherapy

After the mastectomy, it is common for the patient to undergo chemotherapy and/or radiotherapy to treat subclinical disease that may remain. Previous studies have shown significant improvement in the overall and local survival rates for patients who received radiotherapy after a mastectomy (Overgaard *et al.*, 1997; Ragaz *et al.*, 1997; Overgaard *et al.*, 1999). Specifically, three recent randomized trials have demonstrated a 9% benefit in survival 10 to 15 years in patients randomized to comprehensive locoregional radiotherapy after chemotherapy or hormonal therapy. Radiotherapy was delivered to the chest wall and regional nodes, including the internal mammary nodes, in these studies (Overgaard *et al.*, 1997; Ragaz *et al.*, 1997; Overgaard *et al.*, 1999). The extent of radiotherapy after mastectomy is based on how many lymph nodes have cancer and the size of the primary tumor. The National Institutes of Health consensus panel and the NCCN (2014) recommend post-mastectomy radiotherapy (PMRT) in patients with 4 or more positive axillary lymph nodes or T3 (>5cm diameter) or T4 (spread to chest wall) staged lesions (Eifel *et al.*, 2001). And strong consideration of PMRT should be given to patients with 1 to 3 positive axillary lymph nodes (NCCN, 2014).

Post-mastectomy irradiation should be performed with CT-based treatment planning to limit radiation dose to the heart, lungs and other critical structures. The recommended radiation dose is 50.4 Gy in fractions of 1.8 to 2.0 Gy to the ipsilateral chest wall, mastectomy scar, and

regional lymph nodes. Figure 1.1 depicts a typical treatment area for PMRT. This area includes the chest wall (CW), axillary lymph nodes (AX), supraclavicular lymph nodes (SC), and internal mammary lymph nodes (IMN). Chest wall has the greatest risk of cancer recurrence in patients undergoing mastectomy and is given dose coverage priority (NCCN, 2014).

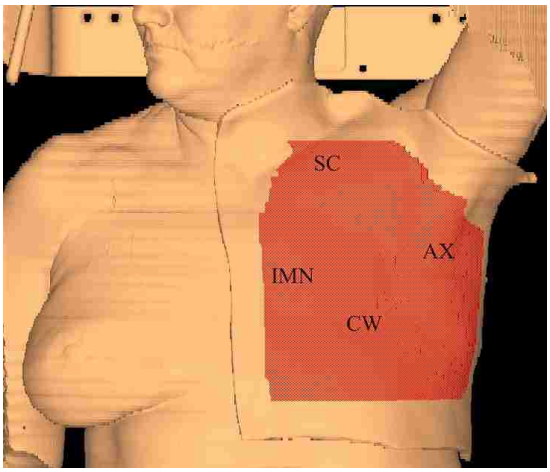

Figure 1.1 Radiation treatment field from beam's eye view of a post-mastectomy radiotherapy patient.

1.2.1 Common PMRT Treatment Techniques

Post-mastectomy radiotherapy was historically delivered by conventional mixed-beam technique, where low energy electrons were used to treat the medial CW and IMN and oblique electrons to treat the lateral CW. The SC and AX nodes were treated with either anterior or parallel-opposed x-rays (Pierce *et al.*, 2002; Ashenafi *et al.*, 2010). However, this technique causes hot-spots or excess dose in the regions where the fields abut. Controlling this dose inhomogeneity requires careful dosimetry planning such as matching the penumbras of the beams with each other and feathering the junction during treatment to spread the hot spot out over a larger area (Ashenafi *et al.*, 2010). Each of these techniques requires significant effort from dosimetrists, therapists, and physicists.

The previously mentioned treatment problems associated with field junctioning can be reduced by using static or dynamic intensity modulated radiation therapy (IMRT) techniques (Ashenafi *et al.*, 2010). Such techniques used to treat PMRT include static IMRT, Helical Tomotherapy (HT), and Volumetric Modulated Arc Therapy (VMAT) (Ashenafi *et al.*, 2010; Teoh *et al.*, 2011). HT was compared to the conventional mixed beam radiotherapy for post-mastectomy patients by Ashenafi *et al.* in 2010 and HT achieved significantly better PTV coverage and sparing of organs at risk. However, HT resulted in increased dose to the contralateral breast as well as larger volumes of low dose to normal tissues.

1.2.2 Volumetric Modulated Arc Therapy

Unlike HT, VMAT is performed using a standard linear accelerator by rotating the gantry in a 360˚(max) arc(s). The modulated portion of the planning is accomplished by varying the multileaf collimator leaf position along with the dose rate and gantry rotation speed simultaneously during the treatment delivery. Currently there are several arc-based IMRT systems available including RapidArc by Varian, SmartArc by Phillips, and Elekta VMAT by Elekta. A study performed by Nichols *et al.* (2012) compared VMAT and HT for 15 PMRT patients, and found that both modalities provided clinically acceptable treatment plans, with VMAT achieving better conformity index and low-dose OAR sparing while HT achieved better dose homogeneity. The study also showed VMAT required less treatment time compared to HT. This is particularly advantageous to reduce treatment errors associated with intrafraction patient motion, both internal and external. Another benefit of VMAT over HT is the ability to deliver the radiotherapy plan using a conventional linear accelerator, provided the systems have been configured for VMAT capability (Teoh *et al.*, 2011). This usually includes a software upgrade as opposed to buying a whole new HT unit and treatment planning system.

1.3 Complications of PMRT

While VMAT can provide clinically acceptable PMRT plans, there is still an increase in low dose radiation to the surrounding normal tissues (Teoh *et al.*, 2011). This increase in low dose to the normal tissues can lead to radiation induced complications especially in organs with strong dose-volume response such as the heart and lungs (Pierce *et al.*, 2002). There are two categories of complications that occur after radiation treatments, acute and late effects.

Acute effects occur during or shortly after the radiation treatments. Common acute effects that occur for PMRT include skin irritation, radiation pneumonitis, hair loss, nausea, and fatigue (Macdonald *et al.*, 2013b). Late effects are characterized as occurring months, years, or even decades after radiation treatments. Late effects for PMRT include pericardial disease, congestive heart failure, secondary malignant neoplasms, and coronary atherosclerosis (Macdonald *et al.*, 2013b).

Radiation pneumonitis occurs in 1 to 5% of patients treated for breast cancer (Marks *et al.*, 2010) or as high as 14.6% with concurrent chemotherapy (Macdonald *et al.*, 2013a). Radiation pneumonitis is the inflammation of the lungs due to radiation therapy and most commonly occurs between 1 to 6 months after completing treatment and has five grades of severity. Usually Grade 2 or higher is considered clinically relevant (Graham *et al.*, 1999). Radiation pneumonitis is known to have a dose-volume response and therefore limits the maximal safe radiation dose that can be delivered to the chest wall (Seppenwoolde *et al.*, 2003; Marks *et al.*, 2010). It is essential to minimize the dose delivered to the lungs while maximizing the dose to the target volume (Marks *et al.*, 2010).

Second malignant neoplasms (SMNs) and cardiovascular disease (CVD) are two of the most frequent and important life-threatening adverse events associated with radiotherapy (Travis

et al., 2011). Radiotherapy-associated CVD refers to a wide spectrum of diseases. Ischemic heart disease is one such CVD that arises from PMRT with the risk being higher for women treated for left-sided breast cancer than right-sided (Darby *et al.*, 2013). Darby *et al.* (2103) found that the risk of a major coronary event increases linearly with the mean dose to the heart with a risk value of 7.4% per gray, with no apparent threshold. The risk of radiation-induced cardiovascular disease begins to increase 5 to 10 years after irradiation and is progressive with time (Andratschke *et al.*, 2011; Darby *et al.*, 2013). Other breast cancer studies have shown a statistically significant increase in coronary artery disease and/or nonfatal myocardial infarction associated with left-sided radiotherapy compared with right-sided radiotherapy or no radiotherapy (Travis *et al.*, 2011). These complications are of great concern because although local control rates are increasing with better radiotherapy techniques the survival benefit is offset by an increase in deaths from cardiovascular disease (Andratschke *et al.*, 2011). About 1% more deaths due to causes other than breast cancer were observed among patients having received loco-regional post-mastectomy radiotherapy due primarily to radiogenic cardiac complications and to a lesser extent secondary malignancies, particularly pulmonary (Weber *et al.*, 2006). Photon breast cancer radiotherapy has also been associated with a small but incremental increase of long-term risk of contralateral breast cancer in a large SEER series and data stemmed from randomized trials conducted by the Early Breast Cancer Trialists' Collaborative Group overview (Gao *et al.*, 2003).

1.4 Proton Therapy

Comparative treatment planning studies have consistently shown proton beam therapy can substantially decrease dose to OARs for the treatment of early or locally-advanced breast cancers (Johansson *et al.*, 2002; Weber *et al.*, 2006; Ares *et al.*, 2010; Jimenez *et al.*, 2013;

Macdonald *et al.*, 2013a). In a study by Johansson *et al.* (2002) passively scattered proton therapy appeared to have major advantages in terms of lower complication risks for cardiac mortality and radiation pneumonitis when compared with treatments using conventional radiation techniques for treating node-positive left-sided breast cancer after breast-conserving surgery. In another study, Ares *et al.* (2010) found intensity modulated proton therapy was advantageous for complex left-sided whole breast target volumes, patients with unfavorable thoracic anatomy or placement of intrathoracic organs, and for patients with reduced organ tolerance from pre-existing cardiac or pulmonary diseases compared to 3D conformal radiotherapy and static multi-field IMRT. Proton therapy has also recently emerged as a new PMRT technique. MacDonald *et al*. (2013) completed the first known *clinical* investigation of passively scattered proton therapy for PMRT and assessed the patients for skin toxicity, fatigue and radiation pneumonitis while late effects were not reported. The study reported that passively scattered proton RT is feasible, well tolerated, and advantageous for patients with unfavorable cardiac anatomy.

The advantage seen with proton therapy mentioned above is attributed to the physical properties of the charged particle. Protons, at therapeutic energies (70-250 MeV), interact almost exclusively with atomic electrons via Coulombic collisions, yielding nearly straight trajectories culminating in a rapid increase in energy loss rate near the end of range (Bragg peak). Since protons lose the majority of their energy near the end of range, there is nearly zero exit dose (ICRU, 2007). This sharp distal dose distribution is a major reason for using protons for radiotherapy.

There are two main methods for proton radiotherapy delivery: passive and active (dynamic). Figure 1.2 shows the differences between the two proton therapy modalities. A

passive beam setup uses a double-scattering system to spread the beam laterally, a block to shape the beam laterally, a rotating variable-thickness propeller to spread out the Bragg peak in depth, and a field-specific collimator to shape the dose distribution to the distal edge of the target (ICRU, 2007). Active beam-scanning systems can position a single narrow Bragg peak from a near monoenergetic proton beam anywhere in the patient. Lateral positioning of the Bragg peak is accomplished by scanning magnets, and penetration depth is controlled by changing the energy at the nozzle entrance. The ability to control the Bragg peak placement within the patient allows the implementation of intensity modulated proton therapy (IMPT). In IMPT a narrow beam (spot) is moved laterally across the tumor and its intensity can be modulated according to the beam energy and position. The weights of all these beam spots is calculated by the proton treatment planning optimizer, much like IMRT techniques in photon therapy (Mohan *et al.*, 2010).

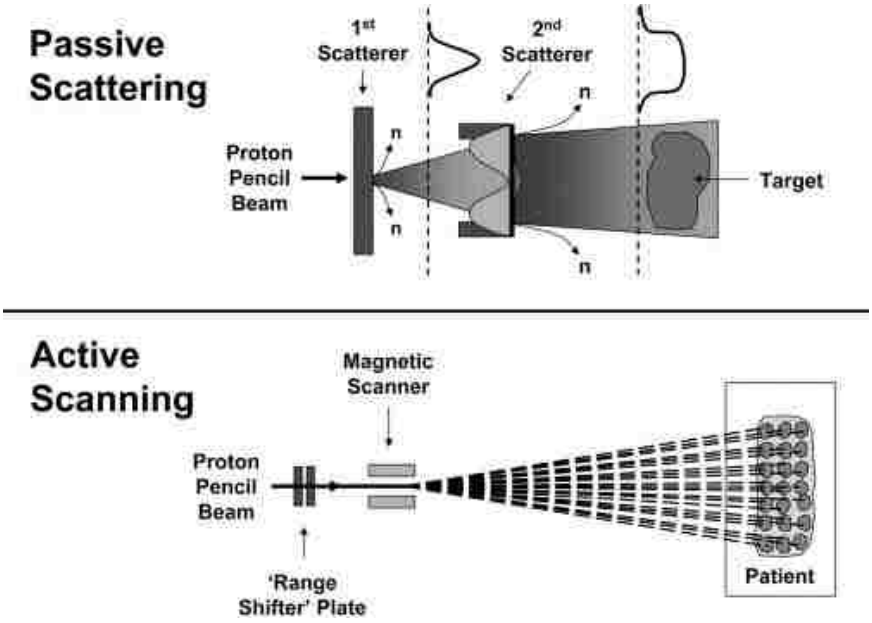

Figure 1.2 Passive scattering proton therapy vs. active scanning proton therapy (Hall, 2006)

1.5 Statement of the Problem

Post-mastectomy radiotherapy improves local tumor control however; toxicities associated with this treatment can be significant due to the complex target volume and proximity of normal tissues. Therefore, the challenge with planning PMRT using any modality is reducing the dose to the organs at risk while not compromising target coverage. Previous studies have shown that both VMAT and proton PMRT can accomplish the necessary target coverage while minimizing the dose to organs at risk (Weber *et al.*, 2006; Ares *et al.*, 2010; Macdonald *et al.*, 2013b; Nichols *et al.*, 2014). Several comparative planning studies hypothesize that protons will provide a decrease in acute and late cardiopulmonary toxicities for patients requiring radiotherapy for advanced or left-sided breast cancer compared to conventional and IMRT photon techniques (Lomax *et al.*, 2003; Weber *et al.*, 2006; Ares *et al.*, 2010). However, no study has compared VMAT and proton modalities for PMRT to compare the predicted risks of late effects. The goal of this study sets out to accomplish such a comparison for left-sided post-mastectomy patients.

1.6 Hypothesis and Specific Aims

We proposed to test the following hypothesis: For a clinically representative cohort of post-mastectomy patients, passively scattered and intensity modulated proton therapy can improve normal tissue sparing while maintaining equal or better target coverage than volumetric modulated arc therapy photon plans ultimately resulting in significantly lower ($p<0.05$) predicted risks of late effects for the heart, lungs, and contralateral breast.

To test this hypothesis, we compared photon and proton PMRT treatment plans on the basis of *dosimetric* and *radiobiological* endpoints, along with the uncertainties associated with each such calculation for eight randomly selected left-sided PMRT patients previously treated with VMAT. Left-sided patients were selected due to the proximity of the heart to the treatment

field. We estimated the risk of radiogenic second cancers, lung toxicity, and cardiac toxicity for all. To accomplish these goals, we proposed the following specific aims:

Aim 1: Determine if the mean dose-volume treatment plan metrics between VMAT, passively scattered proton therapy and intensity modulated proton therapy are statistically significantly different from each other for a clinically representative sample of patients.

Aim 2: Determine if 1) tumor control probability, 2) normal tissue complication probability for whole heart, myocardium, and lungs, and 3) the second cancer complication probability for contralateral breast and lungs between VMAT and proton therapies are statistically significantly different from each other.

Aim 3: Evaluate impact of positional uncertainty, proton range uncertainty, and dose-risk model sensitivities on dosimetric and radiobiological results from Aim 1 and Aim 2 respectively.

Chapter 2 Methods

2.1 Patient Selection

Eleven patients that received a left-sided modified radical mastectomy and volumetric modulated arc therapy radiation treatments at Mary Bird Perkins Cancer Center from June 2013 to November 2013 were consecutively identified. All patients were treated by the same radiation oncologist and fell within the age range of 20 to 80 years. Eight of these eleven patients were selected for the study. Three patients were excluded from the study due to the presence of a chemotherapy port within the treatment site, an immediate reconstruction of the left breast, or data transfer errors.

Once the patients were selected from the photon treatment planning system to be transferred to the proton treatment planning system, sensitive patient information was anonymized. Each patient was assigned a research number in the format CW-X, where x is an index from 1 to 8. In the proton TPS, the patient's last name and medical record number (MRN) were replaced by this research number, and all other personally identifiable information was deleted. Table 2.1 lists the cases used for this study, indicating subjects' age, original treatment site, original treatment modality, target volume, and type of mastectomy. The average age was 54 y and the average volume of the planning target volume was 953.5 cm^3.

All patients were planned with both passively scattered and intensity modulated proton therapy techniques (Eclipse version 11). All patients were planned to the same prescription dose, 50.4 Gy (RBE) in 28 fractions, as were the original VMAT plans.

Table 2.1 Anonymized patient cohort with a VMAT prescription dose of 50.4 Gy in 28 fractions for a left-sided unilateral mastectomy treatment site

Research Index	Age	Treatment Site	Planning Target Volume (cm^3)
CW-1	69	Left CW	1040.8
CW-2	56	Left CW	778.9
CW-3	27	Left CW	774.6
CW-4	42	Left CW	1389.1
CW-5	63	Left CW	1260.6
CW-6	62	Left CW	781
CW-7	46	Left CW	966.2
CW-8	67	Left CW	637.1

2.2 VMAT Treatment Planning

VMAT treatment plans were created in Pinnacle^3 v9.2 by certified radiation dosimetrists at Mary Bird Perkins Cancer Center following the current standard of care. Patients were treated on a linear accelerator (Elekta Ltd., Infinity, Crawley, UK), with two 6 MV photon arcs to a prescribed dose of 50.4 Gy in 28 fractions. The beam geometry consisted of a 0 degree couch angle and a 45 degree collimator angle. Due to the close proximity of the lungs, heart, and contralateral breast, PMRT is considered a complex case and thus two partial arcs were used for every patient. Each arc subtended an angle of 220˚ each with around 56 control points and 4-degree final gantry spacing. The first arc was delivered counterclockwise with a starting angle of around 170-180˚ and ending at 310-320˚. The second arc was delivered clockwise with the start and stop angles opposite that of the first arc. The SmartArc optimization algorithm was used for VMAT treatment planning and optimization.

2.3 Contours

Patients were treated in the supine position and the free breathing CT scans were obtained from the top of the head to the lower abdomen. Planning target volumes (PTV) were generated by the same radiation oncologist for all original VMAT plans and subsequently transferred to the proton TPS. As per ASCO guidelines, the PTV included the chest wall, and regional lymph nodes. The PTV also included a 1 cm tissue-equivalent bolus, which was placed on the surface of the treatment area prior to the patient's initial CT scan and used during the course of treatment. Recording the dose within the bolus was not necessary for this study, and therefore the original PTV was altered to exclude the bolus for plan evaluation purposes and was closest to a clinical target volume. For accurate proton dose calculations a "Body" contour was created for each patient using an auto-contour tool called "search body" that outlined the entire patient anatomy and bolus (Rah *et al.*, 2013). Any voxel outside of this body contour was excluded from any dose calculation.

Figure 2.1 depicts the contours added or altered within the proton TPS. The green contour is the original physician drawn PTV used in VMAT dose calculations. The red contour is the new PTV without bolus structure that is identical to the original PTV drawn by the physician except it begins at the patient surface and not the bolus surface. The yellow contour is a 5 mm shell "skin" contour and is used to report the dose at the surface. The blue contour is a scanning target volume (STV) structure that was used for IMPT planning purposes, and is discussed in more detail below.

To account for systematic range uncertainties within the proton treatment plans, proximal and distal margins for the PTV were added. For passively scattered proton treatment plans, all margins were added using the "Target Margin" tool within the field properties in the treatment

planning system and applied to the PTV without bolus, automatically. However, for active scanning proton plans the margins needed to be added manually to the PTV without bolus structure. These margins needed to be added to the PTV specifically because the treatment planning system for Intensity Modulated Proton Therapy does not incorporate the distal and proximal margins when added through the field properties.

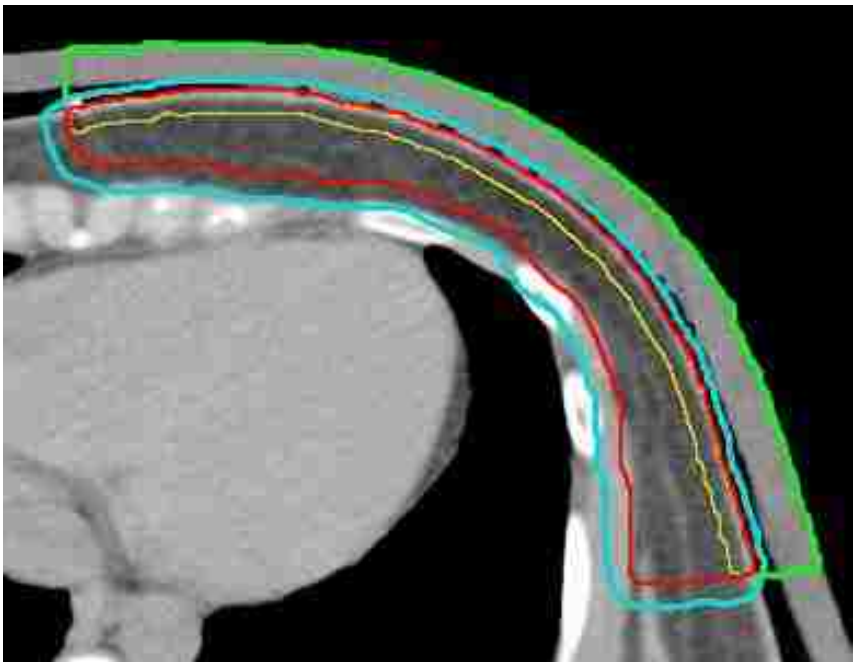

Figure 2.1 Planning target volumes for VMAT (green + red), PS (red), and IMPT (blue) along with a skin contour (yellow)

Although the correct PTV concept for proton planning is beam specific, it is technically impossible to design a single volume from theoretical deduction in which to place spots that accounts for range uncertainties for multidirectional beams. Therefore, the PTV without bolus contour was expanded proximally by 1 mm, and 4 to 6 mm distally for all IMPT patient structure sets to create the scanning target volume (STV) used for IMPT planning (Figure 2.1 blue contour). These margin values are from the beam angle which necessitates the largest margin. The treatment planning system does incorporate lateral margins and therefore lateral margins

were not added to the scanning target volume. These altered proton PTVs were then approved by the same radiation oncologist who created the original PTV prior to proton planning.

Despite having different planning target volumes between modalities all plans were compared, except conformity, using the PTV without bolus structure (red contour) for simplicity and consistency. From here on out, dose reported to the PTV will refer to this evaluation PTV structure and not the volumes used for planning purposes. Table 2.2 summarizes the planning target volumes for each modality of proton therapy.

Table 2.2 Planning target volume for proton plans

Plan	Planning Target Volume
IMPT	STV: Includes VMAT PTV without bolus volume with a 5 to 6 mm distal expansion and 1 mm proximal expansion. Blue contour in Figure 2.1
PS	PsTV: Includes the original physician-drawn PTV but excludes the portion of the treatment volume that includes any part of the bolus. Red contour in Figure 2.1

The organs at risk (OARs) contours were created by either the physician or dosimetrist for the original VMAT plan. OARs that were contoured for the patients included the lungs (left and right), whole heart, contralateral breast, esophagus, trachea, and spinal cord. A new contour for the myocardium was created has a shell having an external contour 2 mm inside the external heart surface and a thickness varying from 1 cm to 2 cm, with the thickness on the left side being twice that on the right side (Zhang *et al.*, 2013).

2.4 Passive Scatter Proton Planning

Once all contours were complete a passive scatter plan was created similar to techniques used in previous proton PMRT studies (Ares *et al.*, 2010; Macdonald *et al.*, 2013a). The total prescribed dose was 50.4 Gy (1.8 Gy per fraction) relative biological effectiveness (RBE) (i.e. 45.8 Gy x 1.1 to reflect the biological effectiveness of protons relative to photons) to 100% of

the PTV. The use of a generic RBE value of 1.1 is in accordance with the recommendations on dose prescription and reporting in International Commission on Radiation Units and Measurements Report 78 (ICRU, 2007).

One left-anterior oblique (LAO) field was used for six of the eight patients with beams angles ranging from 25˚-45˚. Angles were chosen to be as en-face as possible to the chest wall while allowing adequate margins within the snout (field) size. A snout size of 25x25 cm^2 was the largest possible size we had PS commissioning data for and was used for all plans. Due to an inadequate dose distribution with a single LAO field, patient CW-2 used an anterior-posterior (AP) and LAO field combination with different beam weighting. Patient CW-4 was unable to have a passive scatter plan due to the extent of the target size and snout size limitation of 25x25 cm^2.

Uncertainty margins were designed for each treatment field to ensure coverage of target volumes. Beam specific proximal (PM) and distal margins (DM) were calculated using a methodology similar to that used in previous proton planning studies (Macdonald *et al.*, 2013a) and following the methods originally outlined by Moyers and Miller (2003) and Moyers *et al.* (2001). To approximate the proximal margin and distal margins the following equations were used:

$$DM = [(3.5\% \; x \; range) + range \; uncertainty \; (RU)] \quad (1)$$

$$PM = [(3.5\% \; x \; \{range - SOBP\}) + RU] \quad (2)$$

where the 3.5% accounts for CT HU conversion to stopping power inaccuracies, range is the nominal range defined by 90% dose on distal part of the Bragg peak or SOBP expressed in water equivalent depth. Range uncertainty (RU) for passively scatter protons for this study was 3 mm and is used to account for variations in accelerator energy, material thickness in the scattering

system, and compensator density (Giebeler *et al.*, 2013). SOBP is the width of the spread out Bragg peak. Distal margins ranged from 0.6-0.7 cm for all patients and a proximal margin of 0.3 cm was used for each patient.

Once an angle was chosen, a brass block was added with a lateral uncertainty margin of 0.8 to 1.2 cm. The minimum lateral margin needed was calculated using the following equation (Giebeler *et al.*, 2013):

$$LM = 95\% - 50\%\, penumbra + IM + SM\ (cm) \tag{3}$$

where IM is the internal margin and for all plans was set to zero since this margin was already accounted for in the VMAT planning target volume. SM is the setup margin and again needed no further expansion from the PTV boundary. Therefore the only parameter needed to estimate the lateral margin needed was the beam energy and from that the 95%-50% penumbra. This minimum lateral margin was around 0.5 cm for a 160 MeV beam, however, this margin did not provide adequate lateral coverage of the PTV and thus an additional user defined margin of 3 to 4 mm was added. This value was the smallest margin that provided adequate coverage.

Once the block margins were determined and set from the PTV without bolus structure a lucite compensator was added to the plan. Compensators conform the dose distribution to the distal end of the PTV. A smearing radius of 3 mm was used to account for any uncertainty in the alignment of the compensator to the patient and possible motion of the patient during the treatment. A border smoothing radius of 1 cm (default) was used for all patients. Border smoothing is used to avoid steep gradients of the compensator immediately below the block edge. Dose was then calculated for the patient and checked for adequate coverage both laterally and distally. If the dose distribution was not adequate, edits were made to the compensator and dose was recalculated. All passively scattered proton plans were then approved by the same

radiation oncologist who approved the original VMAT plans. Figure 2.2, shows the workflow for planning passively scattered proton therapy treatment plans.

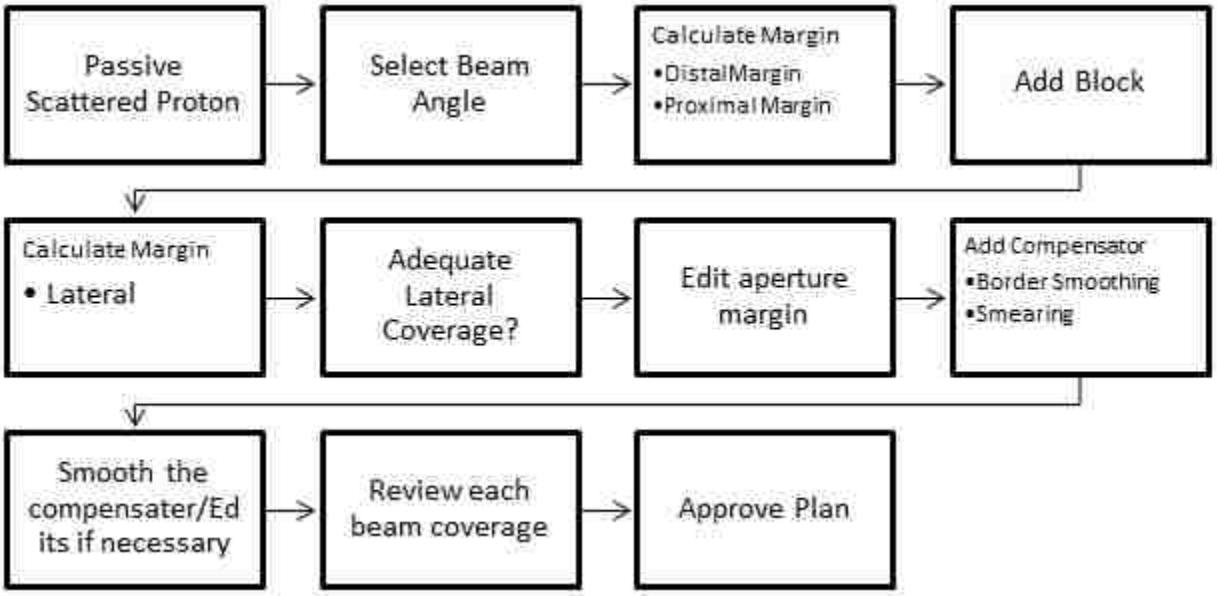

Figure 2.2 Passive scatter proton treatment planning workflow

2.5 Intensity Modulated Proton Therapy Planning

50.4 Gy (RBE) at 1.8 Gy (RBE) per fraction was prescribed to 100% of the PTV. Two fields were used for all patients: an anterior posterior field 0˚ and a left anterior oblique field with angles ranging from 30˚ to 45˚. Angles were chosen to get the best dose distribution within the supraclavicular region (AP beam) and chest wall region (LAO) and were consistent with methods used in a previous proton treatment study for breast cancer (Jimenez *et al.*, 2013). A snout size of 40x30 cm^2 was the largest possible size we had active scanning commissioning data for, and was used for all plans.

The proximal margin and distal margins were calculated using the same methodology as passively scattered proton therapy (section 2.4). However, the range uncertainty value for IMPT was 1 mm instead of 3 mm since no compensator was present. Lateral margins are one of the

many influential IMPT parameters and were required to get adequate lateral coverage of the target. Lateral margins were set to the same value, 0.8 cm, as the block margins used in PS proton plans (Eq. 3). Unlike passive scatter proton plans, these uncertainty margins were not applied by the TPS due to limitations in the computer algorithm, and were thus applied manually to the planning target volume to create a scanning target volume. Figure 2.3 shows the treatment planning workflow for the IMPT technique.

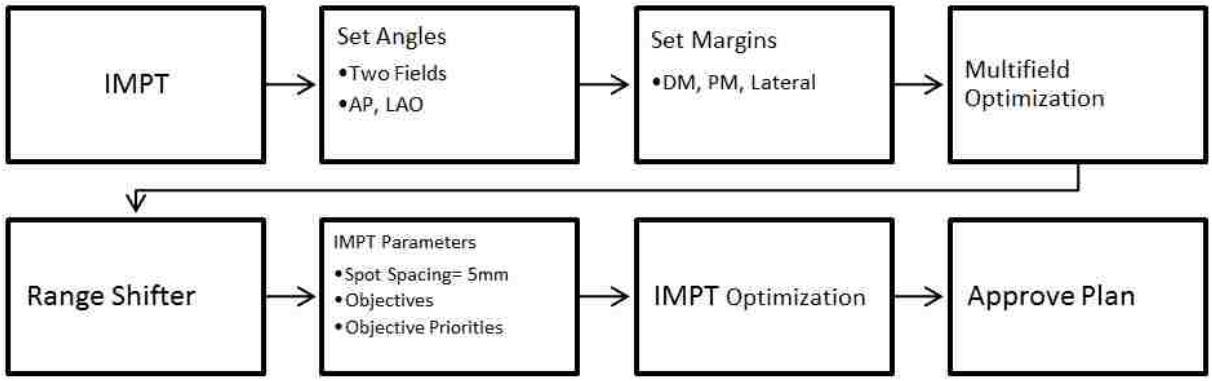

Figure 2.3 Intensity modulated proton therapy treatment planning workflow

Intensity modulated proton planning in the proton TPS was enabled by selecting Multi Field Optimization. This allowed spot weights from both fields to be optimized at the same time to cover the target area and spare organs at risk. Two range shifters were added to the plan in order to achieve lower energies to cover the target volume. The energy range available for IMPT ranged from 70 to 250 MeV, however, our plans only required between 170 to 190 MeV. Prior to optimization a beam-line calculation was performed. This task located all possible spot positions from the range to the target plus margins, available energies, and definition of spot pattern. Optimization of the spot weights was done using Simultaneous Spot Optimization (SSO). SSO algorithm minimizes the objective function which consists of a basic part that accounts for the target dose prescription with a specific fall-off, and the contributions of the user-defined dose

volume objectives. No repainting was chosen during the optimization process. Therefore a dose layer was only "painted" once.

Dose volume constraints for all fields were set up prior to dose optimization. Constraints were made for the PTV, STV, and OARs. Table 2.3 shows the starting constraints for all IMPT plans:

Table 2.3 Preliminary IMPT dose volume objectives

Organ	Type of Constraint	Volume	Dose	Priority
PTV	Upper	0%	51.5 Gy	150
	Lower	100%	50.4 Gy	100
STV	Upper	0%	51.5 Gy	150
	Lower	100%	50.4 Gy	100
Lungs	Upper	0%	40 Gy	50
	Upper	15%	15 Gy	50
Heart	Upper	5%	5 Gy	50
R Breast	Upper	2%	5 Gy	50
Cord	Upper	5%	5 Gy	50
Esophagus	Upper	10%	15 Gy	50
Airway	Upper	10%	20 Gy	50

2.6 Plan Acceptance Criteria

VMAT, PS, and IMPT plans were all normalized so that the evaluation PTV received the same amount of dose for all modalities. This was accomplished by normalizing all plans to a mean dose of 50.4 Gy (RBE) within the evaluation PTV. After normalization, a proton plan was considered optimized when PTV $D_{95\%}$ was at least 47.8 Gy (RBE), $V_{107\%}$ was <2%, $V_{20Gy\ (RBE)}$ was <20% of total lung volume, and heart $V_{22.5Gy\ (RBE)}$ was <20%. The dose constraint to the lung was chosen because it has been established as the threshold for risk of radiation pneumonitis in clinical practice. Similarly, the dose constraint to the heart correlates with increased rates of myocardial perfusion defects (Gagliardi *et al.*, 2001). Target coverage was given priority over normal tissue dosage. The rationale for choosing PTV $D_{95\%}$ at 95% of the

prescription dose, contrary to the International Commission on Radiation Units and Measurements (ICRU) recommendations of PTV $D_{100\%}$ 95%, was due to the difficulties with VMAT acquiring ICRU coverage recommendation at the level of the skin; consequently, the PTV $V_{95\%}$ > 95% is the more frequently used clinical value in breast radiotherapy (Ares *et al.*, 2010). Similarly, we allowed a PTV V_{107}% of up to 2% value because this is more robust than evaluating a single point maximum dose.

2.7 Dosimetric Plan Evaluation Metrics

The goal of aim one is to determine if the *dose-volume* treatment plan metrics between VMAT and proton therapies are statistically significantly different from each other for each patient. The goal of radiotherapy has always been to deliver 100% of the prescribed dose homogeneously to the entire target volume while simultaneously limiting dose to healthy tissues. Every radiotherapy treatment plan is subsequently optimized to meet this goal. Evaluation of treatment plans for the determination of best plan among different plans is accomplished by analysis of the dose volume histogram (DVH) as well as two-dimensional and three-dimensional spatial dose distributions.

2.7.1 Planning Target Volume (PTV)

The same evaluation planning target volume for all modalities was compared on the following dose-volume treatment plan metrics:

<u>Planning target volume (PTV):</u>

1. Dose volume histogram with clinical target volume shown as well
2. Mean, maximum, and minimum dose to the PTV and standard deviation
3. Dose that 95% of the PTV volume receives
4. Volume that receives at least 95% of the prescription dose
5. Volume that receives 107% or more of the prescription dose
6. Dose Homogeneity Index (DHI)
7. Conformity Index (CI)

According to ICRU Report 68 the maximum and minimum dose to a region of interest are defined as the dose to 2% and 98% of each ROI respectively. This formalism was chosen to ignore small, clinically-insignificant hot or cold spots that may appear due to dose algorithm approximations. The dose to 98% of the PTV ($D_{98\%}$) will be used in conjunction with the dose to 2% of the PTV to determine the level of dose homogeneity within the PTV using the following equation:

$$DHI = \frac{D_{max} - D_{min}}{D_{RX}}, \tag{4}$$

where D_{max} is the dose to 2% of the PTV volume and D_{min} is the dose to 98% of the PTV volume and D_{RX} is the prescribed dose (Wu *et al.*, 2003). A value of zero would be the ideal homogeneity index. The PTV was also evaluated and compared on the conformity index (CI) or conformity number proposed by van't Riet *et al.* (1997) using the following equation:

$$CI = \frac{TV_{RI}}{TV} \times \frac{TV_{RI}}{V_{RI}}, \tag{5}$$

where TV is the target volume, RI is the reference isodose, and TV_{RI} is the volume of the target that is covered by the reference isodose (Feuvret *et al.*, 2006). 47.8 Gy (RBE) was used as the reference isodose. This conformity index takes into account irradiation of the target volume and irradiation of health tissues. The conformity index ranges from 0 to 1, where 1 is the ideal number. The PTV was also evaluated for acceptable coverage using $V_{95\%}$ and $V_{107\%}$ or the volume of the PTV that received at least 95% and no more than 107% of the prescribed dose.

2.7.2 Organs at Risk (OARs)

The following parameters from the dose volume histograms were compared between plans for each patient:

Organs at Risk (OARs):

1. Dose volume histogram for each organ (lungs, heart, contralateral breast, skin, esophagus, airway, spinal cord, and unspecified normal tissue)
2. Mean and maximum dose to each OAR and standard deviations
3. Volume of lungs receiving 5, 10, and 20 Gy (RBE) or more
4. Volume of heart receiving 5, 10, 22.5 and 30 Gy (RBE) or more
5. Volume of contralateral breast receiving at least 5 Gy (RBE) or more

The organs at risk that we are most interested in are the lungs, heart, contralateral breast, skin, esophagus, airway, spinal cord, and unspecified normal tissue. DVH values of interest for the total lung volume included the mean dose, $V_{20Gy\ (RBE)}$, $V_{10Gy\ (RBE)}$, $V_{5Gy\ (RBE)}$, and their respective standard deviations. The volume that receives at least 20 Gy (RBE) should be less than or equal to 20% of the total lung volume ($V_{20Gy} \leq 20\%$) and was the metric we were most concerned with for the lungs since it is a well-established threshold for risk of radiation induced pneumonitis in clinical practice (Ares *et al.*, 2010). The volume receiving at least 5 Gy (RBE) should be kept under 42% since this volume is associated with an increase in lung toxicity (Ares *et al.*, 2010). The volume receiving at least 10 Gy (RBE) and the mean dose to each lung will also be compared.

The heart will be evaluated on the volumes receiving 5, 10, 22.5, and 30 Gy (RBE). Studies have shown that doses below 30 Gy (RBE) to the heart demonstrate no increase in cardiac mortality (Gagliardi *et al.*, 1996; Gagliardi *et al.*, 1998). Other studies quote that a dose of 22.5 Gy (RBE) has been shown to correlate with increased rates of reduced myocardial blood flow (Ares *et al.*, 2010). The volume receiving 5 Gy (RBE) was used to evaluate the low dose contribution to the organ.

2.8 Radiobiological Metric Comparison

Not only should radiation treatment plans be evaluated on physical quantities such as the DVH values discussed above, but also biological responses. It has been shown that the inclusion

of non-dosimetric factors such as normal tissue complication probability, tumor control probability, and secondary cancer complication probability for organs at risk with dose volume metrics increase the predictive power of complication incidence and provide a more robust method of comparing different radiotherapy treatment plans (Li *et al.*, 2012).

The goal of aim two was to determine if the following treatment plan metrics between VMAT and proton therapies were statistically significantly different from each other: normal tissue complication probability for the heart and lungs, tumor control probability, and the second cancer complication probability for the contralateral breast and lungs.

Since the biological parameters used in the various dose-response models were derived from 2 Gy (RBE) fraction sizes and the current study delivered 1.8 Gy (RBE) fraction sizes, it was desired to correct the dose distributions for this fraction size discrepancy. Therefore, prior to the calculation of TCP, NTCP, and SCCP the linear quadratic model was used to correct each dose step in the corresponding differential DVH (dDVH) for fractionation with an α/β ratio of 3 Gy (RBE) resulting in the normalized total dose distribution.

2.8.1 Tumor Control Probability (TCP)

Tumor control probability was calculated using the Webb and Brenner model (Brenner, 1993; Webb and Nahum, 1993; Li *et al.*, 2012), which accounts for repopulation. Since α, β, and n values for the chest wall are not available in literature, the chest wall was considered as a whole breast to retrieve said values. The model for the overall TCP is the product sum of probabilities of tumor control in each PTV dose bin *i* of the differential dose-volume histogram:

$$TCP = \prod_i TCP_i. \tag{6}$$

The tumor control probability in each tumor sub-volume was calculated as

$$TCP_i = e^{-N \cdot SF_i}, \quad (7)$$

where N is the number of clonogens initially in the tumor and was found by the following equation:

$$N = nV\ , \quad (8)$$

where n is the tumor cell density and is generically taken to be $2.0 \times 10^8 cm^3$ (Wigg, 2001), and V is the volume of the PTV. SF in Equation 7 is defined as the survival fraction as a function of dose, and is most commonly predicted with the linear-quadratic model for cell survival:

$$SF_i = e^{(-\alpha D_i - G\beta D_i^2)}, \quad (9)$$

where α and β are constants representing the rate of lethal and sublethal cell damage respectively, and G is a constant that takes fractionation, and the half-time for sublethal damage repair into account where, $G=1/x$ with x being the number of fractions. The parameter values suggested for TCP calculation are listed below in Table 2.4.

Table 2.4 TCP parameter values

Parameter	Value	Source
α	0.51 Gy^{-1}(RBE)	(Wigg, 2001)
β	0.061 Gy^{-2}(RBE)	

2.8.2 Normal Tissue Complication Probability (NTCP)

The Lyman-Kutcher-Burman (LKB) (Lyman, 1985; Kutcher and Burman, 1989; Mohan *et al.*, 1992; Seppenwoolde *et al.*, 2003) model was used to calculate the NTCP for the lungs. NTCP for the lungs was calculated with radiation pneumonitis grade two or higher as an endpoint:

$$NTCP = \frac{1}{\sqrt{2\pi}} \int_{-\infty}^{t} e^{\frac{-x^2}{2}} dx, \quad (10)$$

where

$$t = \frac{EUD - TD_{50}}{m \cdot TD_{50}}. \quad (11)$$

Since an inhomogeneous dose was delivered to the lungs, the treatment plan dDVH values were reduced to an equivalent uniform dose using the following equation (Seppenwoolde *et al.*, 2003).

$$EUD = \left(\sum_i D_i^{\frac{1}{n}} \frac{v_i}{v_{tot}} \right)^n, \quad (12)$$

where EUD is the dose, that if given uniformly to the entire volume, will lead to the same NTCP as the actual non-uniform dose distribution. D_i is the dose per fraction to sub volume *i*, v_i is the volume irradiated with dose D_i in bin number *i*, and V_{tot} is the total lung volume. D_i was corrected for fractionation using the linear-quadratic model with an α/β ratio of 3. TD_{50} is the uniform dose given to the entire organ that results in 50% complication risk, *m* is a measure of the slope of the dose-response curve, and *n* is the volume effect parameter. Table 2.5 gives the model parameter values used to calculate NTCP for the lungs.

Table 2.5 Parameters to calculate NTCP (radiation pneumonitis) for the lungs

Parameter	Value	95% CI	Source
m	0.37	[0.28-0.56]	(Seppenwoolde *et al.*, 2003)
n	0.99	[0.6-2.8]	
TD_{50}	30.8 Gy (RBE)	[23-46]	

NTCP for the whole heart and myocardium was calculated using the relative seriality model (Kallman *et al.*, 1992) which describes response of an organ with a mixture of serial- and parallel-arranged functional subunits (Li *et al.*, 2012). NTCP is given by the following equation with cardiac mortality as the endpoint:

$$NTCP = \left\{ 1 - \prod_i^n (1 - P(D_i)^s)^{v_i} \right\}^{1/s}, \quad (13)$$

where v_i is the fractional organ volume receiving a dose D_i, n is the number of sub volumes in the dose volume histogram, s is the relative seriality of the organ which is defined as the ratio between the number of serial functional subunits to the total number of functional subunits. $P(D_i)$ is the probability of complication, and is defined by the following equation:

$$P(D_i) = 2^{-e^{e\gamma(1-\frac{D_i}{D_{50}})}}, \quad (14)$$

where γ is the maximum relative slope of the dose-response curve describing excess cardiac mortality at 15 years, and D_{50} is the dose associated with 50% complication probability. Table 2.6 gives the parameters used to calculate NTCP for the heart.

Table 2.6 Parameters to calculate NTCP (cardiac mortality) for the whole heart and myocardium

Structure	Parameter	Value	68% CI	Source
Whole Heart	D_{50}	52.3 Gy	-3.3, +4.7	(Gagliardi *et al.*, 2001)
	γ	1.28	-0.24, +0.36	
	s	1	-0.27	
Myocardium	D_{50}	52.2 Gy	-3.4, +4.7	
	γ	1.25	-0.24, +0.37	
	s	0.87	-0.24	

2.8.3 Second Cancer Complication Probability (SCCP)

Second cancer complication probability was calculated for the contralateral breast and lung using the Schneider model (Schneider *et al.*, 2005):

$$SCCP = In_{org} OED_{org,} \quad (15)$$

where In_{org} is the organ specific absolute cancer incidence rate in percent per gray (RBE). These values represent lifetime risk, and assume a residual life expectancy of 50 years. Therefore, any age related effect of radiation-induced breast cancer was ignored in this study. In_{org} for the breast was estimated using atomic bomb survivor data and applies to whole-body irradiation. OED_{org} is the organ equivalent dose and represents the corresponding dose in gray for an inhomogeneous

dose distribution, which if distributed evenly throughout the organ, causes the same radiation-induced cancer incidence (Schneider *et al.*, 2005). OED was calculated using three different dose-response models: linear, linear-exponential, and linear-plateau based on the differential DVHs (Abo-Madyan *et al.*, 2014)

$$OED_{T,linear} = \frac{1}{V_T}\sum_i (v_i \cdot D_i), \tag{16}$$

$$OED_{T,linear-exp} = \frac{1}{V_T}\sum_i (v_i \cdot D_i \cdot e^{-\alpha D_i}), \tag{17}$$

$$OED_{T,plateau} = \frac{1}{V_T}\sum_i \left(v_i \cdot \frac{\left(1 - e^{-\delta_{org} D_i}\right)}{\delta_{org}}\right), \tag{18}$$

where v_i is the volume receiving dose D_i and the summation runs over all voxels of organ T with volume V_T. The parameters α and δ are the organ specific model parameters for their respective dose-response models. Parameters that were used to calculate SCCP are listed in Table 2.7.

Table 2.7 Parameters used to calculate SCCP

Organ	α (Gy^{-1})	δ (Gy^{-1})	In_{org} (% / Gy)	Source
Breast	0.085	0.139	0.78 [0.6-1.0]	(Schneider and Kaser-Hotz, 2005b; Abo-Madyan *et al.*, 2014)
Lungs	0.085	0.15	1.68 [1.1-2.3]	(Schneider and Kaser-Hotz, 2005b, a)

2.9 Uncertainty Analysis

Many uncertainties are associated with treatment planning with both photon and proton treatment planning modalities. Uncertainties analyzed within this work included the impact of isocenter shifts, proton range uncertainty on dose distribution and predicted risks, and sensitivity analysis of the risk models for NTCP and SCCP. The proton range uncertainty was evaluated

using the range uncertainty dose calculation tool within the proton TPS for a representative patient (CW-3).

The two factors manipulated within the treatment planning range uncertainty tool were positional uncertainty and HU to relative linear stopping power (RLSP) calibration curve error. Positional uncertainty was simulated by an isocenter shift of 1 cm in all directions for one patient for all modalities (Wang *et al.*, 2013). In the proton treatment planning system, the default coordinate system is defined as follows and for simplicity is referenced to a patient head first supine: the +X direction is to the patient's left, +Y is posterior, and +Z is superior.

The HU to relative stopping power calibration curve was changed by ±3.5% and ±10% (Lomax *et al.*, 2001; Wang *et al.*, 2013) simulating a large systematic over- or under-shoot calibration error for the proton modalities. A positive percentage change indicated the proton stopping power value increased and the range became shorter compared to the range of the nominal plan. Conversely, a negative percentage change simulated a decrease in stopping power value and the range moved further from the source. This percentage was relative to the HU value in the calibration curve, therefore as the values on the curve increased, the correction also increased. Range uncertainty DVH data cannot be exported from the TPS. However, it was possible to simulate the isocenter shift and export that DVH data. The data from the calibration curve error was manually extracted from the TPS generated range uncertainty DVH at 0.5 Gy (RBE) intervals and then converted to a differential DVH for predicted risk calculations. New NTCP and SCCP values were generated for the isocenter shifts and calibration curve errors data.

The sensitivity of the NTCP and SCCP models was analyzed using the nominal dose distributions. The sensitivity analysis for NTCP was accomplished by varying the model parameter values within the equations to their respective minima and maxima within the 95%

confidence interval. NTCP values were calculated for each patient for each parameter by taking all other parameters as a constant except for the parameter being varied within its 95% confidence interval. Then the average NTCP values for each set of parameters were calculated. In the case of lung NTCP, the parameters varied were the slope of the dose-response curve (*m*), D_{50}, and the volume effect parameter (*n*). NTCP using the relative-seriality model varied the following parameters: the normalized dose response curve slope parameter (γ), D_{50}, and the relative seriality parameter *s*. The parameter *s* describes the relative seriality of the organ and is defined as the ratio of the number of serial subunits to all subunits. According to this interpretation the *s* value should be between 0 and 1. However, an *s* value greater than 1 was allowed for this sensitivity analysis.

Sensitivity analysis of SCCP consisted of comparing the second cancer risk between three different dose-response models: linear, linear-exponential, and linear-plateau. The organ equivalent dose used in the calculation of SCCP was calculated using these models for the lungs and contralateral breast. At low doses (D < 2 Gy RBE) OED is the average organ dose because for low doses the risks are proportional to dose or the linear model. However, for doses higher than 2 Gy (RBE), radiation induced cancer incidence rates are not necessarily a linear function of dose. Therefore, comparing the results for the different risk models allows estimating the magnitude of the effect of the unknown shape of the dose-response curve.

Since there are large uncertainties associated with the dose-response models used, the ratios of NTCP (RNTCP) and SCCP (RSCCP) from the nominal proton PMRT and photon PMRT plans were also compared. To compare the risk values for NTCP we defined the ratio as: $RNTCP = NTCP_{ps\ or\ IMPT}/NTCP_{VMAT}$. To compare the risk values for SCCP we defined the ratio for the linear (baseline model) as: $RSCCP_{linear} = SCCP_{ps\ or\ IMPT}/SCCP_{VMAT}$.

Chapter 3 Results

3.1 Patient CW-3

Minimal differences were observed between patients with regards to the dosimetric and radiobiological findings. For this reason, only one representative patient is presented here; meaning this patient had the most, not all, metrics closest to the mean of the sample population. Patient CW-3 was a 27 year old woman diagnosed with invasive ductal carcinoma of the upper-outer quadrant of the left breast. After receiving a modified radical mastectomy the patient underwent post-mastectomy radiotherapy of the CW and regional lymph nodes using VMAT at Mary Bird Perkins Cancer Center. Results for the patient will be presented in the following fashion:

1. Isodose distribution comparison
2. DVH Comparison
3. Dosimetric and radiobiological results for planning target volume
4. Dosimetric and radiobiological results for lungs, heart, contralateral breast, and skin
5. Impact of proton range uncertainties

3.1.1 Isodose Distribution Comparison

Isodose distributions for the VMAT, PS, and IMPT plans are shown for a transverse slice through VMAT beam isocenter (Figure 3.1). VMAT distributions are placed in the middle for ease of comparison between it and the proton plans. All treatment plans were normalized to the mean dose of the evaluation PTV, shown as the red contour. Color coding for the isodose distributions is listed in Table 3.1.

Table 3.1 Color coding for isodose distributions

Isodose Value Gy or Gy (RBE)	Color
55.0	Yellow
52.9	Green
50.4	Blue
47.9	Cyan
35.0	Orange
25.0	Magenta
15.0	Dark Green
5.0	Red

All techniques met the required PTV coverage, with 95% of the PTV receiving more than 95% of the prescribed dose (47.9 Gy or Gy RBE), and the volume receiving 107% or more of the prescription dose (53.9 Gy or Gy RBE) was less than 2% of the PTV volume. All three techniques showed a high degree of conformity, with better conformity in the proton plans. The VMAT plan had higher maximum dose located medially than the proton plans. Both proton modalities significantly reduced the dose to the organs at risk, especially at the 5 Gy (RBE) level. The max dose to the target was reduced from VMAT to PS and IMPT, with IMPT having the lowest maximum dose, indicating a more homogeneous dose distribution. The dose to the contralateral breast was greatly reduced from VMAT to IMPT and PS, with PS having the lowest dose. IMPT shows a low dose increase in the left posterior portion of the patient due to the AP beam used for dose coverage of the supraclavicular area that is not seen in the PS plans.

Isodose distributions for VMAT, PS, and IMPT plans are shown for a transverse slice through a plane in the supraclavicular region of the PTV (Figure 3.2). Similar to the dose distributions through isocenter, all three modalities showed a high degree of dose homogeneity. However, there were several small spots receiving 52.9 Gy (RBE) in the anterior portion of the PTV in the PS plan due to the oblique entry angle of the beam. The 47.9 Gy (95%) isodose line extends further posteriorly in the VMAT plan than in the proton plans indicating a higher degree of

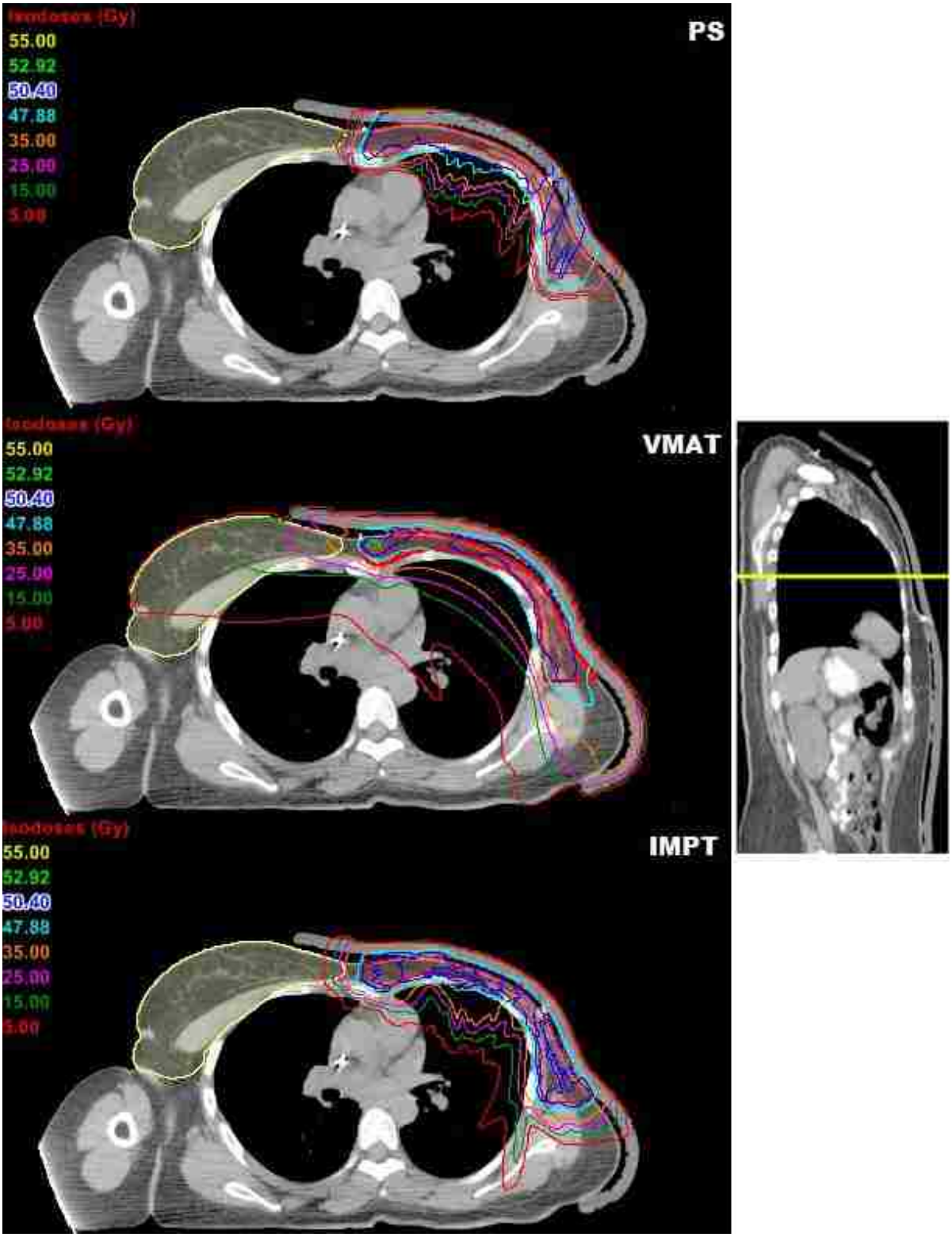

Figure 3.1 Isodose distributions in transverse slice for PS, VMAT, and IMPT treatment plans. Shown through VMAT isocenter, indicated by yellow line in sagittal view

conformity for the proton plans. Also similar to the previous figure, the 5 and 15 Gy (RBE) isodose lines extended farther through the patient in the VMAT plan.

3.1.2 DVH Comparison

Figure 3.3 contains the cumulative dose volume histograms for VMAT and PS plans for this patient. Regions of interest included in the figure include the evaluation PTV, heart, lungs, and contralateral breast. Color coding for all dose volume histograms is listed in Table 3.2.

Table 3.2 Color coding for regions of interest included in dose volume histograms for all treatment plans

Region of Interest	Color
Contralateral Breast	Green
Heart	Magenta
Lungs	Blue
Evaluation PTV	Red

To describe DVHs a few terms must be defined. First the "shoulder" of the graph pertains to the PTV curve and describes the region where the curve begins to bend away from 100% of the PTV volume. Next the "falloff" of the graph also pertains to PTV curve and describes the vertical drop from prescription dose to zero dose. An ideal PTV curve would appear as having no shoulder and whose falloff would be a perfect vertical line from 100% volume to 0% volume at the prescription dose. For this patient, the VMAT and PS plans have nearly identical DVH curves for the PTV. Both curves for the PTV have a narrow shoulder and sharp distal falloff, representing a high degree of dose homogeneity. The major difference between these two plans becomes apparent when comparing the OARs.

The VMAT plan had significantly higher volumes of the heart, lung, and contralateral breast receiving more dose than the PS plan. The volume of the lungs receiving 10 Gy (RBE) or less was about twice as large for the VMAT plan as it was for the PS plan. However, the volume

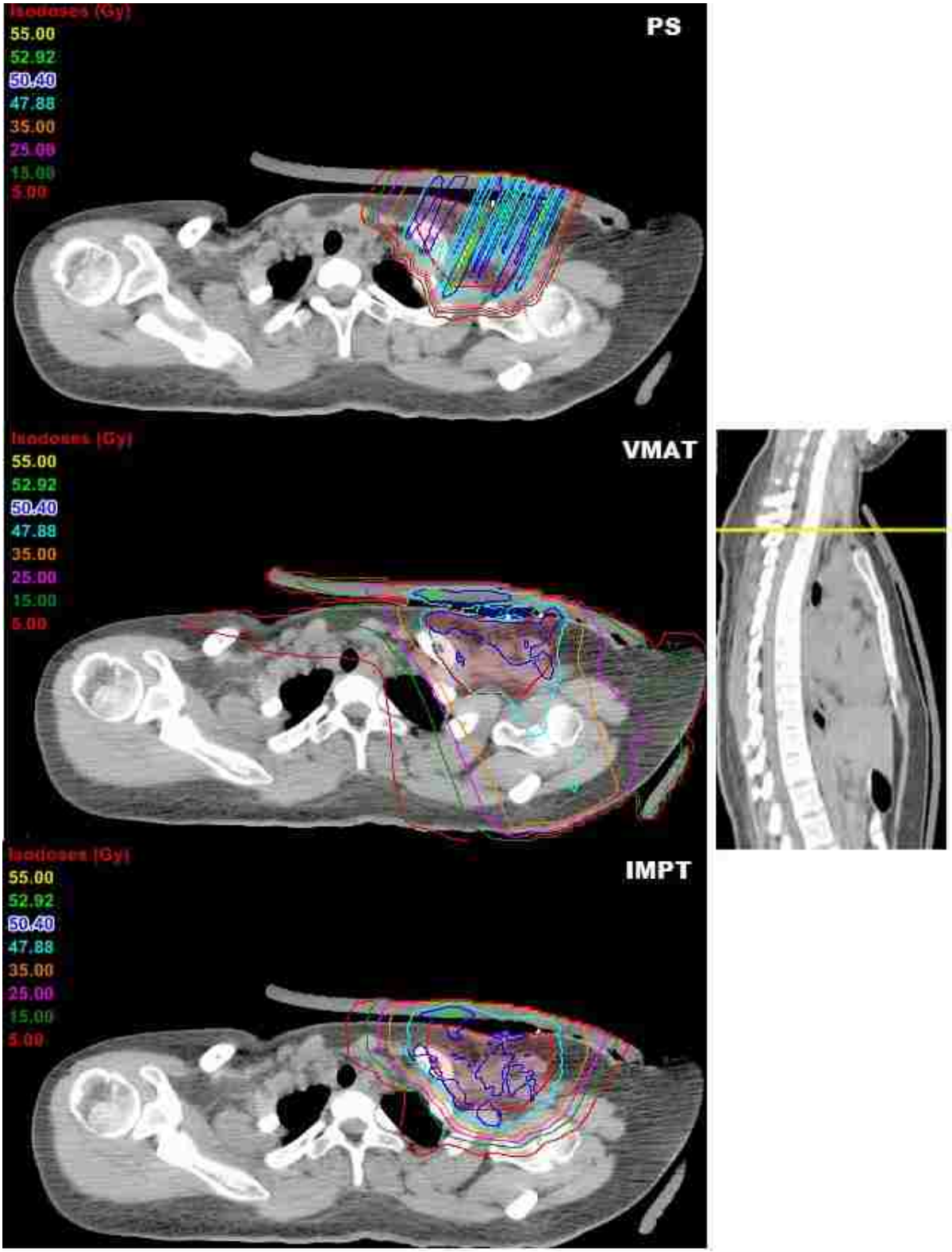

Figure 3.2 Isodose distribution for PS, VMAT, and IMPT in the supraclavicular region as indicated by yellow line in sagittal view

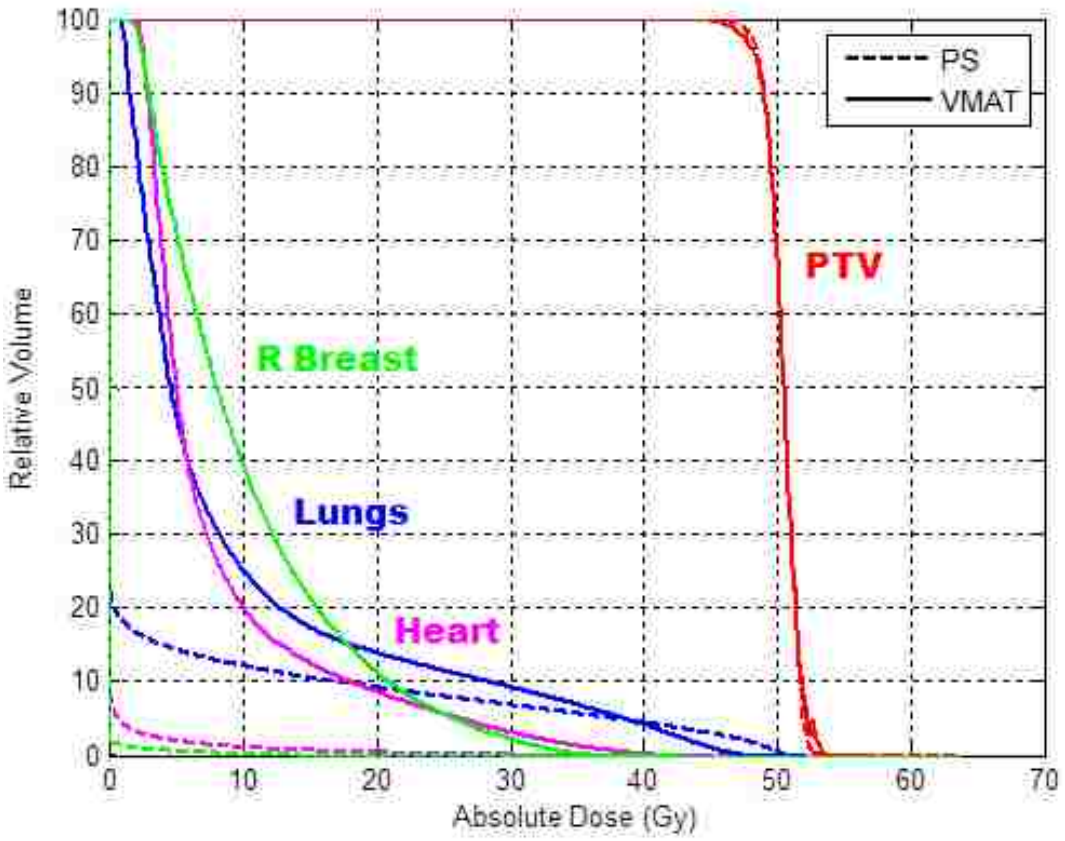

Figure 3.3 DVH comparing PS (dashed line) to VMAT (solid line) for patient CW-3

of the lungs receiving above 40 Gy (RBE) was marginally higher for PS. The volume of the heart receiving 10 Gy (RBE) or less was about 20 times lower for the PS plan than VMAT. There was even more of a reduction seen, about 40 times, in the volume of the contralateral breast receiving 10 Gy (RBE) or less for the PS plan versus VMAT.

Figure 3.4 contains the cumulative dose volume histograms for VMAT and IMPT plans for this patient. Regions of interest included in the figure include the PTV (PTV-Bolus), heart, lungs, and contralateral breast. The PTV DVH for IMPT exhibits a narrower shoulder and steeper distal falloff than VMAT. This indicates IMPT had a better degree of conformity and homogeneity than VMAT. There was not as large as a reduction in dose to the OARs from VMAT to IMPT as was seen in the PS plan however, there was still a reduction. The volume of

the lungs receiving 10 Gy (RBE) or less was about 1.5 times as large for VMAT versus IMPT. The volume of the heart receiving 10 Gy (RBE) or less was about 4 times lower IMPT. There was even more of a reduction seen, about 20 times, in the volume of the contralateral breast receiving 10 Gy (RBE) or less for the IMPT plan versus VMAT.

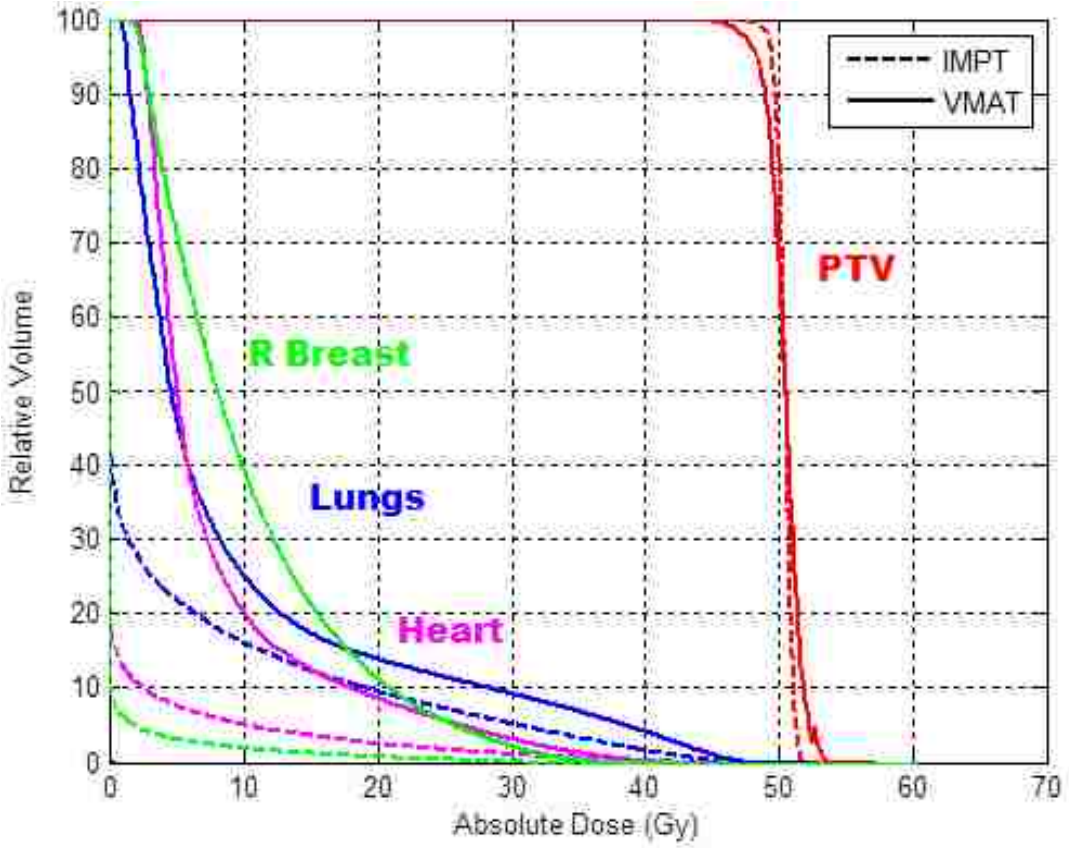

Figure 3.4 DVH comparing IMPT (dashed line) and VMAT (solid line) for patient CW-3

3.1.3 PTV

Results for patient CW-3 pertaining to the evaluation PTV are shown Table 3.3. No difference was seen between mean dose for all plans since normalization was set to the mean dose of the PTV. Maximum dose was defined as the dose to 2% of the PTV volume. Both proton modalities had slightly lower maximum doses. Minimum dose was defined as the dose to 98% of

the PTV volume. There was little difference between the minimum doses for VMAT and PS. There was however a more noticeable difference between the minimum doses for IMPT and VMAT, as was also shown in Figures 3.3 and 3.4. Dose coverage for 95% of the PTV volume exceeded the 47.9 Gy or Gy (RBE) dose requirements for all three plans. Better conformity was achieved with both proton plans, with IMPT having the highest degree of conformity. This trend also applied to DHI, where IMPT had superior dose homogeneity. Both proton modalities achieved 100% tumor control and VMAT achieved 99.99% tumor control.

Table 3.3 Evaluation metrics for the PTV for patient CW-3

Plan	D_{mean} [Gy (RBE)]	D_{max} [Gy (RBE)]	D_{min} [Gy (RBE)]	$D_{95\%}$ [Gy (RBE)]	$V_{95\%}$ [%]	$V_{107\%}$ [%]	CI	DHI	TCP [%]
VMAT	50.4	52.6	47.3	48.3	96.7	0.0	0.60	0.11	99.99
PS	50.4	52.2	47.9	48.5	98.1	0.1	0.80	0.09	100.00
IMPT	50.4	51.5	49.1	49.5	99.8	0.0	0.85	0.05	100.00

3.1.4 Lungs

Table 3.4 summarizes the evaluation metrics used for the total lung volume in patient CW-3. Mean dose was lower by ~50% from VMAT to both proton modalities. Maximum dose was defined as the dose to 2% of total lung volume. Maximum doses were comparable between VMAT and IMPT modalities with IMPT having slightly lower dose. Maximum dose for PS was about 25% lower than VMAT. 43.7% of the lungs received a dose of 5 Gy (RBE) or higher whereas only 14.5% and 22% received this dose for PS and IMPT, respectively. The volume of lungs receiving 10 Gy (RBE) or more was again highest for VMAT with 25.5% and lowest for the PS plan with 12.3% and IMPT had 16.4%. The same trend was seen for the volume of the lungs receiving 20 Gy (RBE) or more, however PS and IMPT were more comparable at this dose level with 9.4% and 9.8% respectively. VMAT had the highest mean dose and larger volumes receiving dose especially at the 5 Gy (RBE) level. Consequently, VMAT had the highest NTCP

with 1.9% and highest SCCP with 12.1%. NTCP for PS and IMPT were comparable with 0.9%. SCCP was lowest for PS with 6.2% and with IMPT SCCP was 6.4%. SCCP values reported here are calculated using the linear OED model (see section 2.8.3).

Table 3.4 Evaluation metrics for the lungs for patient CW-3

Plan	D_{mean} [Gy (RBE)]	D_{max} [Gy (RBE)]	$V_{5Gy\ (RBE)}$ [%]	$V_{10Gy\ (RBE)}$ [%]	$V_{20Gy\ (RBE)}$ [%]	NTCP [%]	SCCP [%]
VMAT	9.4	43.7	46.7	25.5	14.2	1.93	12.06
PS	4.3	31.3	14.5	12.3	9.4	0.89	6.24
IMPT	4.8	39.5	22.0	16.4	9.8	0.90	6.37

3.1.5 Heart

Table 3.5 summarizes the evaluation metrics for the whole heart and myocardium for patient CW-3. VMAT had the highest mean dose with 8.0 Gy (RBE) to the whole heart with a maximum dose of 33.5 Gy (RBE). PS and IMPT had lower mean and maximum doses with PS having the most drastic reduction in dose. PS had a mean dose of 0.4 Gy (RBE) and a max dose of 5.8 Gy (RBE). IMPT had a mean dose of 1.6 Gy (RBE) and a maximum dose closer to VMAT of 24.8 Gy (RBE). Over 50% of the whole heart received 5 Gy (RBE) or more when using VMAT, but only 2.2% and 7.8% received this dose for PS and IMPT respectively. Differences in volume percentage receiving 30 Gy (RBE) or more became less drastic with 3.4%, 0.3% and 1.4% of the whole heart for VMAT, PS, and IMPT respectively. VMAT had to highest NTCP for both the whole heart and myocardium, with 0.22% and 0.13% respectively. PS had the lowest NTCP at <0.01%. NTCP for IMPT was reduced from VMAT with 0.15% for the whole heart and 0.04% for the myocardium.

Table 3.5 Evaluation metrics for the heart for patient CW-3

Plan	D_{mean} [Gy (RBE)]	D_{max} [Gy (RBE)]	V_{5Gy} (RBE) [%]	V_{10Gy} (RBE) [%]	$V_{22.5Gy}$ (RBE) [%]	V_{30Gy} (RBE) [%]	Whole Heart NTCP [%]	Myocardium NTCP [%]
VMAT	8.0	33.5	51.2	20.5	7.3	3.4	0.22	0.13
PS	0.4	5.8	2.2	1.3	0.5	0.3	0.03	0.00
IMPT	1.6	24.8	7.8	5.3	2.3	1.4	0.15	0.04

3.1.6 Contralateral Breast

Table 3.6 reports the doses, volumes, and second cancer complication probabilities for the contralateral breast for patient CW-3. There was a significant reduction in dose to the right breast using either proton modality compared to VMAT. The mean dose was 10.3 Gy (RBE) for VMAT, more than 10 times higher than both PS and IMPT. Maximum dose was 30.8 Gy (RBE) when using VMAT and only 0.3 Gy (RBE) for the PS treatment plan. When this patient was planned with IMPT a maximum dose of 10.9 Gy (RBE) was observed. 71.7% of the breast received 5 Gy (RBE) or more for the VMAT plan and this volume was drastically reduced to 0.8% and 3.3% for PS and IMPT respectively. Consequently, the second cancer complication probability was highest for VMAT with 5.7%. SCCP for PS was 0.09% and 0.37% for IMPT. SCCP values reported here were calculated using the linear OED model (see section 2.8.3).

Table 3.6 Evaluation metrics for the contralateral breast for patient CW-3

Plan	D_{mean} [Gy (RBE)]	D_{max} [Gy (RBE)]	$V_{5Gy\ (RBE)}$ [%]	SCCP [%]
VMAT	10.3	30.8	71.7	5.70
PS	0.1	0.3	0.8	0.09
IMPT	0.6	10.9	3.3	0.37

3.1.7 Skin

Table 3.7 reports the mean, maximum, and minimum doses to the skin for patient CW-3. All three modalities had comparable mean doses and were slightly higher than prescription dose

of 50.4 Gy and 50.4 Gy (RBE) for proton plans. VMAT and PS plans had similar maximum doses of 52.5 Gy and 52.4 Gy (RBE) corresponding to 4% increase above prescription dose. The maximum dose reported for the IMPT plan was lower at 51.5 Gy (RBE) which corresponds to only a 2% increase above prescription. Again, VMAT and PS had comparable minimum doses with 48.2 Gy and 48.1 Gy (RBE), respectively. This corresponds to a 4% decrease from prescription. IMPT had a more homogeneous dose distribution to the skin, indicated by the maximum dose previously mentioned and a minimum dose of 49.5 Gy (RBE), or about 98% of the prescription dose.

Table 3.7 Evaluation metrics for the skin (5 mm shell) for patient CW-3

Plan	D_{mean} [Gy (RBE)]	D_{max} [Gy (RBE)]	D_{min} [Gy (RBE)]
VMAT	50.7	52.5	48.2
PS	50.7	52.4	48.1
IMPT	50.6	51.5	49.5

3.1.8 Plan Robustness

Dosimetric and radiobiological uncertainties associated with an isocenter shift and proton range were assessed for the representative patient, CW-3. A 1 cm isocenter shift in all directions was simulated in the proton TPS for both proton modalities and in the photon TPS for the VMAT plan. Cumulative and differential DVH data were exported. In the proton TPS, the default coordinate system was used and the X, Y, and Z directions are defined for a head-first supine patient as the following: +X refers to the patient's left, +Y is posterior, and +Z is superior. In the photon TPS the coordinate system +X is to the patient's left, +Y is anterior, and +Z is inferior. All shifts refer to the point shifting, meaning that the patient table shifted in the opposite direction.

3.1.8.1 Positional Uncertainty for Patient CW-3

Figures 3.5, 3.6, and 3.7 show the change in dose-volume statistics after a 1 cm isocenter shift was simulated for a VMAT treatment plan in all directions. The solid line in all following DVHs indicates the nominal plan, meaning no shift was applied to the calculated dose distribution. For each plan and shift the evaluation PTV, lungs, heart, and contralateral breast were plotted. Figure 3.5 shows the DVH for VMAT when a lateral shift to the left or right was made. The shift degraded the dose coverage within the PTV, with a shift to the right resulting in the lowest $V_{95\%}$.

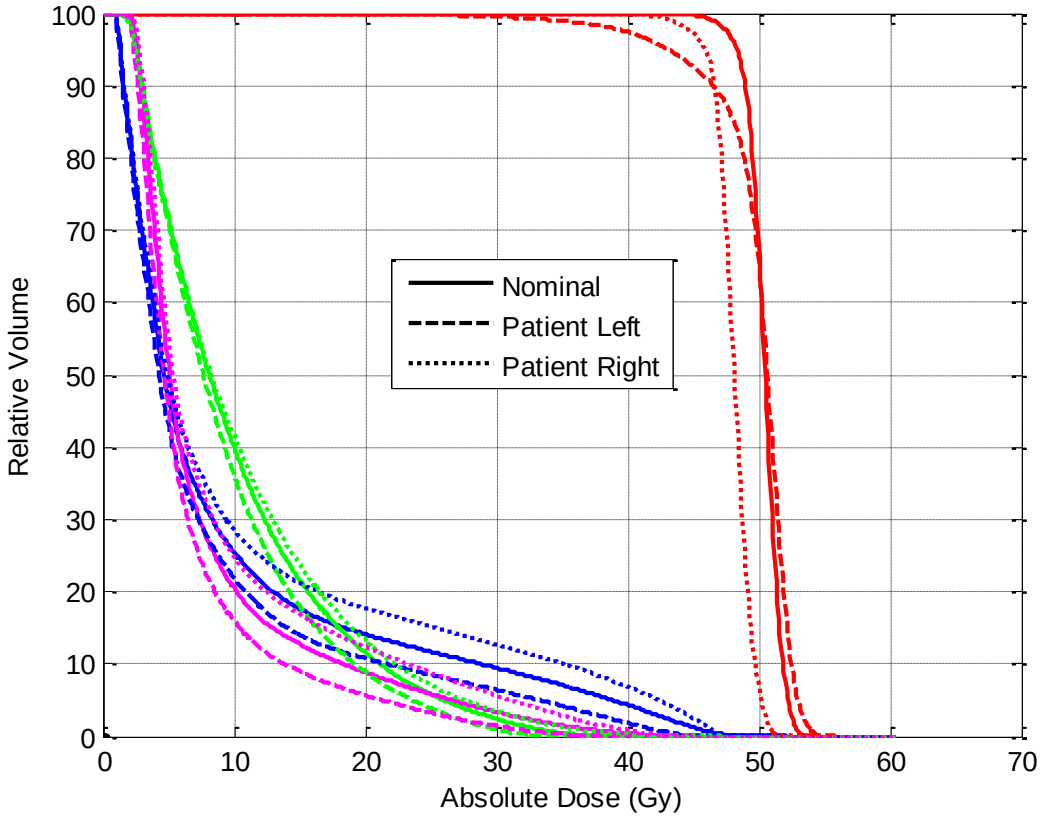

Figure 3.5 DVH showing PTV (red), lungs (blue), heart (magenta), and breast (green) after 1 cm isocenter shift laterally for VMAT

A shift to the patient's right also caused the mean dose to increase in all organs, due to the organs shifting more into the beams eye view or treatment area. Despite the increase in OAR

volume receiving dose, no OARs were beyond their dose tolerances. We see a more pronounced cold dose shoulder for the PTV when the isocenter was shifted to the left. This shift also produced lower mean doses to the OARs.

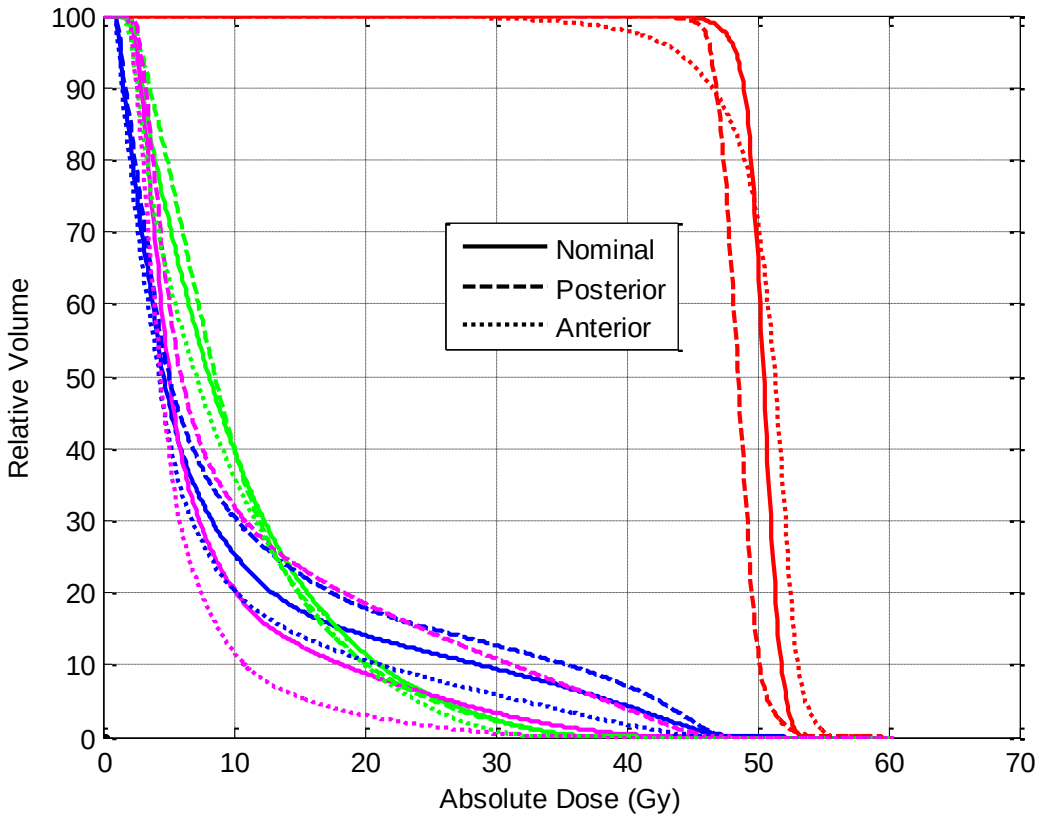

Figure 3.6 DVH showing PTV (red), lungs (blue), heart (magenta), and breast (green) after 1.0 cm isocenter shift anterior or posterior for VMAT

Figure 3.6 shows how the nominal VMAT dose distribution changed for a shift in the ±y-direction. There was a significant dose shoulder for the PTV for an anterior shift, but the dose coverage, $D_{95\%}$, was higher for an anterior shift than posterior. A posterior shift greatly increased $V_{5Gy\ (RBE)}$, $V_{10Gy\ (RBE)}$, $V_{22.5Gy\ (RBE)}$, and $V_{30Gy\ (RBE)}$ to the heart which resulted in the highest risk of cardiac mortality at 1.22%.

Figure 3.7 shows us that PTV coverage was diminished for both an inferior and superior shift for VMAT. An inferior shift caused $V_{107\%}$ to increase from 0.0% to 1.6%, but a superior

shift resulted in poorer dose coverage within the PTV with $D_{95\%}$ at only 43.7 Gy. Mean dose and NTCP to the lungs was increased for an inferior shift but was decreased for a shift in the opposite direction. SCCP for the lungs remained around the same as the nominal risk estimate. Dose statistics for the contralateral breast and heart were very similar to the nominal plan.

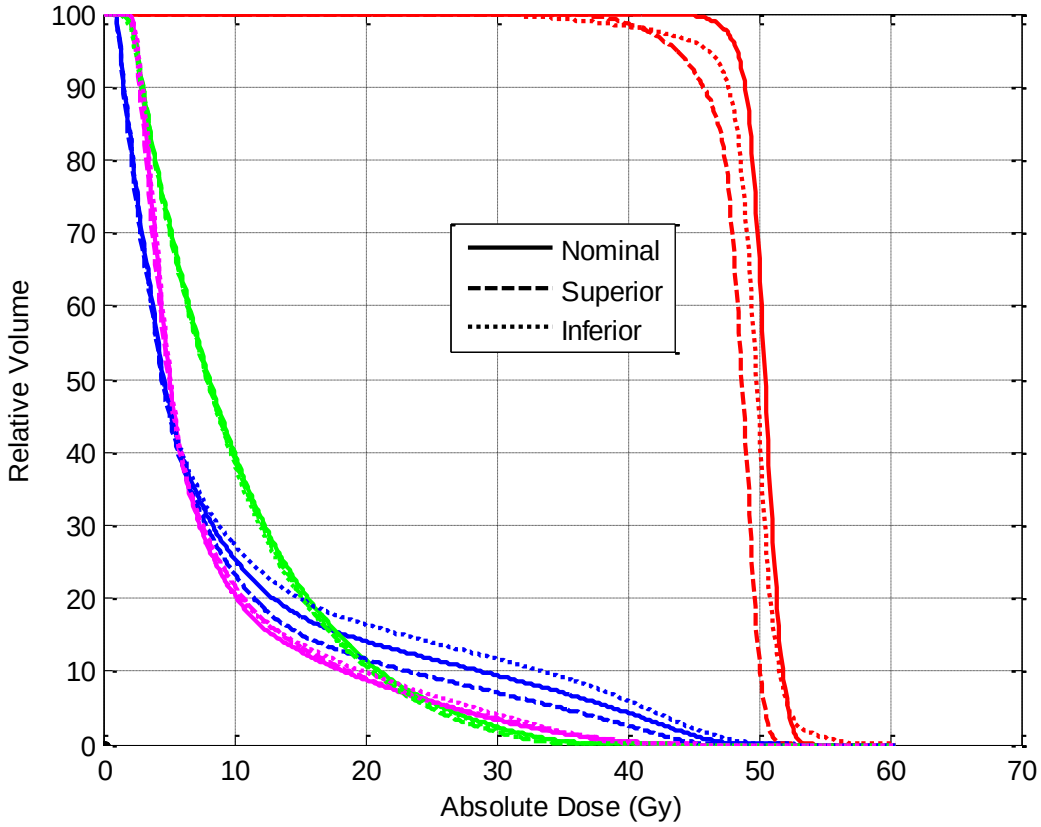

Figure 3.7 DVH showing PTV (red), lungs (blue), heart (magenta), and breast (green) after 1 cm isocenter shift superior or inferior for VMAT

Table 3.8 lists of all dose-volume, NTCP, and SCCP values associated with the PTV, lungs, heart, and contralateral breast for a VMAT plan after a 1 cm isocenter shift was applied in each. For clarification on D_{max}, D_{min}, etc. please refer to section 2.7. NTCPmyo refers to the predicted risk for the myocardium and nominal refers to no shift or the original dose distribution. The criterion for an acceptable plan was $D_{95\%} \geq 47.8$ Gy of the PTV volume while keeping OARs

within their tolerance doses. All bolded values fail to meet the acceptance criterion. This VMAT plan failed to pass the PTV dose coverage criterion for a 1 cm in all directions; however no OARs received doses beyond their respective tolerance levels. Therefore this VMAT plan was not considered robust for an isocenter shift of 1 cm or greater.

Table 3.8 Dose-volume and risk metrics for PTV, lungs, heart, and contralateral breast following a 1 cm isocenter shift in all directions to nominal VMAT plan for patient CW-3

ROI		Nominal	Patient's Left	Patient's Right	Posterior	Anterior	Superior	Inferior
PTV	D_{max}	52.6	53.6	50.6	51.9	54.4	50.8	53.5
	D_{min}	47.3	38.7	44.5	45.9	39.6	41.1	41.2
	$D_{95\%}$	48.3	**43.1**	**45.9**	**46.4**	**43.9**	**43.7**	**46.1**
	$V_{95\%}$	96.7	**86.0**	**58.0**	**68.6**	**85.7**	**72.2**	**88.5**
	$V_{107\%}$	0.0	0.9	0.0	0.3	**3.5**	0.0	1.6
Lungs	D_{mean}	9.4	8.0	10.7	11.0	7.8	8.5	10.2
	D_{max}	43.7	39.7	45.5	45.3	39.4	41.2	45.4
	V_{5Gy}	46.7	42.7	49.1	50.4	42.0	45.3	46.3
	V_{10Gy}	25.5	22.0	28.6	30.5	20.3	23.3	27.3
	V_{20Gy}	14.2	10.8	17.7	17.9	10.7	11.7	16.4
	NTCP	1.93	1.47	2.49	2.60	1.41	1.59	2.27
	SCCP*	12.06	9.96	14.10	14.46	9.66	10.59	13.35
Heart	D_{mean}	8.0	6.8	9.2	11.4	6.0	8.0	8.3
	D_{max}	33.5	28.3	36.9	42.7	23.2	34.1	34.5
	V_{5Gy}	51.2	45.1	54.8	61.1	40.2	49.8	52.1
	V_{10Gy}	20.5	16.0	24.9	32.0	11.8	21.8	20.8
	$V_{22.5Gy}$	7.3	4.4	10.5	16.5	2.2	7.4	8.3
	$V_{30\ Gy}$	3.4	1.4	5.7	10.9	0.6	3.6	4.1
	NTCP	0.22	0.06	0.40	1.22	0.02	0.21	0.25
	$NTCP_{myo}$	0.13	0.02	0.31	1.05	0.01	0.15	0.15
R Breast	D_{mean}	10.3	9.5	10.7	10.4	9.4	10.0	10.0
	D_{max}	30.8	27.8	33.2	30.5	27.8	29.4	30.4
	V_{5Gy}	71.7	70.9	71.0	79.3	63.7	70.6	71.5
	SCCP*	5.70	5.20	6.00	5.75	5.15	5.53	5.56

*Linear OED dose- response model
BOLDED values fail to meet plan acceptance criteria

Figures 3.8, 3.9, and 3.10 show the DVHs for passively scattered proton therapy plans after an isocenter shift was applied. A lateral shift in either direction, as seen in Figure 3.8, decreased the dose coverage within the PTV by about 3%; however 95% of the PTV still received 95% of the prescription dose. An isocenter shift to the patient's right increased the volume over the whole range of dose to the lungs, however decreased the volume in the heart and contralateral breast that received each dose level. A shift left had the opposite effect. Despite the increase of volume receiving dose, all critical organs were well within their tolerance doses.

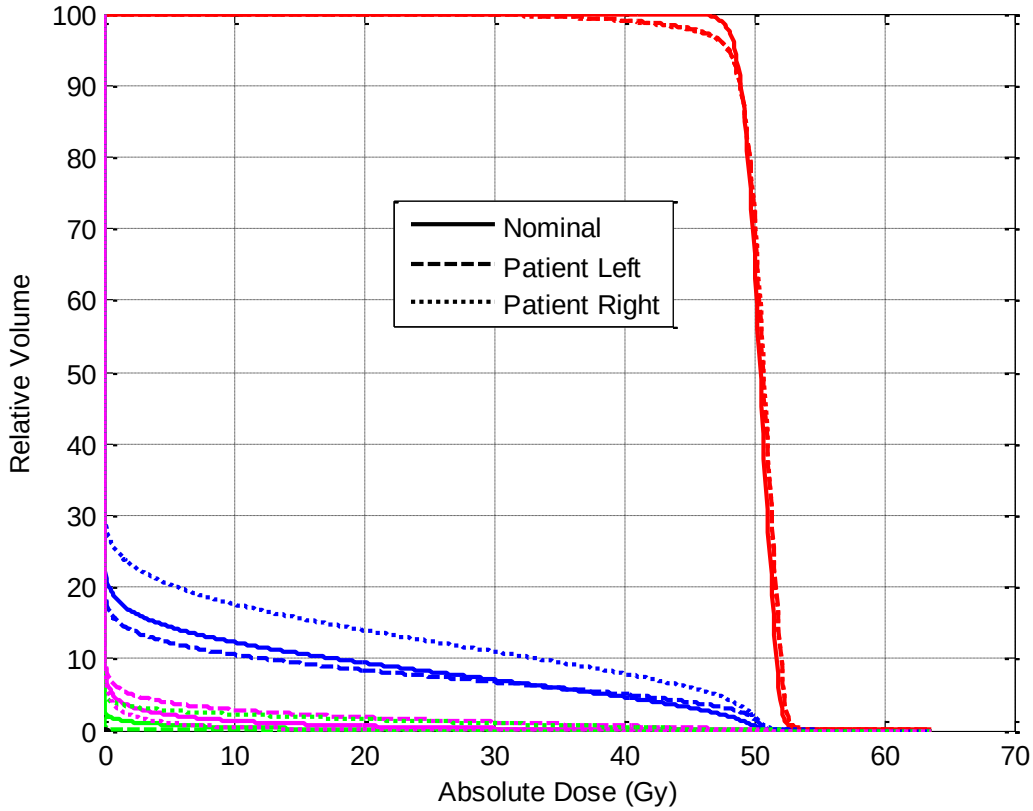

Figure 3.8 DVH showing PTV (red), lungs (blue), heart (magenta), and breast (green) after 1 cm isocenter shift laterally for PS.

A shift posteriorly or anteriorly did not affect the dose coverage, $D_{95\%}$, in the PTV. A posterior shift decreased the volume receiving 10 Gy (RBE) or more to the OARs aside from the

heart where the dose was increased from 1.3% to 2.1%. An anterior shift increased the mean dose to the lungs as well as the contralateral breast.

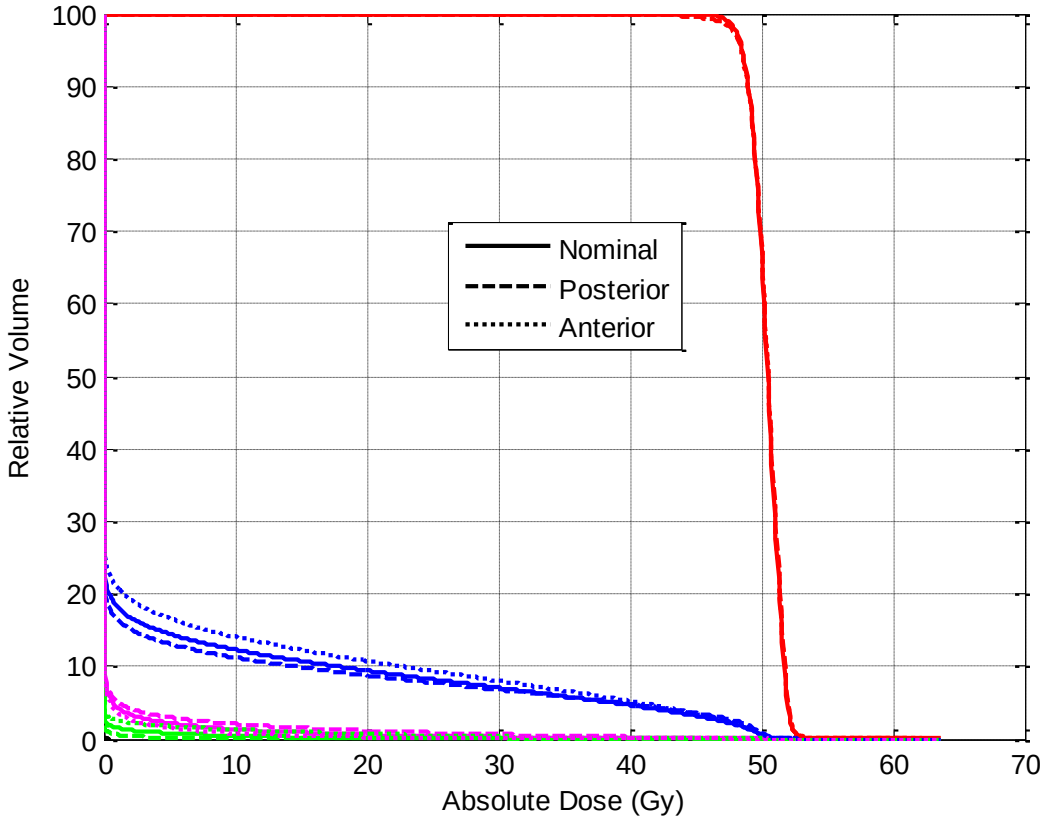

Figure 3.9 DVH showing PTV (red), lungs (blue), heart (magenta), and breast (green) after 1 cm isocenter shift anterior or posterior for PS

A shift inferior or superior for a passively scattered proton therapy plan had the greatest impact on dose coverage and dose to the OARs as seen in Figure 3.10. Shifting the isocenter point superiorly or a patient shift inferior causes $V_{47.9\ Gy\ (RBE)}$ to decrease 3.4%. A shift inferiorly decreased PTV coverage more with a 4.2% change from the nominal dose coverage of 98.1% of the PTV volume. Mean dose to the lungs increased when the point shifted inferior meaning the patient shifted superiorly causing more volume of the lung to be irradiated. All dose-volume metrics for the heart were decreased for an inferior isocenter shift.

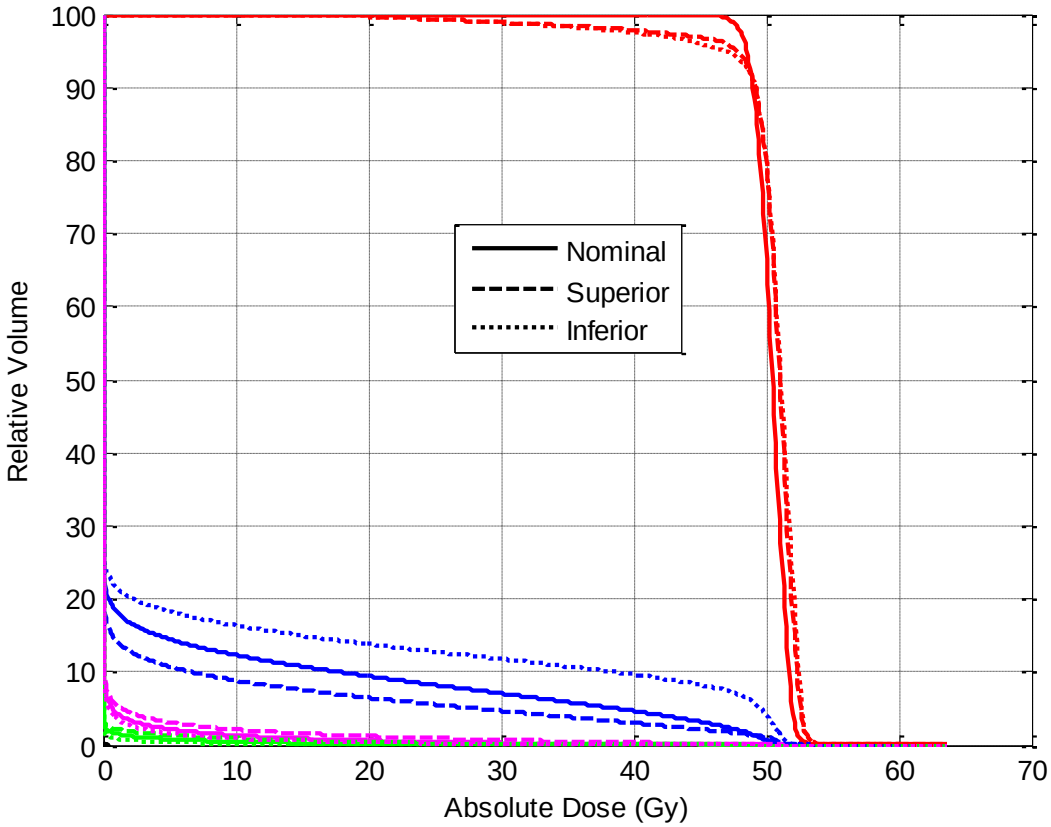

Figure 3.10 DVH showing PTV (red), lungs (blue), heart (magenta), and breast (green) after 1 cm isocenter shift superior or inferior for PS

Table 3.9 summarizes all of the dose-volume and radiobiological metrics for the PTV, lungs, heart, and contralateral breast for a passively scattered proton therapy plan for patient CW-3 after a 1 cm isocenter shift was applied in each direction. For clarification on D_{max}, D_{min}, etc. please refer to section 2.7. NTCPmyo refers to the predicted risk for the myocardium and nominal refers to no shift or the original dose distribution. The criterion for an acceptable plan was $D_{95\%} \geq$ 47.8 Gy (RBE) of the PTV volume while keeping OARs within their tolerance doses. A 1 cm shift inferiorly failed to meet the dose coverage for the PTV by 1 Gy (RBE), but the OARs were still within acceptable limits. Therefore, this PS plan was considered robust (meet most or all criteria) up to 1 cm shift.

Table 3.9 Dose-volume and risk metrics for PTV, lungs, heart, and contralateral breast following a 1 cm isocenter shift in all directions to nominal PS plan for patient CW-3

ROI		Nominal	Patient's Left	Patient's Right	Posterior	Anterior	Superior	Inferior
PTV	D_{max}	52.2	52.6	52.6	47.7	47.7	52.9	52.9
	D_{min}	47.9	44.8	44.5	52.3	52.3	38.9	37.1
	$D_{95\%}$	48.5	48	47.9	48.5	48.5	47.8	**46.8**
	$V_{95\%}$	98.1	95.4	95.1	97.5	97.4	94.8	**94.0**
	$V_{107\%}$	0.1	0.2	0.2	0.1	0.1	0.2	0.2
Lungs	D_{mean}	4.3	4.0	6.4	4.7	4.9	3.6	6.6
	D_{max}	48.0	49.6	50.0	48.9	48.2	45.9	50.8
	$V_{5Gy\ (RBE)}$	14.5	12.3	20.4	13.1	16.6	10.8	18.3
	$V_{10Gy\ (RBE)}$	12.3	10.6	17.7	11.2	14.1	8.8	16.4
	$V_{20Gy\ (RBE)}$	9.4	8.4	14.0	8.8	10.8	6.5	13.8
	NTCP	0.89	0.85	1.40	0.86	1.00	0.68	1.49
	SCCP*	6.24	5.89	9.51	5.96	7.08	4.41	9.97
Heart	D_{mean}	0.4	0.9	0.2	0.6	0.3	0.7	0.3
	D_{max}	5.8	17.8	2.3	10.4	3.4	10.9	3.5
	$V_{5Gy\ (RBE)}$	2.2	3.9	1.1	3.0	1.5	3.1	1.6
	$V_{10Gy\ (RBE)}$	1.3	2.9	0.5	2.1	0.8	2.1	1.0
	$V_{22.5Gy\ (RBE)}$	0.5	1.6	0.1	1.0	0.2	1.1	0.3
	$V_{30\ Gy\ (RBE)}$	0.3	1.2	0.0	0.6	0.1	0.7	0.2
	NTCP	0.03	0.24	0.00	0.10	0.01	0.12	0.01
	$NTCP_{myo}$	0.00	0.04	0.00	0.01	0.00	0.01	0.00
R Breast	D_{mean}	0.1	0.0	0.7	0.3	0.4	0.3	0.7
	D_{max}	0.3	0.1	13.3	0.1	3.4	1.5	0.1
	$V_{5Gy\ (RBE)}$	0.8	0.0	2.8	0.2	1.8	1.3	0.4
	SCCP*	0.09	0.03	0.48	0.04	0.24	0.17	0.06

*Linear OED dose- response model
BOLDED values fail to meet plan acceptance criteria

Figure 3.11 shows the DVH after a 1 cm isocenter shift was applied in the lateral directions for an IMPT dose distribution on patient CW-3. A shift to the patient's left decreased $D_{95\%}$ from 49.5 Gy (RBE) to 47 Gy (RBE), which fails to meet the 47.9 Gy (RBE) plan acceptance criteria. This shift also caused D_{max} to increase from 51.5 Gy (RBE) to 54.3 Gy (RBE) and $V_{107\%}$ increased from 0% to 3%. Despite not having acceptable PTV dose coverage and poor dose homogeneity, a shift to the patient's left decreased the mean dose to the lungs and

contralateral breast. An isocenter shift to the patient's right by 1 cm caused an even greater decrease in $D_{95\%}$, 45.1 Gy (RBE), but had a lower D_{max} to the PTV. This shift also caused an increase in mean dose to the lungs, and contralateral breast, but decreased the mean dose to the heart. A shift to the patient's right increased the risk of radiation pneumonitis the most from 0.9% to 1.31% and also had the highest SCCP risk.

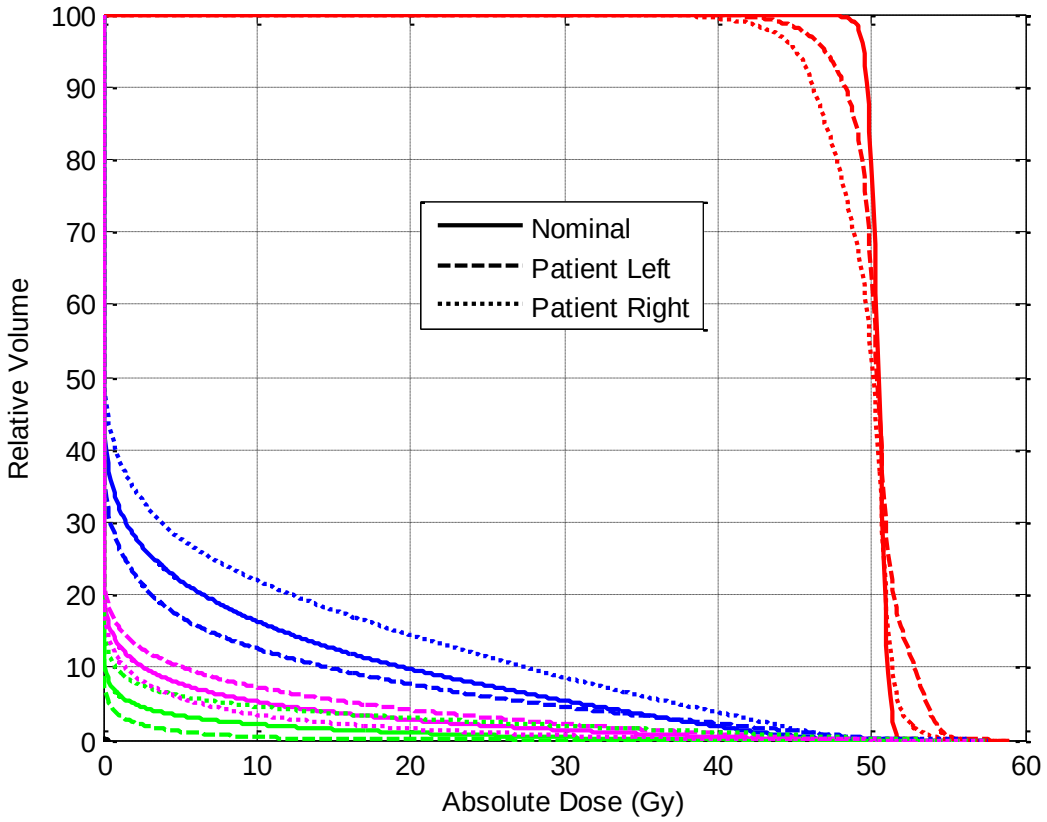

Figure 3.11 DVH showing PTV (red), lungs (blue), heart (magenta), and breast (green) after 1 cm isocenter shift laterally for IMPT

A shift posteriorly or anteriorly in the IMPT plan decreased $D_{95\%}$ from 49.5 Gy (RBE) to 46.0 Gy (RBE) and 47.6 Gy (RBE) respectively as seen in Figure 3.12. However, the dose to 20% of the lungs or greater was very similar to the nominal dose distribution. D_{max} for the PTV increased for both shifts and D_{min} decreased which indicates less dose homogeneity and

conformity. A posterior shift increased the mean dose to the heart but decreased the mean dose to the lungs and contralateral breast.

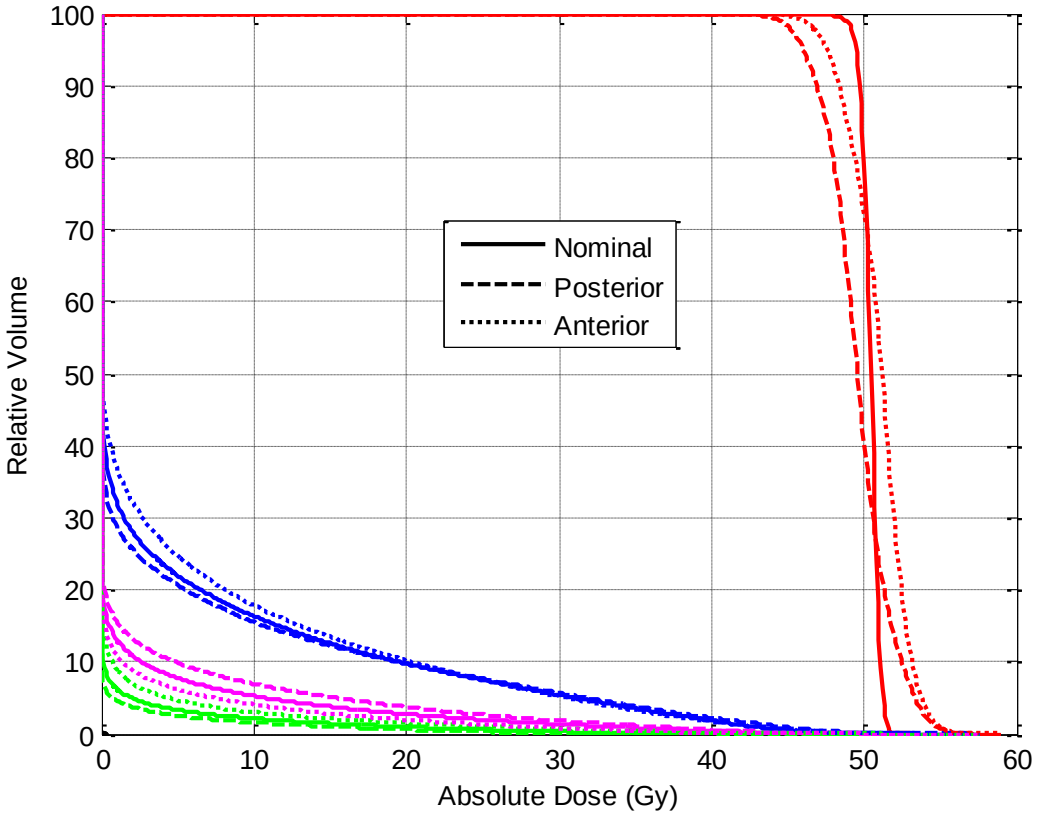

Figure 3.12 DVH showing PTV (red), lungs (blue), heart (magenta), and breast (green) after 1 cm isocenter shift anterior or posterior for IMPT

Figure 3.13 demonstrates how the nominal dose distribution for an IMPT plan changed for an inferior or superior isocenter shift of 1 cm. The PTV received similar dose coverage statistics for both *z*-shifts, however a shift inferior resulted in worse dose homogeneity. This shift did not cause much change from the nominal distribution for the heart and contralateral breast; however the mean dose to the lung increased. Due to the increased volume receiving dose in the lungs, the risk of radiation pneumonitis increased from 0.9% to 1.51%.

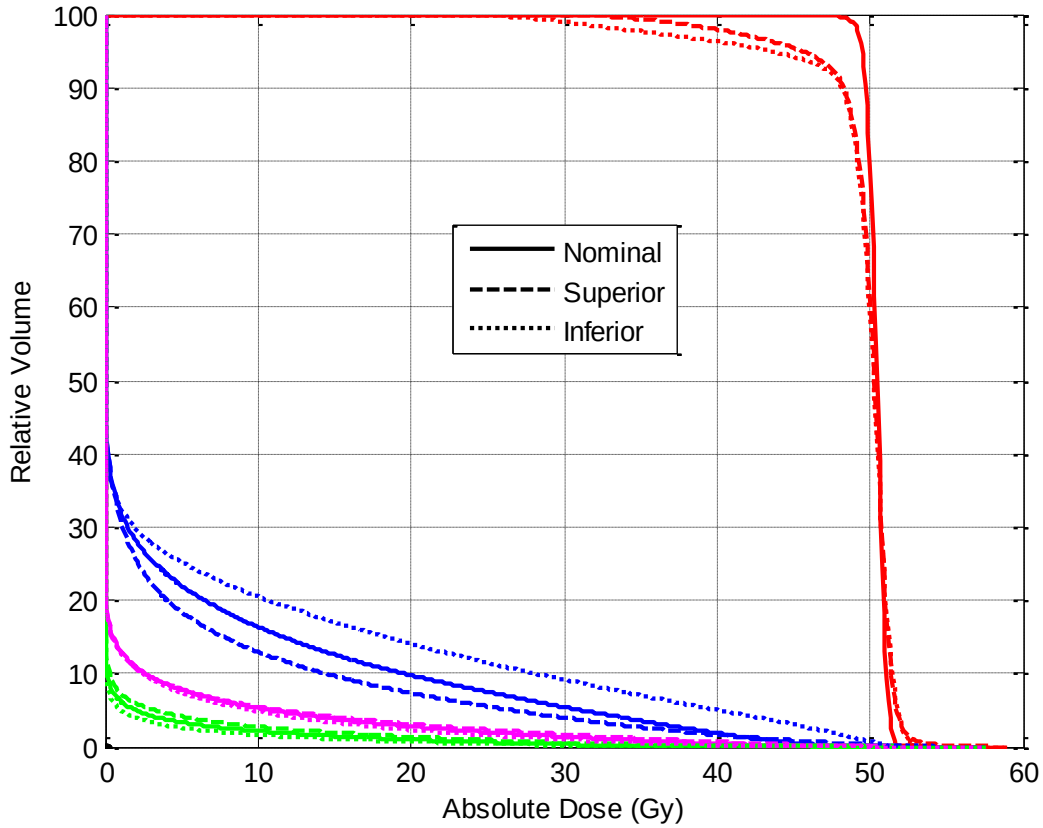

Figure 3.13 DVH showing PTV (red), lungs (blue), heart (magenta), and breast (green) after 1 cm isocenter shift superior or inferior for IMPT

In summary, an isocenter shift of 1 cm in any direction (x,y,or z) for IMPT caused the dose coverage in the PTV to drop below 47.9 Gy (RBE) to 95% of the volume which was a criterion for plan acceptance. Despite poor dose coverage within the PTV, no OARs were out of their respective tolerance doses (see section 2.6). Table 3.10 lists all the dose-volume and radiobiological metrics for the PTV, lungs, heart, and contralateral breast following a 1 cm isocenter shift in all directions for patient CW-3 for an IMPT treatment plan. For clarification on D_{max}, D_{min}, etc. please refer to section 2.7. NTCPmyo refers to the predicted risk for the myocardium and nominal refers to no shift or the original dose distribution.

Table 3.10 Dose-volume and risk metrics for PTV, lungs, heart, and contralateral breast following a 1 cm isocenter shift in all directions to nominal IMPT plan for patient CW-3

ROI		Nominal	Patient's Left	Patient's Right	Posterior	Anterior	Superior	Inferior
PTV	D_{max}	51.5	54.3	52.7	54.2	54.5	52.3	52.2
	D_{min}	49.1	45.3	43.1	45.1	46.7	39.8	33.7
	$D_{95\%}$	49.5	**47.0**	**45.1**	**46.0**	**47.6**	**45.6**	**43.6**
	$V_{95\%}$	99.8	**91.7**	**78.7**	**80.9**	**93.3**	**91.6**	**91.0**
	$V_{107\%}$	0.0	**3.0**	0.5	**2.5**	**3.8**	0.4	0.0
Lungs	D_{mean}	4.8	3.9	6.7	4.7	5.2	4.0	6.5
	D_{max}	39.5	41.2	44.1	40.8	39.0	38.0	47.4
	$V_{5Gy\ (RBE)}$	22.0	17.0	27.8	20.7	24.7	18.4	25.2
	$V_{10Gy\ (RBE)}$	16.4	12.6	22.0	15.6	17.9	13.0	20.5
	$V_{20Gy\ (RBE)}$	9.8	7.7	14.5	9.8	10.2	7.3	14.1
	NTCP	0.90	0.77	1.31	0.89	0.96	0.76	1.31
	SCCP*	6.37	5.29	9.05	6.26	6.80	5.21	9.06
Heart	D_{mean}	1.6	2.2	1.6	2.0	1.2	1.7	1.4
	D_{max}	24.9	31.4	16.7	29.0	20.0	27.4	22.0
	$V_{5Gy\ (RBE)}$	7.8	10.1	5.8	9.9	6.2	7.8	7.4
	$V_{10Gy\ (RBE)}$	5.3	7.3	3.5	7.0	4.1	5.4	4.8
	$V_{22.5Gy\ (RBE)}$	2.3	3.6	1.3	3.2	1.7	2.7	1.9
	$V_{30\ Gy\ (RBE)}$	1.4	2.2	0.6	1.8	0.9	1.7	1.0
	NTCP	0.15	0.28	0.06	0.20	0.07	0.23	0.09
	$NTCP_{myo}$	0.04	0.10	0.01	0.07	0.01	0.07	0.02
R Breast	D_{mean}	0.6	0.2	1.5	0.4	0.9	0.8	0.5
	D_{max}	10.9	2.7	29.5	7.5	15.8	14.5	7.7
	$V_{5Gy\ (RBE)}$	3.3	1.2	6.1	2.6	4.7	4.1	2.6
	SCCP*	0.37	0.11	0.97	0.26	0.55	0.48	0.29

*Linear OED dose response model
BOLDED values fail to meet plan acceptance criteria

3.1.8.2 Proton Range Uncertainty for Patient CW-3

Using the Eclipse range uncertainty tool a ±3.5% and ±10% HU to relative stopping power calibration curve error was introduced to the nominal proton plan for IMPT and PS for the representative patient (CW-3). Figures 3.14 and 3.15 show the changes in the nominal DVH after a ±3.5% error was applied for IMPT and PS proton plans, respectively.

Figure 3.14 Range uncertainty DVH for patient CW-3 for PTV (red), lungs (blue), heart (magenta), and contralateral breast (green) for a ±3.5% simulated HU to relative stopping power calibration curve error (dotted lines) introduced to the nominal IMPT plan (solid line)

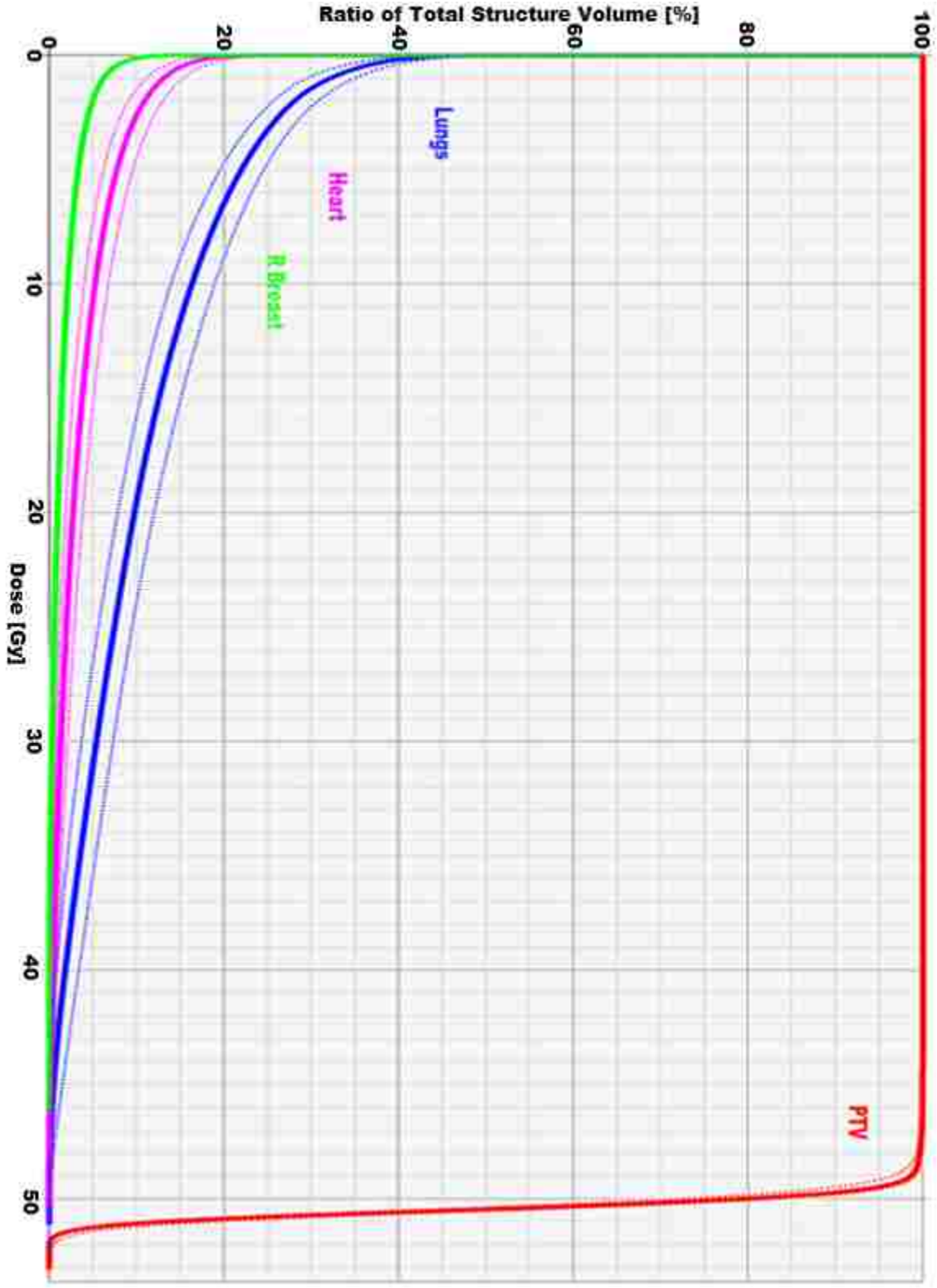

Figure 3.15 Range uncertainty DVH for patient CW-3 for PTV (red), lungs (blue), heart (magenta), and contralateral breast (green) for a ±3.5% simulated HU to relative stopping power calibration curve error (dotted lines) introduced to the nominal PS proton plan (solid line)

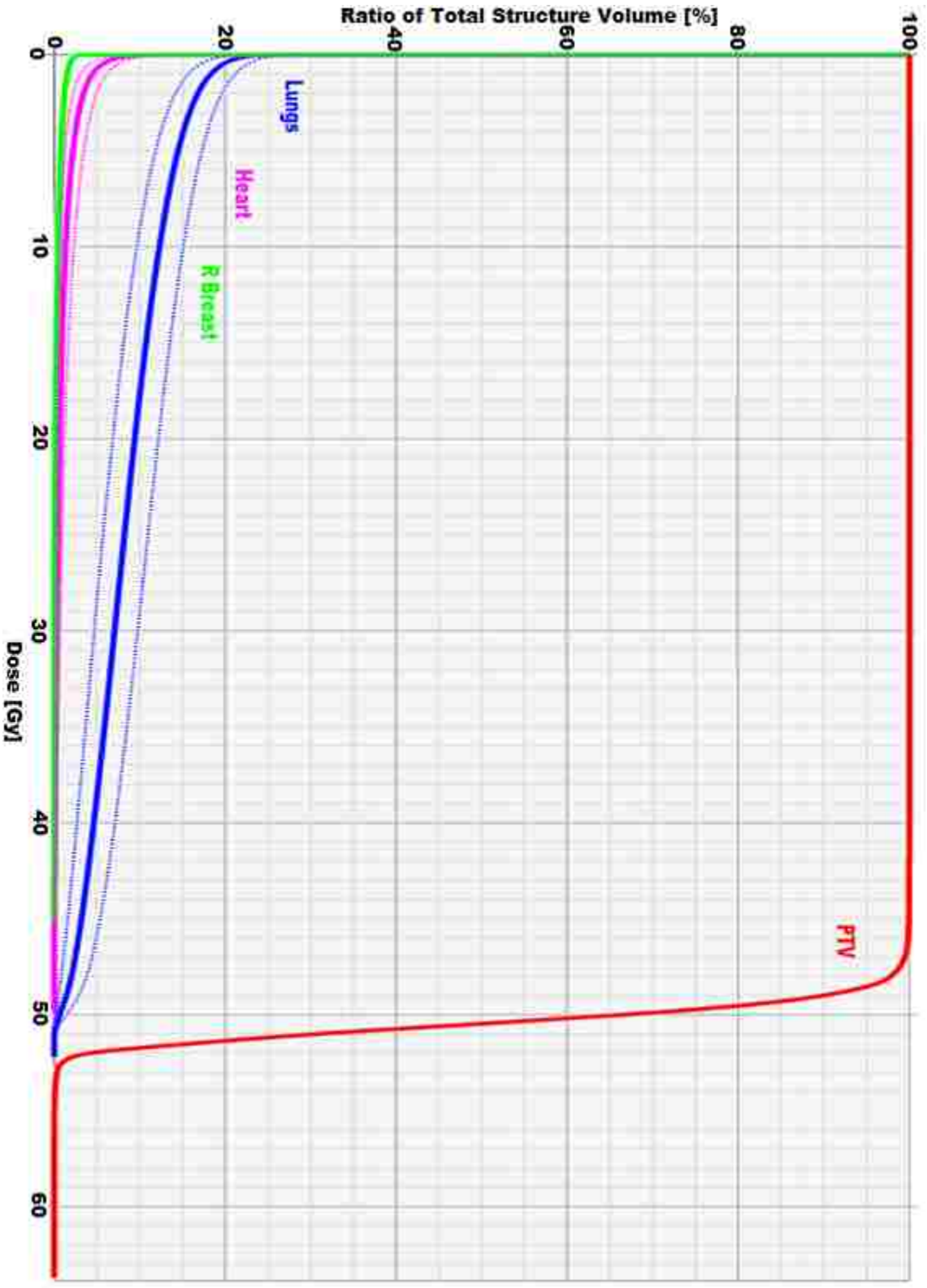

A negative 3.5% relative linear stopping power (RLSP) error increased the mean dose to the lungs and heart for both IMPT and PS due to the increase in range. A positive 3.5% had the opposite effect because of the decrease in range. This decrease in range caused the dose coverage in the PTV for the IMPT plan to slightly decrease in the 48 to 50 Gy (RBE) shoulder region. Despite the small change, the IMPT plan with a +3.5% RLSP error was still able to meet all plan acceptance criteria and therefore was deemed a robust plan. The PTV DVH for the PS plan did not change and was also determined to be a robust plan.

A ±10% RLSP error was also applied to the same IMPT and PS proton plans and provided a worst-case scenario. Figures 3.16 and 3.17 display these range uncertainty DVHs for IMPT and PS proton plans, respectively. A -10% RLSP error caused a large systematic increase in the DVH statistics for the lungs and heart for both proton modalities. However, a +10% error decreased the mean dose to those organs. Neither a positive or negative error appeared to alter the nominal dose distribution for the contralateral breast. The dose to the PTV for IMPT increased for a -10% error starting at 80% of the volume and lower, with the largest increase in dose occurring to only 5% of the PTV. When a +10% error was applied, the PTV DVH was impacted the most seen by the decrease in $D_{95\%}$. The IMPT plan still met the plan acceptance PTV criteria of $D_{95\%} > 47.9$ Gy (RBE) and was considered robust for up to a ±10% RLSP error.

Similarly, the passively scattered proton plan was also deemed robust, since all dose-volume acceptance criteria were met. The same DVH trends for the OARs from IMPT were seen for the PS proton plan. However, the PS range uncertainty DVH was different from the IMPT plan with regards to the PTV coverage. The nominal PTV dose-volume statistics for PS did not change for either (±10%) RLSP error simulation (Figure 3.17).

Figure 3.16 Range uncertainty DVH for patient CW-3 for PTV (red), lungs (blue), heart (magenta), and contralateral breast (green) for a ±10% simulated HU to relative stopping power calibration curve error (dotted lines) introduced to the nominal IMPT plan (solid line)

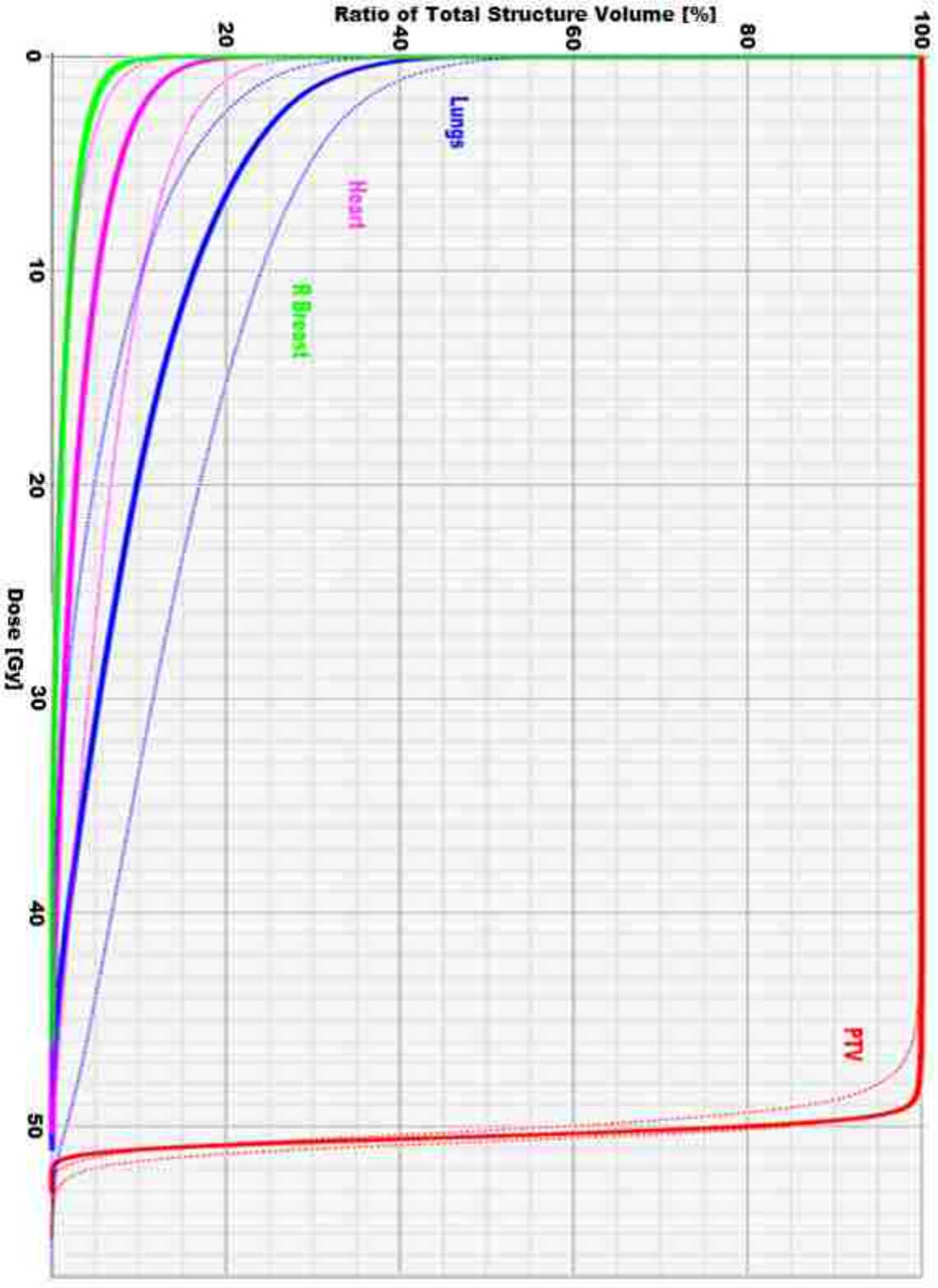

Figure 3.17 Range uncertainty DVH for patient CW-3 for PTV (red), lungs (blue), heart (magenta), and contralateral breast (green) for a ±10% simulated HU to relative stopping power calibration curve error (dotted lines) introduced to the nominal PS proton plan (solid line)

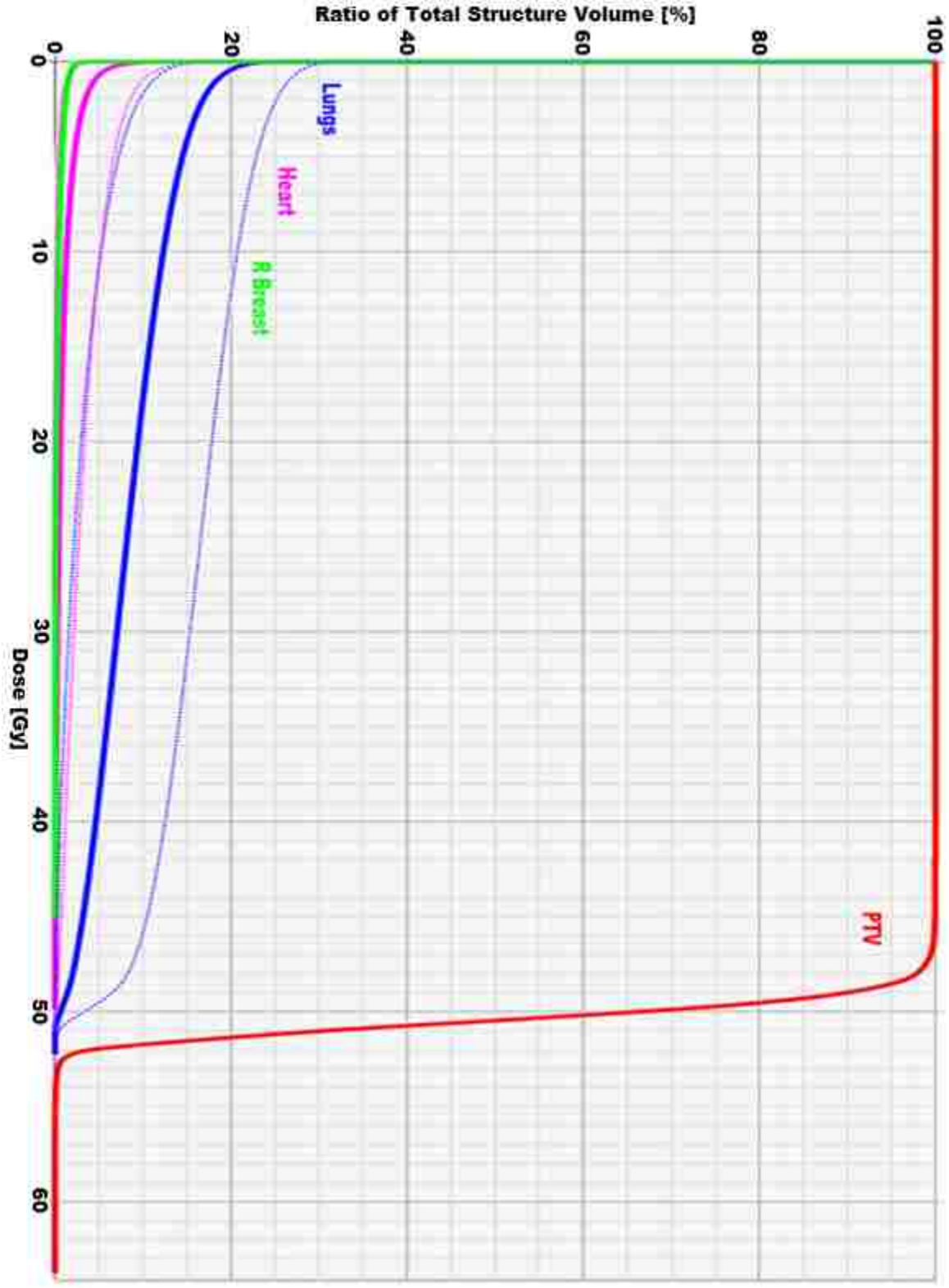

Since a 3.5% calibration curve error did not change the IMPT and PS proton dose distributions as much as the ±10% RSLP error did, it was decided to only recalculate the normal tissue complication risks for the lung, heart, myocardium and risk of second cancer for the lung and contralateral breast for the ±10% RSLP error DVHs. Table 3.11 summarizes these range uncertainty risks for both proton modalities.

Table 3.11 NTCP (%) and SCCP (%) for the lungs, heart, and contralateral breast for patient CW-3 for a simulated 10% HU to relative stopping power calibration curve error introduced to the nominal IMPT and PS plan.

Calibration Curve Error		$NTCP_{lung}$ (%)	$SCCP_{lung}$ (%)	$NTCP_{heart}$ (%)	$NTCP_{myo}$ (%)	$SCCP_{breast}$ (%)
IMPT	Nominal (0%)	0.90	6.37	0.15	0.04	0.37
	-10%	1.74	10.91	0.74	0.41	0.39
	10%	0.60	3.73	0.01	0.00	0.36
PS	Nominal (0%)	0.89	6.24	0.03	0.00	0.09
	-10%	2.09	12.25	0.53	0.23	0.09
	10%	0.48	2.31	0.00	0.00	0.09
VMAT	Nominal (0%)	1.93	12.06	0.22	0.13	5.7

There was a systematic increase in all risks when a -10% error was assumed for both the IMPT and PS proton plans. SCCP (linear) for the lung for both IMPT and PS increased the most for a 10% undershoot in HU to stopping power conversion. This change from the nominal risk was 4.54% for IMPT and 6.01% for PS plans. NTCP for the lungs and heart and also SCCP for the lungs calculated for a -10% RLSP error in the PS plan were predicted to be slightly higher than values associated with VMAT plan for this same patient. Also, NTCP for the heart calculated for a -10% RLSP error in the IMPT plan were predicted to be higher than VMAT. SCCP for the breast was still substantially lower than VMAT despite the introduced RLSP error. However the differences between the proton range uncertainty risks and VMAT were small. It

was therefore concluded that IMPT and PS proton plans were robust for up to a 10% over- or undershoot in stopping power conversion.

3.2 Overview of Results for the Sample of Patients

Results for patients in this sample are presented in the following sections. Patient CW-4 had no results for a PS plan because the PTV was larger than the maximum snout size of 25x25 cm^2. Despite having one less patient in the PS cohort, statistical power of >80% for the results was obtained. Mean values (± 1σ) are given for each evaluation metric. Statistical significance was determined for each comparison (VMAT vs. PS and VMAT vs. IMPT) using a paired, two-tailed Student's t-test and Wilcoxon signed-rank test with a significance level of $p = 0.05$.

3.2.1 PTV

Tables 3.12 and 3.13 list the dose volume and radiobiological metrics results used to evaluate the PTV for VMAT, PS, and IMPT radiotherapy treatment plans. PS and IMPT showed a statistically significant advantage in dose coverage with a mean dose to 95% of the PTV of 48.6±0.4 Gy (RBE) ($p = 0.043$) for PS and 49.4±0.4 Gy (RBE) ($p = 0.001$) for IMPT compared to VMAT. The dose to 95% of the PTV for VMAT was lower, 47.8±0.6 Gy. PS and IMPT achieved significantly better ($p = 0.016$ and $p = 0.001$, respectively) dose conformity than VMAT. Mean conformity values for VMAT, PS and IMPT were 0.72±0.08, 0.81±0.03 and 0.86±0.02, respectively. PS and IMPT also had significantly better dose homogeneity over VMAT. However, there were no statistically significant differences found between modalities in terms of TCP. There was also no statistical difference between VMAT and PS in maximum dose to the PTV. The mean dose value for VMAT was 52.7±0.4 Gy and the mean dose value for PS was 52.3±0.3 Gy (RBE). However, there was a statistical difference between VMAT and IMPT modalities in patient averaged maximum dose ($p = 0.001$). IMPT had a lower $\overline{D}_{max}$ with a mean

value of 51.7±0.3 Gy (RBE). Mean values for the minimum dose ($D_{98\%}$) for both PS and IMPT were found to be statistically different from the corresponding mean value for VMAT. The average minimum dose for VMAT was 46.4±0.7 Gy, 48.0±0.6 Gy (RBE) (p = 0.009) for PS, and 48.7±0.4 Gy (RBE) (p < 0.001) for IMPT.

3.2.2 Lungs

Results for the lungs for each patient are listed in Tables 3.14 and 3.15. $\overline{D}_{mean}$ in the lungs was statistically significantly lower for both PS and IMPT when compared to VMAT (p < 0.001). $\overline{D}_{mean}$ for PS was 4.0±1.9 Gy (RBE), 4.2±1.2 Gy (RBE) for IMPT, and 9.8±0.7 Gy for VMAT. No statistically significant difference was detected between PS and VMAT for the patient averaged maximum dose; however $\overline{D}_{max}$ for IMPT was statistically significantly lower than that for VMAT (p < 0.001). On average more than half the lung volume, 53.2%±10.6%, received 5 Gy (RBE) or more with VMAT compared to only 13.1%±4.6% with PS and 19.0%±3.9% with IMPT, with both proton modalities producing statistically significant reductions in $\overline{V}_{5Gy\,(RBE)}$ (p < 0.001). The mean volume of the lungs receiving 10 Gy (RBE) or more was statistically significantly lower for both proton modalities with $\overline{V}_{10Gy\,(RBE)}$ values of 11.2%±4.4% for PS (p < 0.001), 14.4%±3.5% with IMPT (p = 0.001) and 28.4%±4.6% with VMAT. There was also a statistically significant reduction in $V_{20Gy\ (RBE)}$ for both proton modalities with comparable average $V_{20Gy\ (RBE)}$ values of 8.7%±4.1% (p = 0.002) with PS and 8.7%±3.0% (p < 0.001) with IMPT compared to VMAT, which had an average V_{20Gy} of 14.2%±1.6%. Consequently, $\overline{NTCP}$ and $\overline{SCCP}$ were statistically significantly lower for PS and IMPT compared to VMAT (p < 0.001). $\overline{NTCP}$ was reduced from 2.0%±0.2% in VMAT to 0.9%±0.4% in PS and 0.8%±0.2% in IMPT. $\overline{SCCP}$ values were reduced from 12.5%±0.9% in VMAT to 5.9%±2.9% in PS and 5.61%±1.81% in IMPT.

3.2.3 Heart

Tables 3.16 and 3.17 list the dose volume and radiobiological metrics used to evaluate the heart for each patient. The first metric compared between the modalities was the patient averaged mean dose ($\overline{D}_{mean}$) to the whole heart. $\overline{D}_{mean}$ values were statistically significantly lower ($p < 0.001$) for PS (0.4±0.3 Gy (RBE)) and IMPT (0.5±0.5 Gy (RBE)) compared to VMAT (12.4±2.0 Gy). $\overline{D}_{max}$ values were also statistically significantly lower for both proton modalities ($p < 0.001$) compared to VMAT with $\overline{D}_{max}$ values of 5.9±6.0 Gy (RBE), 8.5±7.7 Gy (RBE), and 39.2±5.3Gy for PS, IMPT, and VMAT, respectively. The volume receiving 5 Gy (RBE) or more was statistically significantly reduced from 88.0±16% with VMAT to 2.0±1.2% and 3.1±2.3% using PS and IMPT ($p < 0.001$), respectively. Similarly, the patient averaged volume receiving 10 Gy (RBE) or more was statistically significantly reduced using both proton modalities compared to that of VMAT ($p < 0.001$) with $\bar{V}_{10Gy(RBE)}$ values of 1.3%±0.9%, 1.8%±1.6%, and 47.2%±15.1% for PS, IMPT, and VMAT, respectively. $\bar{V}_{22.5Gy(RBE)}$ and $\bar{V}_{30Gy(RBE)}$ were also statistically significantly lower ($p \leq 0.001$) for both proton modalities compared to VMAT; with <1% of the whole heart volume receiving these doses using PS and IMPT compared to 12.1%±3.2% ($\bar{V}_{22.5Gy}$) and 7%±3.1% ($\bar{V}_{30Gy}$) using VMAT. Subsequently, the patient averaged predicted risk of cardiac mortality ($\overline{NTCP}$) for the whole heart was statistically significantly lower for PS ($p < 0.017$) and IMPT ($p = 0.014$) when compared to VMAT. The mean risk of cardiac mortality was also statistically significantly lower for the myocardium for PS ($p = 0.019$) and IMPT ($p = 0.020$) compared to VMAT. $\overline{NTCP}$ for the whole heart and myocardium were <0.05% for both proton modalities and around 1% for VMAT.

Table 3.12 Selected PTV evaluation metrics for VMAT, PS, and IMPT plans. Abbreviations: D_{max} = maximum dose; D_{min} = minimum dose; $D_{95\%}$ = dose that 95% of the volume receives; PS p-value = VMAT vs. PS; IMPT p-value = VMAT vs. IMPT.

Patient	D_{max} [Gy (RBE)]			D_{min} [Gy (RBE)]			$D_{95\%}$ [Gy (RBE)]			$V_{95\%}$ [%]		
	VMAT	PS	IMPT	VMAT	PS	IMPT	VMAT	PS	IMPT	VMAT	PS	IMPT
1	53.3	52.2	51.4	45.6	48.0	49.3	46.9	48.4	49.9	90.8	98.3	99.9
2	52.4	52.9	52.2	47.1	46.8	48.1	48.5	47.8	49.2	96.9	94.9	99.1
3	52.6	52.2	51.5	47.3	47.9	49.1	48.3	48.5	49.5	96.7	98.1	99.8
4	52.8	-	51.5	46.3	-	48.6	47.5	-	49.5	93.2	-	99.4
5	52.6	52.4	51.6	45.7	47.7	48.6	47.6	48.6	49.7	94.1	97.7	99.7
6	52.8	52.1	52.0	45.9	48.5	48.3	47.7	49.0	49.5	94.3	99.1	99.4
7	52.1	52.2	51.4	47.3	48.7	49.1	48.4	49.1	49.8	96.7	99.7	100.0
8	52.8	51.9	51.6	45.8	48.4	48.6	47.3	48.9	49.3	93.0	99.1	99.6
Mean	52.7	52.3	51.7	46.4	48.0	48.7	47.8	48.6	49.4	94.5	98.1	99.6
σ	0.3	0.3	0.3	0.7	0.6	0.4	0.6	0.4	0.4	2.2	1.6	.0.3
p-value	PS	IMPT*		PS*	IMPT*		PS**	IMPT*		PS*	IMPT*	
	0.123	0.001		0.009	<0.001		0.043	<0.001		0.026	<0.001	

* Statistical significance detected using both Student's t-test and Wilcoxon signed-rank test
** Statistical significance only found using Student's t-test

Table 3.13 Selected PTV evaluation metrics for VMAT, PS, and IMPT plans. Abbreviations: $V_{107\%}$ = volume that receives at least 107% of the prescription dose; CI = conformity index; DHI = dose homogeneity index; TCP = tumor control probability.

Patient	$V_{107\%}$ [%]			CI			DHI			TCP		
	VMAT	PS	IMPT	VMAT	PS	IMPT	VMAT	PS	IMPT	VMAT	PS	IMPT
1	0.8	0.0	0.0	0.79	0.84	0.89	0.15	0.09	0.04	97.5%	100.0%	100.0%
2	0.0	0.5	0.0	0.79	0.82	0.85	0.11	0.12	0.08	92.7%	99.3%	99.7%
3	0.0	0.1	0.0	0.60	0.80	0.85	0.11	0.09	0.05	100.0%	100.0%	100.0%
4	0.1	-	0.0	0.61	-	0.87	0.15	-	0.06	100.0%	-	100.0%
5	0.0	0.0	0.0	0.72	0.81	0.88	0.14	0.09	0.06	100.0%	100.0%	100.0%
6	0.1	0.0	0.0	0.72	0.76	0.83	0.14	0.07	0.07	100.0%	100.0%	100.0%
7	0.2	0.0	0.0	0.80	0.85	0.89	0.10	0.07	0.05	100.0%	100.0%	100.0%
8	0.1	0.0	0.0	0.74	0.78	0.85	0.13	0.07	0.06	100.0%	100.0%	100.0%
Mean	0.2	0.1	0.0	0.72	0.81	0.86	0.13	0.09	0.06	98.8%	99.9%	100.0%
σ	0.3	0.2	0.0	0.08	0.03	0.02	0.02	0.02	0.01	2.6%	0.2%	0.1%
p-value	PS	IMPT		PS*	IMPT*		PS*	IMPT*		PS	IMPT	
	0.628	0.134		0.016	0.001		0.013	<0.001		0.220	0.220	

* Statistical significance detected using both Student's t-test and Wilcoxon signed-rank test

Table 3.14 Selected lung evaluation metrics for VMAT, PS, and IMPT plans. Abbreviations: D_{mean} = mean lung dose; D_{max} = maximum dose; $V_{5Gy\ (RBE)}$ = volume that receives at least 5 Gy (RBE); PS p-value = VMAT vs. PS; IMPT p-value = VMAT vs. IMPT.

Patient	D_{mean} [Gy (RBE)]			D_{max} [Gy (RBE)]			$V_{5Gy\ (RBE)}$ [%]		
	VMAT	PS	IMPT	VMAT	PS	IMPT	VMAT	PS	IMPT
1	9.9	2.4	3.1	37.3	40.9	30.7	65.2	8.9	16.6
2	8.7	1.8	3.6	43.2	31.3	35.6	40.5	7.5	17.7
3	9.4	4.3	4.8	43.7	48.0	39.5	46.7	14.5	22.0
4	10.4	-	2.4	38.7	-	31	64.5	-	11.6
5	9.5	5.4	5.0	47.2	49.4	43.4	43.9	16.1	20.1
6	10.4	7.1	6.2	46.4	50.2	45.3	45.5	19.7	24.1
7	9.4	2.7	3.6	43.1	44.6	34.6	53.3	9.4	17.9
8	10.9	4.7	4.8	43.4	47.9	39.1	66.1	15.9	22.0
Mean	9.8	4.0	4.2	42.9	44.6	37.4	53.2	13.1	19.0
σ	0.7	1.9	1.2	3.4	6.7	5.4	10.6	4.6	3.9
p-value	PS*	IMPT*		PS	IMPT*		PS*	IMPT*	
	<0.001	<0.001		0.625	<0.001		<0.001	<0.001	

* Statistical significance detected using both Student's t-test and Wilcoxon signed-rank test

Table 3.15 Selected lung evaluation metrics for VMAT, PS, and IMPT plans. Abbreviations: $V_{10Gy\ (RBE)}$ = volume that receives at least 10 Gy (RBE); $V_{20Gy\ (RBE)}$ = volume that receives at least 20 Gy (RBE); NTCP = normal tissue complication probability; SCCP = second cancer complication probability; PS p-value = VMAT vs. PS; IMPT p-value = VMAT vs. IMPT.

Patient	$V_{10Gy\ (RBE)}$ [%]			$V_{20Gy\ (RBE)}$ [%]			NTCP [%]			SCCP [%]		
	VMAT	PS	IMPT	VMAT	PS	IMPT	VMAT	PS	IMPT	VMAT	PS	IMPT
1	31.9	7.2	11.5	12.3	5.1	5.8	1.94	0.59	0.64	12.14	3.40	3.99
2	22.7	5.7	13.1	14.2	3.6	7.3	1.74	0.50	0.72	11.24	2.42	4.77
3	25.5	12.3	16.4	14.2	9.4	9.8	1.93	0.89	0.90	12.06	6.24	6.37
4	36.0	-	8.7	13.3	-	4.8	2.10	-	0.56	12.74	-	3.08
5	24.0	14.2	16.1	14.4	11.7	11.2	2.03	1.14	0.98	12.46	8.02	6.97
6	28.6	17.8	19.7	17.3	15.2	13.8	2.37	1.64	1.24	13.69	10.69	8.65
7	26.3	7.8	12.8	12.7	5.7	6.9	1.88	0.63	0.71	11.88	3.88	4.67
8	32.4	13.5	16.7	15.1	10.3	10.1	2.40	0.96	0.90	13.80	6.78	6.37
Mean	28.4	11.2	14.4	14.2	8.7	8.7	2.05	0.91	0.83	12.50	5.92	5.61
σ	4.6	4.4	3.5	1.6	4.1	3.0	0.23	0.39	0.22	0.88	2.91	1.81
p-value	PS*	IMPT*		PS*	IMPT*		PS*	IMPT*		PS*	IMPT*	
	<0.001	0.001		0.002	<0.001		<0.001	<0.001		<0.001	<0.001	

* Statistical significance detected using both Student's t-test and Wilcoxon signed-rank test

Table 3.16 Selected heart evaluation metrics for VMAT, PS, and IMPT plans. Abbreviations: D_{mean} = mean dose; D_{max} = maximum dose; $V_{5Gy\ (RBE)}$ = volume that receives at least 5 Gy (RBE); $V_{10Gy\ (RBE)}$ = volume that receives at least 10 Gy (RBE).

Patient	D_{mean} [Gy (RBE)]			D_{max} [Gy (RBE)]			$V_{5Gy\ (RBE)}$ [%]			$V_{10Gy\ (RBE)}$ [%]		
	VMAT	PS	IMPT	VMAT	PS	IMPT	VMAT	PS	IMPT	VMAT	PS	IMPT
1	13.0	0.1	0.5	30.8	0.4	7.4	98.0	0.6	2.8	62.0	0.3	1.4
2	12.4	0.3	0.4	38.2	3.4	5.4	93.9	1.7	2.1	50.8	1.1	1.1
3	8.0	0.4	1.6	33.5	5.8	24.8	51.2	2.2	7.8	20.5	1.3	5.3
4	12.7	-	0.1	38.0	-	0.7	99.7	-	0.7	58.0	-	0.3
5	11.3	0.3	0.2	45.3	3.5	2.2	79.9	1.6	1.2	27.3	0.9	0.6
6	14.7	1.0	0.8	45.9	18.6	14.1	91.8	4.4	4.6	57.0	3.2	2.9
7	13.1	0.4	0.4	39.4	6.9	5.4	95.0	2.5	2.1	48.2	1.5	1.1
8	13.5	0.2	0.5	42.3	2.4	7.9	94.2	1.2	3.0	53.7	0.7	1.5
Mean	12.4	0.4	0.5	39.2	5.9	8.5	88.0	2.0	3.1	47.2	1.3	1.8
σ	2.0	0.3	0.5	5.3	6.0	7.7	16.0	1.2	2.3	15.1	0.9	1.6
p-value	PS*	IMPT*		PS*	IMPT*		PS*	IMPT*		PS*	IMPT*	
	<0.001	<0.001		<0.001	<0.001		<0.001	<0.001		<0.001	<0.001	

* Statistical significance detected using both Student's t-test and Wilcoxon signed-rank test

Table 3.17 Selected heart evaluation metrics for VMAT, PS, and IMPT plans. Abbreviations: $V_{22.5Gy\ (RBE)}$ = volume that receives at least 22.5 Gy (RBE); $V_{30Gy\ (RBE)}$ = volume that receives at least 30 Gy (RBE); NTCP = normal tissue complication probability.

Patient	$V_{22.5Gy\ (RBE)}$ [%]			$V_{30Gy\ (RBE)}$ [%]			Whole Heart NTCP [%]			Myocardium NTCP [%]		
	VMAT	PS	IMPT	VMAT	PS	IMPT	VMAT	PS	IMPT	VMAT	PS	IMPT
1	9.3	0.1	0.3	2.6	0.0	0.1	0.10	0.00	0.00	0.09	0.00	0.00
2	11.4	0.4	0.3	6.8	0.2	0.1	0.48	0.01	0.01	0.40	0.00	0.00
3	7.3	0.5	2.3	3.4	0.3	1.4	0.22	0.03	0.15	0.13	0.00	0.04
4	10.2	-	0.0	5.2	-	0.0	0.48	-	0.00	0.51	-	0.00
5	12.8	0.3	0.2	10.2	0.1	0.1	1.77	0.02	0.00	2.12	0.00	0.00
6	17.0	1.6	0.9	11.3	1.0	0.3	1.85	0.17	0.02	1.92	0.01	0.00
7	14.7	0.3	0.2	7.7	0.1	0.1	0.65	0.01	0.00	0.50	0.00	0.00
8	14.2	0.2	0.3	9.1	0.1	0.1	1.02	0.01	0.00	1.10	0.00	0.00
Mean	12.1	0.5	0.6	7.0	0.3	0.3	0.82	0.04	0.02	0.85	0.002	0.005
σ	3.2	0.5	0.8	3.1	0.3	0.5	0.67	0.06	0.05	0.79	0.005	0.014
p-value	PS*	IMPT*		PS*	IMPT*		PS*	IMPT*		PS*	IMPT*	
	<0.001	<0.001		0.001	0.001		0.017	0.014		0.019	0.020	

* Statistical significance detected using both Student's t-test and Wilcoxon signed-rank test

3.2.4 Contralateral Breast

Table 3.18 lists the evaluation metrics for the contralateral breast for each patient. A statistically significant difference was found in $\overline{D}_{mean}$ and $\overline{D}_{max}$ for both proton modalities when compared to VMAT ($p < 0.001$). $\overline{D}_{mean}$ for VMAT was 7.3±2.5 Gy, 0.2±0.1 Gy (RBE) for PS, and 0.3±0.2 Gy (RBE) for IMPT. VMAT had the highest $\overline{D}_{max}$ at 22.0±5.9 Gy. IMPT had the next highest $\overline{D}_{max}$ at 5.6±3.0 Gy (RBE), and PS had the lowest at 1.4±1.6 Gy (RBE). The volume of the contralateral (right) breast receiving 5 Gy (RBE) or more was statistically significantly lower using both proton techniques ($p \leq 0.001$). $\overline{V}_{5Gy(RBE)}$ for VMAT was 56.9±23.5% which was 57 times higher than that from PS and 28.4 times higher than that from IMPT. Patient averaged SCCP for VMAT was 3.89%±1.41% and was statistically significantly lower for PS (0.12±0.06%) and IMPT (0.20±0.09%) with $p < 0.001$.

Table 3.18 Selected contralateral breast evaluation metrics for VMAT, PS, and IMPT plans. Abbreviations: D_{mean} = mean dose; D_{max} = maximum dose; $V_{5Gy\ (RBE)}$ = volume that receives at least 5 Gy (RBE).

Patient	D_{mean} [Gy (RBE)]			D_{max} [Gy (RBE)]			$V_{5Gy\ (RBE)}$ [%]			SCCP [%]		
	VMAT	PS	IMPT	VMAT	PS	IMPT	VMAT	PS	IMPT	VMAT	PS	IMPT
1	8.7	0.0	0.2	22.8	0.0	4.1	73.0	0.0	1.6	4.63	0.03	0.14
2	5.8	0.3	0.3	19.7	2.9	5.9	45.6	1.6	2.3	3.01	0.17	0.20
3	10.3	0.1	0.6	30.8	0.3	10.9	71.7	0.8	3.3	5.70	0.09	0.37
4	9.8	-	0.5	27.7	-	8.3	75.3	-	3.1	5.36	-	0.29
5	4.1	0.1	0.1	11.1	0.2	1.7	28.1	0.5	0.6	2.06	0.06	0.08
6	3.8	0.3	0.4	20.1	2.7	6.2	18.7	1.5	2.4	1.97	0.17	0.20
7	7.8	0.1	0.3	23.8	0.2	4.9	61.0	0.7	2.0	4.15	0.09	0.19
8	8.0	0.3	0.2	20.1	3.7	2.9	81.7	1.7	1.2	4.19	0.19	0.13
Mean	7.3	0.2	0.3	22.0	1.4	5.6	56.9	1.0	2.1	3.89	0.12	0.20
σ	2.5	0.1	0.2	5.9	1.6	3.0	23.5	0.6	0.9	1.41	0.06	0.09
p-value	PS*	IMPT*		PS*	IMPT*		PS*	IMPT*		PS*	IMPT*	
	<0.001	<0.001		<0.001	<0.001		0.001	<0.001		<0.001	<0.001	
* Statistical significance detected using both Student's t-test and Wilcoxon signed-rank test												

3.2.5 Skin

Table 3.19 lists the mean, maximum, and minimum doses in the skin (5 mm shell) for each patient. $\overline{D}_{mean}$ was statistically significantly lower for PS (p = 0.021) and IMPT (p = 0.006) versus VMAT; with of 50.9±0.3 Gy, 50.6±0.1 Gy (RBE), and 50.5±0.03 Gy (RBE) for VMAT, PS, and IMPT, respectively. There was a 1.2 Gy (RBE) difference between VMAT and IMPT for $\overline{D}_{max}$ (p < 0.001) with IMPT having a statistically significantly lower $\overline{D}_{max}$ at 51.7±0.3 Gy (RBE). However, no statistically significant difference was detected between VMAT and PS for $\overline{D}_{max}$. IMPT had a statistically significantly higher $\overline{D}_{min}$ (p = 0.046) than that for VMAT with values of 49.0±0.5 Gy (RBE) and 47.5±1.8 Gy for IMPT and VMAT, respectively. Again, no statistically significant difference was detected between VMAT and PS for $\overline{D}_{min}$.

Table 3.19 Selected skin (5 mm shell) evaluation metrics for VMAT, PS, and IMPT plans. Abbreviations: D_{mean} = mean dose; D_{max} = maximum dose; D_{min} = minimum dose; PS p-value = VMAT vs. PS; IMPT p-value = VMAT vs. IMPT.

Patient	D_{mean} [Gy (RBE)]			D_{max} [Gy (RBE)]			D_{min} [Gy (RBE)]		
	VMAT	PS	IMPT	VMAT	PS	IMPT	VMAT	PS	IMPT
1	50.9	50.6	50.5	53.5	52.4	51.5	46.1	47.9	49.4
2	50.6	50.7	50.5	52.7	52.9	52.3	44.1	46.5	48.3
3	50.7	50.7	50.6	52.5	52.4	51.5	48.2	48.1	49.5
4	51.6	-	50.6	53.5	-	51.6	49.4	-	49.2
5	51.0	50.5	50.6	52.7	52.6	51.7	48.6	45.9	48.7
6	51.0	50.7	50.5	53.1	52.3	51.9	48.4	47.8	48.4
7	50.9	50.7	50.5	52.4	52.4	51.5	48.9	48.5	49.3
8	50.9	50.5	50.6	53.1	52.0	51.6	46.5	47.8	48.9
Mean	50.9	50.6	50.5	52.9	52.4	51.7	47.5	47.5	49.0
σ	0.3	0.1	0.03	0.4	0.3	0.3	1.8	0.9	0.5
p-value	PS**	IMPT*		PS	IMPT*		PS	IMPT*	
	0.021	0.006		0.086	<0.001		0.724	0.046	

* Statistical significance detected using both Student's t-test and Wilcoxon signed-rank test
** Statistical significance only found using Student's t-test

3.2.6 NTCP and SCCP Sensitivity Analysis

Figure 3.18 plots the patient averaged normal tissue complication probabilities ($\overline{NTCP}$) for various values of model parameters *s*, *γ,* and D_{50} for the whole heart and myocardium for each PMRT technique. $\overline{NTCP}$ for the whole heart ranged from 0.1% to 2.1% for VMAT when the seriality parameter (*s*) was varied between 0.46 and 1.54 (Johansson *et al.*, 2002) with γ = 1.28 and D_{50} = 52.3 Gy. $\overline{NTCP}$ values for the same set of parameter values (*s* = 0.46 to 1.54; γ = 1.28; and D_{50} = 52.3 Gy) were lower for both proton modalities than VMAT with a range of <0.01 to 0.26 and <0.01 to 0.15 for PS and IMPT, respectively. When the slope from the dose-response curve (γ) was varied between 0.8 and 2.00 (Johansson *et al.*, 2002) with *s* = 1.00 and D_{50} = 52.3 Gy (RBE), $\overline{NTCP}$ for the whole heart ranged from 3.1% to 0.25% for VMAT, 0.33% to 0.02% for PS, and 0.33% to 0.01% for IMPT. Similarly, $\overline{NTCP}$ ranged from 1.58% to 0.34% for VMAT, 0.07% to 0.02% for PS, and 0.05% to 0.01% for IMPT when D_{50} varied between 45.7 Gy (RBE) and 61.7 Gy (RBE) with *s* = 1.00 and γ = 1.28.

When these $\overline{NTCP}$ values were compared to the baseline $\overline{NTCP}$ values for each technique, we saw an increase in predicted risk for higher *s* values and lower values of *γ* and D_{50}, with the highest average predicted risk for γ = 0.8. It was also observed that no matter the model parameter value that we considered, the predicted risk of excess cardiac mortality at 15 years due to radiation therapy was consistently higher for VMAT compared to both proton modalities. Evidently, despite the model sensitivity to different parameter *s* values the qualitative findings from the baseline risk results (see section 3.2.3), i.e., that both proton modalities produced lower $\overline{NTCP}$ in the whole heart compared to VMAT was *insensitive* to the risk modeling methods considered here.

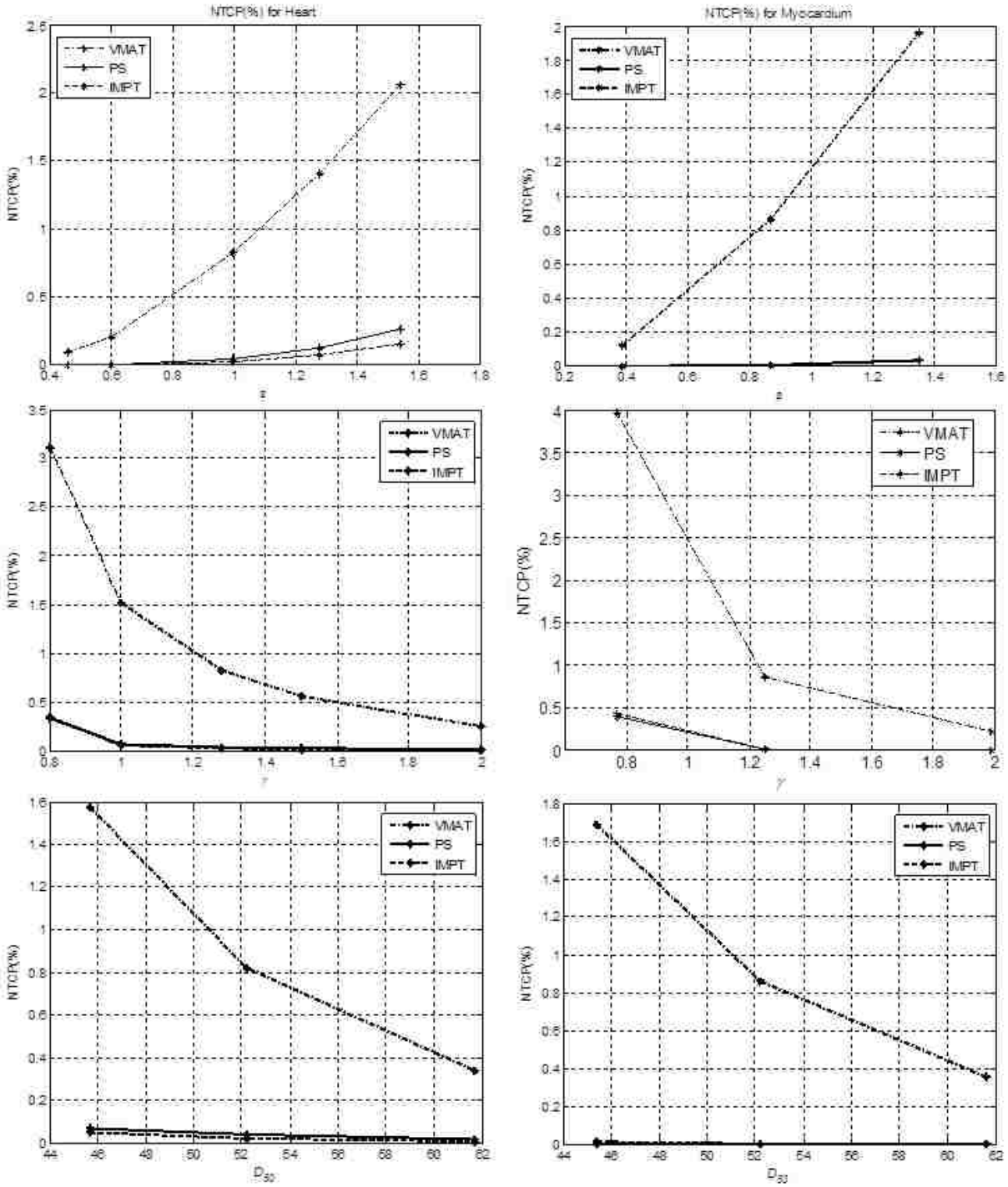

Figure 3.18 Patient averaged NTCP (%) for various values of model parameters s, γ, and D_{50} for the whole heart (left) and myocardium (right) following VMAT (dash-dotted line), PS (solid line), and IMPT (dashsed line). Whole Heart: s varied between 0.46 and 1.54 with γ=1.28, D_{50}=52.3 Gy (RBE). γ varied between 0.80 and 2.00 with s=1.00,D_{50}=52.3 Gy (RBE). D_{50} varied between 45.7 and 61.7 Gy (RBE) with *s*=1, γ=1.28. Myocardium: s varied between 0.39 and 1.35 with γ=1.25, D_{50}=52.2 Gy (RBE). γ varied between 0.77 and 1.99 with s=0.87,D_{50}=52.2 Gy (RBE). D_{50} varied between 45.4 and 61.6 Gy (RBE) with *s*=0.87, γ=1.25.

Similar results were observed for the predicted risk of cardiac mortality in the myocardium. $\overline{NTCP}$ for the myocardium ranged from 0.12% to 1.96% for VMAT when the seriality parameter was varied between 0.39 and 1.35 (Gagliardi *et al.*, 2001) with $\gamma = 1.25$ and $D_{50} = 52.2$ Gy. $\overline{NTCP}$ values for the same set of parameter values were considerably lower for both proton modalities than VMAT with a range of <0.01 to 0.03 for both PS and IMPT. When the slope of the dose-response curve (γ) was varied between 0.77 and 1.99 (Gagliardi *et al.*, 2001) with $s = 1.00$ and $D_{50} = 52.2$ Gy (RBE), $\overline{NTCP}$ for the myocardium ranged from 3.97% to 0.22% for VMAT, 0.40% to <0.01% for PS, and 0.43% to <0.01% for IMPT. Similarly, $\overline{NTCP}$ ranged from 1.68% to 0.35% for VMAT and <0.01% for both proton modalities when D_{50} varied between 45.4 Gy (RBE) and 61.6 Gy (RBE) with $s = 1.00$ and $\gamma = 1.25$ (Gagliardi *et al.*, 2001). Again the model predicted the hightest NTCP values for lower values of γ for all techniques compared to the baseline NTCP estimates, with $\overline{NTCP}$ being greatest for VMAT compared to the proton modalities. In fact, $\overline{NTCP}$ was consistently higher for VMAT than PS and IMPT for all of the model parameter (s, γ, and D_{50}) values. Again this was consistent with the earlier conclusion based off the baseline risk estimates (see section 3.2.3) that both proton modalities statisitcally significantly lowered the predicted risk of cardiac mortality (15 years) in the myocardiun compared to VMAT.

NTCP of radiation pneumonitis for the lungs using the Lyman-Kutcher-Burman (LKB) model (see section 2.8.2) was also calculated for several different model parameter values for each PMRT technique. Figure 3.19 plots the patient averaged NTCP values ($\overline{NTCP}$) for various values of model parameters n, m, and D_{50} for the lungs for each PMRT technique. $\overline{NTCP}$ values for VMAT ranged from 3.9% to 1.2% when the volume effect parameter (n) was varied between 0.6 and 2.8 (Seppenwoolde *et al.*, 2003) with $m = 0.37$ and $D_{50} = 30.8$ Gy. PS and IMPT $\overline{NTCP}$

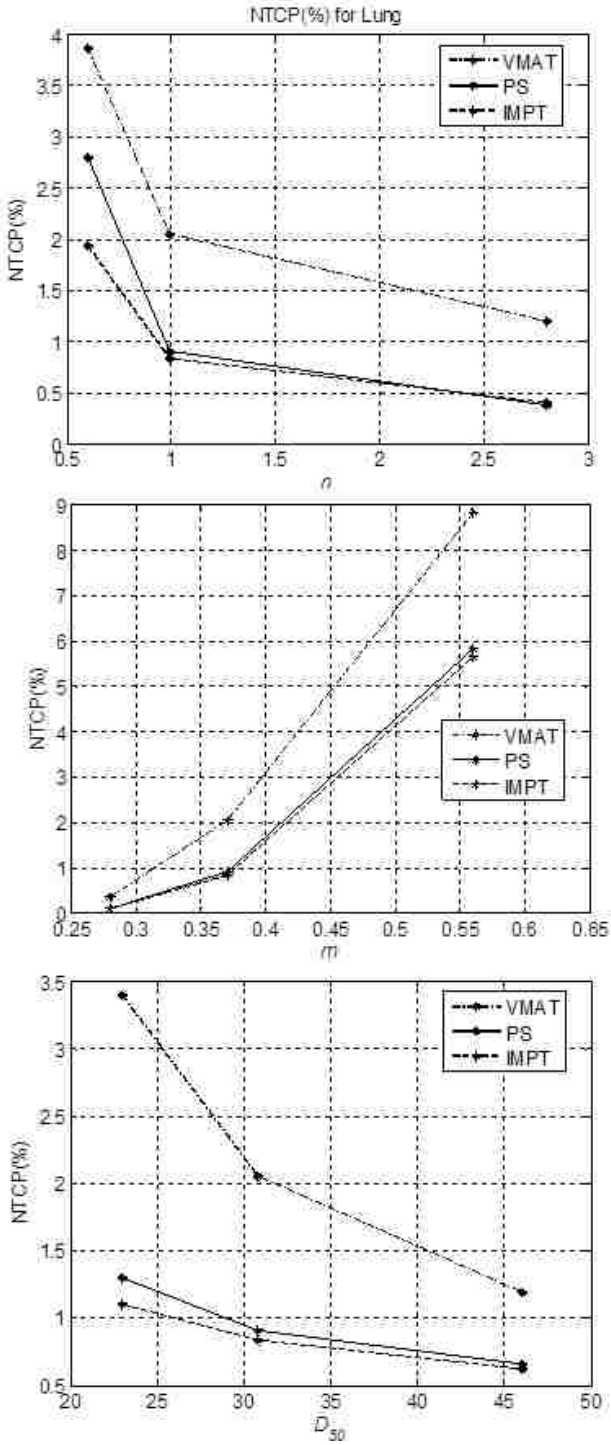

Figure 3.19 NTCP (%) for various values of model parameter *n*, *m*, and D_{50} for the lungs, following VMAT (dash-dotted line), PS (solid line), and IMPT (dashsed line). *n* varied between 0.6 and 2.8 with *m*=0.37, D_{50}= 30.8 Gy (RBE). *m* varied between 0.28 and 0.56 with *n*=0.99, D_{50}=30.8 Gy (RBE). D_{50} was varied between 23-46 Gy (RBE) with *n*=0.99 and *m*=0.37.

values were lower than VMAT for the same interval of *n* values, and ranged from 2.8% to 0.4% and 1.9% to 0.4%, respectively. Like the relative seriality model used for NTCP calculations in the heart, the LKB model was most sensitive to variations in the slope of dose-response curve (*m*) with the highest predicted risk occurring for larger slope values for all techniques. $\overline{NTCP}$ values for the lungs ranged from 0.4% to 8.8% for VMAT, 0.1% to 5.8 % for PS, and 0.1% to 5.6% for IMPT, when *m* was varied between 0.28 and 0.56 with *n* = 0.99 and D_{50} = 30.8 Gy (RBE). When D_{50} was taken as 23 Gy $\overline{NTCP}$ for VMAT was as high as 3.4% while both proton modalities were just above 1%. From these results, it was concluded that the LKB model was sensitive to parameter value selection for calculating the absolute risk for radiation pneumonitis (grade > 2) for each PMRT technique. However, $\overline{NTCP}$ values for VMAT were consistently higher than each proton modality for each variation in the model parameter values used. This result was consistent with the earlier claim stated in section 3.2.2 that said PS and IMPT lowered the predicted risk of radiation pneumonitis compared to VMAT based off baseline estimates. Baseline estimates were calculated using the following model parameter values: *n* = 0.99, *m* = 0.37 and D_{50} = 30.8 Gy and patient averaged NCCP for these values were plotted on Figure 3.19.

Figure 3.20 plots the patient averaged SCCPs (absolute cancer incidence per lifetime) and standard deviations calculated using the linear, linear-exponential, and linear-plateau models for VMAT, PS, and IMPT for the contralateral breast. $\overline{SCCP}$ using the linear (baseline) model was highest for VMAT at 3.9%±1.4% compared to <0.5% for both PS and IMPT. Similarly, $\overline{SCCP}$ values from the linear-exponential and linear-plateau models were highest for VMAT at 2.0%±0.5% and 2.4%±0.7%, respectively. Both proton techniques statistically significantly reduced ($p < 0.001$) $\overline{SCCP}$ compared to VMAT with a predicted risk of ≤0.1% calculated using both the linear-exponential and linear-plateau models. Since $\overline{SCCP}$ was statistically significantly

higher for VMAT compared to each proton modality ($p < 0.001$) for all three different OED models, it was concluded that the ability of PS and IMPT to statistically significantly reduce the predicted risk of absolute cancer incidence per lifetime for the contralateral breast compared to VMAT was not dependent on the selection of models considered in this work.

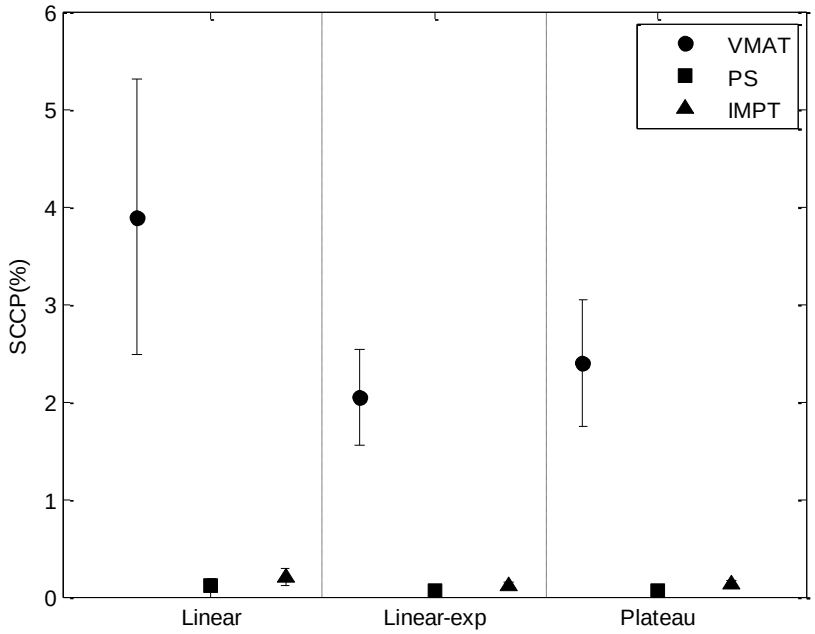

Figure 3.20 Patient averaged SCCP (±1σ) values for the contralateral breast following PMRT using VMAT, PS, and IMPT techniques calculated using linear, linear-exponential, and linear-plateau dose-response models.

Figure 3.21 plots the patient averaged SCCPs (absolute cancer incidence per lifetime) and standard deviations calculated using the linear, linear-exponential, and linear-plateau models for VMAT, PS, and IMPT for the lungs. VMAT had the largest $\overline{SCCP}$ at 12.5%±0.88% when the linear dose model was used. 4.1% and 5.3% $\overline{SCCP}$ values were found when the linear-exponential and linear-plateau models were used to calculate SCCP for the VMAT plans. The PS proton technique had $\overline{SCCP}$ values of 5.9%, 0.7%, and 1.4% when the linear, linear-exponential, and linear-plateau models were used, respectively, and were statistically significantly lower than VMAT ($p < 0.001$) for each model. $\overline{SCCP}$ values for IMPT using the linear, linear-exponential

and linear-plateau models were 5.6%, 1.3%, and 1.9%, respectively, and were also statistically significantly lower than values predicted for VMAT ($p < 0.001$) for each model. Since $\overline{SCCP}$ was statistically significantly higher for VMAT compared to each proton modality ($p < 0.001$) for all three different OED models, it was concluded that the ability of PS and IMPT to statistically significantly reduce the predicted risk of absolute cancer incidence per lifetime for the lungs compared to VMAT was not model dependent.

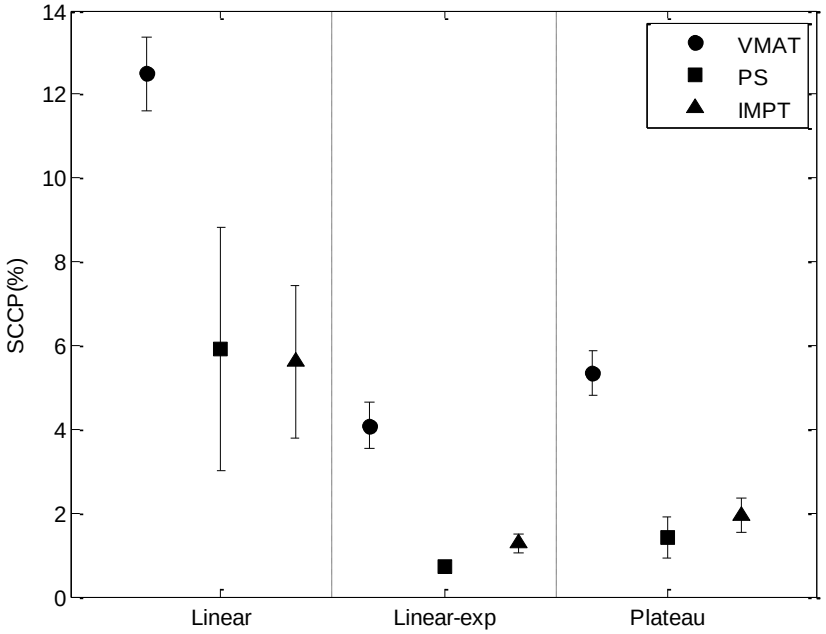

Figure 3.21 Patient averaged SCCP (±1σ) values for the lungs following PMRT using VMAT, PS, and IMPT techniques calculated using linear, linear-exponential, and linear-plateau dose-response models.

Table 3.20 lists the mean, standard deviation, and *p*-value of RNTCP for the lung, heart, and myocardium along with RSCCP for the lung and contralateral breast. RNTCP and RSCCP were calculated for both proton techniques separately. A value of 1.0 indicated no change in risk from photon PMRT to proton PMRT, a value above 1.0 indicated an increase in risk from the proton modalities, and a value less than 1.0 indicated a decrease in predicted risk from the proton modalities. The patient averaged ratios for all organs, were statistically significantly lower than

1.0 for both proton modalities, signifying an advantage for both proton PMRT techniques to lower predicted risks to the lungs, heart, and contralateral breast. These findings are consistent with the earlier absolute risk observations noted in sections 3.2.2 through 0.

Table 3.20 Average predicted RNTCP and RSCCP for cardiopulmonary structures and the contralateral breast based on baseline model parameters. Blanks in RNTCP column indicate organs that did not use an NTCP model. Blanks in RSCCP column indicate organs that did not use an SCCP model. $P < 0.05$ was statistically significant.

		Ratio of PS and VMAT		Ratio of IMPT and VMAT	
Structure		RNTCP	RSCCP	RNTCP	RSCCP
Lung	Mean	0.43	0.46	0.40	0.45
	σ	0.15	0.20	0.09	0.13
	p-value	<0.001	<0.001	<0.001	<0.001
Heart	Mean	0.04	-	0.09	-
	σ	0.05	-	0.24	-
	p-value	<0.001	-	<0.001	-
Myocardium	Mean	2.34E-03	-	0.04	-
	σ	3.55E-03	-	0.11	-
	p-value	<0.001	-	<0.001	-
Contralateral Breast	Mean	-	0.04	-	0.05
	σ	-	0.03	-	0.02
	p-value	-	<0.001	-	<0.001

Chapter 4 Discussion

This study compared passively scattered proton therapy (PS) and intensity modulated proton therapy (IMPT) to volumetric modulated arc therapy (VMAT) for a clinically representative sample of 8 left-sided breast cancer patients treated with post-mastectomy radiotherapy. The goals of this study were to reduce the dose to the surrounding normal tissues while maintaining equal or better PTV dose coverage for both re-planning proton techniques; calculate the corresponding predicted risk of radiogenic second cancers and normal tissue complications; estimate the uncertainties in the predicted dosimetric and radiobiological metrics, and to test for statistically significant predicted differences between the photon and proton modalities. The hypothesis of the study was that for a clinically representative cohort of post-mastectomy patients, passively scattered and intensity modulated proton therapy could improve predicted normal tissue sparing while maintaining equal or better target coverage than volumetric modulated arc therapy photon plans, ultimately resulting in statistically significantly lower ($p < 0.05$) predicted risks of several late effects for the heart, lungs, and contralateral breast. The baseline results of this study support the hypothesis for both passively scattered and intensity modulated proton therapy. Specifically, PS and IMPT significantly lowered average predicted risks for the sample. A sensitivity analysis of patient setup error reinforced the qualitative baseline findings of this study for up to a 0.5 cm isocenter shift, and a sensitivity analysis of proton range uncertainty confirmed the baseline qualitative findings to be robust up to a ±10% HU to proton linear relative stopping power conversion error. A sensitivity analysis of lung NTCP and heart NTCP model parameter selection found that the average NTCP values for PS and IMPT were consistently lower than that of VMAT for different risk model parameter values. A sensitivity analysis of contralateral breast SCCP and lung SCCP modeling methods considered

also found that the average SCCP values for PS and IMPT were consistently statistically significantly lower than that of VMAT for different OED models. Both sensitivity analyses' results were consistent with the baseline NTCP and SCCP findings.

The major outcomes of this work are summarized in sections 4.1 through 4.3, followed by the significance, strengths, weaknesses, and possible future research directions.

4.1 Outcomes of Specific Aim One

Aim one determined if certain PTV and OAR dose-volume metrics were statistically significantly different between VMAT and both proton modalities for the sample. To accomplish this, PS and IMPT treatment plans were created for PMRT. Out of the eight patients selected for this work, seven were planned with PS and eight were planned with IMPT. All proton plans met the dosimetric planning goals when normalized to the mean evaluation PTV dose, and all were approved by the same radiation oncologist who approved the original VMAT plan. VMAT plans met most dosimetric planning goals. Five of the eight patients treated with VMAT did not meet the goal of $D_{95\%} \geq 47.8$ Gy. However, these objectives were meant to be conservative, and a radiation oncologist deemed each of the VMAT plans clinically acceptable and the patients were thus treated.

Both proton plans showed statistically significantly better PTV conformity and dose homogeneity ($p < 0.05$) compared to VMAT. As expected and by design, no statistically significant difference was observed for tumor control probability, since all treatment techniques had nearly 100% TCP. Both proton modalities were able to statistically significantly reduce the volume of the heart, lungs, and contralateral breast receiving dose. These results strongly suggest that either PS or IMPT for the treatment of subclinical disease after a mastectomy would be advantageous for patients requiring OAR doses below those delivered with VMAT. Such

patients would include those with prior/current cardiopulmonary complications or unfavorable anatomy since they are already at an increased risk of cardiovascular diseases (Weber *et al.*, 2006).

Because skin is an oncologic target of treatment for post-mastectomy patients, erythema is expected with any radiotherapy technique. The doses reported to the skin (5 mm shell) were similar between PS, IMPT, and VMAT with doses just above the prescription dose. However, the skin received a statistically significantly higher maximum dose when treated with VMAT than IMPT, with no observed statistically significant difference between VMAT and PS. The mean dose to the skin was also closer to the desired prescribed dose of 50.4 Gy (RBE) for both proton modalities. A recent study (Macdonald *et al.*, 2013b) assessed acute skin toxicity for 12 post-mastectomy patients treated with two matched passively scattered proton fields. Skin reactions were mostly superficial and often with moderate to severe erythema and moderate to large areas of dry superficial desquamation. After 4 to 8 weeks cosmesis was favorable and patients only had mild erythema.

The dosimetric results agreed well with previous photon and proton treatment planning comparisons for breast cancer patients. In a study by Ares *et al.* (2010), IMPT improved target coverage and reduction of low doses to OARs for complex-target whole breast irradiation for breast cancer patients when compared to static field IMRT and three-dimensional conformal radiotherapy (3D-CRT). In another study, passively scattered proton therapy decreased dose to surrounding normal structures without compromising target coverage for a cohort of post-mastectomy patients (Macdonald *et al.*, 2013a; Macdonald *et al.*, 2013b).

4.2 Outcomes of Specific Aim Two

Specific aim two predicted and compared the absolute risk of radiation pneumonitis Grade 2 or greater at 6 months, excess cardiac mortality at 15 years, and radiogenic second cancer incidence per lifetime for patients planned with VMAT, PS, and IMPT and compared the corresponding risks. NTCP models are important tools for estimating complication risks. In some clinical sites, however, the complication events used to deduce the dose-response curves are infrequent, which has limited confidence to use NTCP estimates for clinical decision making. Until additional clinical data are available to validate the predictive models, NTCP estimates are best used for relative comparison between techniques rather than for absolute risk assessment (Pierce *et al.*, 2002). That being said, predicted risks investigated within this study were statistically significantly reduced for both proton modalities when compared to VMAT. The predicted risks between the two proton techniques were not statistically different from one another.

The average NTCP for the lung with radiation pneumonitis (RP) Grade 2 or higher was 2.05%±0.23%, 0.91%±0.39%, and 0.83%±0.22% for VMAT, PS, and IMPT, respectively. These values fall within previously reported clinical incidence of 1 to 5% following breast cancer radiotherapy (Marks *et al.*, 2010). Both proton therapy modalities significantly reduced the risk of RP, which was supported by a similar study by Johansson *et al.* (2002) which compared passively-scattered proton beams, static field IMRT (6-beams), mixed electron-photon, and photon tangential techniques for node-positive left-sided breast cancer patients after breast-conserving surgery. They found a mean NTCP value of 0.6±0.8% using the relative seriality model following proton therapy which was significantly lower than all other techniques compared in the study. In a PMRT comparative planning study, Nichols *et al.* (2014) compared

helical tomotherapy and VMAT for the risk of RP computed using the Lyman-Kutcher-Berman model using the following values: D_{50}=24.5 Gy, n=0.87, and m=0.18. No significant difference between the two modalities was found, with an average NTCP value of 0.3%±0.1% for VMAT plans and 0.6%±0.1% for HT plans. These values do not agree with the 2.05%±0.23% risk estimated for VMAT within this study even though $\bar{D}_{mean}$ to the lungs was similar between the two studies. Disagreement in average NTCP values may be attributed to the variation in model parameter values used. The parameter values used in this study are from a more recent publication (Seppenwoolde *et al.*, 2003) than the one used in the study by Nichols *et al.* (2014).

The average baseline SCCP values for the lungs were 12.5%±0.9% in VMAT, 5.9%±2.9% in PS and 5.61%±1.81% in IMPT. Average SCCP values using the linear-exponential model in a PMRT study by Nichols *et al.* (2014) predicted a value of 5.3%±0.1% for VMAT. We had a similar result at 4.1%±0.6% for VMAT using the linear-exponential model as well. SCCP results represent lifetime risk, with a mean residual lifetime of 50 years. Smoking at the time of radiation or earlier increased the 15-year risk of developing a lung cancer after breast conserving surgery and radiation by 6% and 4.7%, respectively compared to 0.26% for non-smokers (Obedian *et al.*, 2000). Beside the inherent increased risk in cancer survivors due e.g. lifestyle, both chemotherapy and radiotherapy are known to further increase the risk of second solid cancers (Abo-Madyan *et al.*, 2014). The proportion of risk attributed to radiotherapy alone has been variably reported and to date there are no clinical analyses reporting second cancer induction after VMAT or proton PMRT due to the limited time span of its clinical availability.

Average NTCP values for the whole heart were 0.82%±0.67%, 0.04%±0.06%, and 0.02%±0.05% for VMAT, PS, and IMPT, respectively. In a previous study, Johansson *et al.* (2002) estimated the risk of cardiac mortality following a left-sided breast cancer radiotherapy

treatment using passively scattered proton therapy for 11 patients. They reported a value of 0.5%±0.5% calculated using the relative-seriality model for a single LAO proton field. The PS results from our study agreed well with their findings. Our average NTCP values for the myocardium were highest for VMAT with 0.85%±0.79% and nearly 0% for both proton modalities. Several previous studies have found protons to be advantageous for the reduction of heart irradiation and late toxicity for breast cancer radiotherapy (Weber *et al.*, 2006; Ares *et al.*, 2010). The predicted decrease in cardiac mortality when using protons for post-mastectomy radiotherapy will not be observed until after a long follow-up (15 years) (Pierce *et al.*, 2002). Studies that report an increased risk of non-breast cancer deaths from myocardial infarction and ischemic heart disease after irradiation did not see these effects until 10 or more years after exposure (Rutqvist *et al.*, 2003; Darby *et al.*, 2013).

No excess breast cancer risk has been found among women irradiated at age 40 years or older. Boice *et al.* (1992) showed radiation exposure after the age of 45 years entails little, if any risk (relative risk, 1.01) of radiation-induced breast cancer for a female population of an average age of 51.7 years exposed with mean radiation dose of 2.51 Gy to the contralateral breast. Therefore, the risk of contralateral breast cancer after radiotherapy for breast cancer appears to be limited to women who are younger than age 40 to 45 years (premenopausal) at exposure, and highest for PMRT patients (Travis *et al.*, 2011). In the current study, the average age for the eight patients was 54. Both proton modalities were able to significantly reduce the mean dose to the contralateral breast and SCCP compared to VMAT. The patient averaged SCCP using the linear dose-risk model for VMAT was 3.89%±1.41%, 0.12%±0.06% for PS, and 0.20%±0.09% for IMPT. It was expected for both proton modalities to produce statistically significantly lower mean SCCP values because both proton techniques also produced statistically significantly lower

$\overline{D}_{mean}$ values. Nichols *et al*., (2014) reported an average SCCP value of 1.0% for VMAT using the linear-exponential dose-response model. This value was similar but lower than our result of 2% using the same model. SCCP results for the contralateral breast represent lifetime risk, with a mean residual lifetime of 50 years. Therefore, the results of our study are especially important for younger patients, whose longer residual lifetime puts them at great risk for radiogenic second malignancies.

4.3 Outcomes of Specific Aim Three

The goal of aim three was to determine the impact of patient setup errors, proton range errors, and risk model choice had on DVH and predicted risk values. In general, patient setup errors tend to cause geometric misalignment of the treatment field, resulting in inadequate target coverage. An isocenter shift of 1 cm in any direction for VMAT and IMPT for the representative patient (CW-3) caused a large degradation in PTV dose coverage. PS was less susceptible to set-up errors and this was largely in part to compensator smearing. It should be noted that in current treatment practice, a patient set-up error of 1 cm is an extreme case but still within a plausible misalignment range. For example, the commonly used vacuum bags in lung cancer treatments can introduce over 1 cm variations in the thickness of soft tissue around the chest wall: and breast position in female patients can introduce additional thickness variations. It is therefore common that no such vacuum bag immobilization devices are used for treatment of tumors in the thorax region using proton therapy and beams that enter female patients through breasts are minimally used (Li, 2012). However, some set-up errors are random and can be averaged out by repainting dose (IMPT) and fractionating treatments over the course of treatment (Wang *et al.*, 2013). The impact of patient-setup errors on NTCP were small (<1%) for the heart and lungs for

all plans. SCCP for the lungs was impacted the most, but didn't deviate more than 4% from the nominal risk predication for either modality.

The uncertainty margins used for proton planning incorporated both set-up errors and errors in CT number to proton linear relative stopping power. The latter error was investigated separately from the patient set-up errors by simulating a 3.5% and 10% error in relative linear proton stopping power conversion. This simulation for a single patient indicated PS and IMPT plans are robust for up to a 10% error. The evaluation PTV maintained adequate dose coverage and predicted risk of late effects had small changes <1.2% from the nominal dose distribution for both PS and IMPT.

Upon a sensitivity analysis for NTCP parameter values for the Lyman-Kutcher-Burman model (radiation pneumonitis) and the relative seriality model (cardiac mortality); we quantified how the absolute risk for each organ (lungs and heart) was dependent on model parameter selection. We found that the models were most sensitive to variations in the slope of the dose-response curve for each technique. The average NTCP values for PS and IMPT were consistently lower than that of VMAT for different risk model parameter values. This same result was observed for SCCP when different dose-risk models were investigated for the contralateral breast and the lungs. The differences obtained in this study between the linear, linear-exponential, and linear-plateau dose-risk models for SCCP were most pronounced for VMAT plans. This was due to the fact that the linear model deviates from the other two models for doses larger than about 5 Gy (RBE) (Abo-Madyan *et al.*, 2014). Dose to the contralateral breast and lungs was considerably higher in the VMAT plans and thus the deviations between the linear model and non-linear models were the greatest for VMAT.

Two different case-control studies of female breast cancer following treatment for Hodgkin lymphoma before age 30 years (Travis *et al.*, 2003) and in childhood cancer survivors (Inskip *et al.*, 2009), found the risk of breast cancer increased with increasing radiation dose to the breast, reaching an odds ratio of 8 or more at doses of 40 Gy or more with no evidence of a downturn in the risk of breast cancer at the highest doses. These studies support the use of the linear OED model for the calculation of SCCP for the contralateral breast. However, there are also studies that show a reduced risk of breast cancer with increasing dose or linear-exponential dose-response model. This effect is due to treatment-related premature menopause for a radiation dose to the ovary exceeding 5 Gy (RBE) (Travis *et al.*, 2011). Therefore, the absolute risks of contralateral second cancer predicted using the linear and linear-exponential models within this study are both relevant and when used together provide a more robust conclusion about which technique would be appropriate for patients.

4.4 Implications and Significance of the Results

In treating post-mastectomy disease, the planning complexity is increased by many factors, such as the high dose prescribed to the tumor and the simultaneous irradiation of regional lymph nodes. The large and complex shaped PTV entail the involvement of many OARs whose dose tolerances are limiting factors for post-mastectomy radiotherapy. Thanks to its innovative delivery characteristic, VMAT plans provide a very conformal dose distribution tailored to the planning target volume, minimizing the dose to selected OARs, but unfortunately spreading out the dose over a large volume of non-target tissues. Because of their finite and energy-dependent range protons improved the dose distributions outside of the PTV, reducing acute and late toxicities to the heart, lungs, and contralateral breast.

Cardiac toxicity has been implicated as the primary reason for excess non-breast cancer mortality in early breast cancer studies (Senkus-Konefka and Jassem, 2007). Studies of PMRT utilizing more modern techniques and fractionation schedules have demonstrated survival benefits and no increase in cardiac mortality (Nixon *et al.*, 1998; Hojris *et al.*, 1999; Correa *et al.*, 2007). However, the increasing use of cardiotoxic chemotherapy agents such as Doxorubicin and Trastuzumab, adds another confounding factor to determining the effect of radiation therapy on cardiac outcomes (Macdonald *et al.*, 2013a). Dose to the heart should therefore be minimized as much as possible. In this study, passively scattered and intensity modulated proton therapy techniques for post-mastectomy patients were able to significantly reduce dose to the heart and subsequently the predicted risk of cardiac mortality in both the whole heart and myocardium structures.

Other normal tissue complications that arise from breast cancer radiotherapy are radiation pneumonitis and radiogenic second cancers. While lung toxicity is less serious than cardiac mortality, it may be troublesome and disabling. Irradiation to the lungs to doses higher than 30 Gy (RBE) may also result in fibrosis and reduced lung capacity (Johansson *et al.*, 2002). The risk of a radiation-induced malignancy is relatively small, but considering the large number of patients treated and the gravity of a second malignancy, it should not be ignored. We showed a potentially significant decrease in the predicted risk of lung toxicity and second cancers with the use of either passively scattered and intensity modulated proton therapy for PMRT.

4.5 Strengths and Limitations

Our study has several strengths. First, we used realistic patient data and treatment plans system and detailed risk calculations. Second, we investigated passively scattered and intensity modulated proton therapies. Third, we calculated both normal tissue complications and

radiogenic second cancers based on recent dose-response models. Gagliardi *et al*. (2010) suggested that clinical outcomes of certain organs are better correlated when NTCP parameters are derived from the DVH of the same organ. Therefore, the inclusion of the myocardium contouring and DVH provided a more robust estimation of the potential clinical outcomes for the heart following VMAT, PS, or IMPT since the whole heart and myocardium risk estimates were similar. Finally, the sensitivity analysis increased confidence in the qualitative findings of this study.

Our study also has several limitations. Only eight patients were used for this work and, although that provided satisfactory statistical power, more patient data would provide more statistical robustness. Our predicted risks were calculated using only the therapeutic doses. Including the stray dose may have changed the predicted outcomes. Another limitation is the inability of the treatment planning systems to accurately report doses out-of-field. Finally, this study did not investigate the effects of respiratory and cardiac motion on the nominal dose distribution. Ares *et al.* (2010) looked at this issue and concluded that the effects were small for en face proton beams because the beam is parallel to the organ motion.

4.6 Future Work

The inclusion of right-sided PMRT patients and/or patients who underwent an immediate breast reconstruction before PMRT is a potential next step for this work. Our methodology could be applied after modifications take into account proton range errors within metallic tissue expanders that are common for reconstructed patients. A treatment planning comparison based on a boarder spectrum of post-mastectomy patients will be helpful to generalize the results of this study to the whole population of post-mastectomy patients. Also, since VMAT is delivered in an arc, a treatment planning comparison between proton arc therapy and VMAT would be

interesting. In a treatment planning comparison study of proton arc therapy and VMAT for three prostate cancer patients, Rechner *et al.* (2012) found the predicted risk of second cancers following proton arc therapy was less than or approximately equal to the risk following VMAT. Another proton arc study demonstrated a potential role for proton arc therapy as an alternative to electron arc therapy when lung dose must be minimized (Sandison *et al.*, 1997).

Given that mastectomy with adjuvant radiotherapy is not the standard of care for early stage breast cancer according to the National Comprehensive Cancer Network (NCCN, 2014), it may be worthwhile comparing VMAT and proton therapy for these patients treated with breast irradiation following conservation surgery. Several comparative planning studies hypothesize that protons will provide a decrease in acute and late cardiopulmonary toxicities for patients requiring radiotherapy for advanced or left-sided breast cancer compared to conventional and IMRT photon techniques (Johansson *et al.*, 2002; Lomax *et al.*, 2003; Weber *et al.*, 2006; Ares *et al.*, 2010), yet no current study exists between VMAT and proton therapies for these patients.

Chapter 5 Conclusion

The rationale for the use of protons to treat post-mastectomy radiotherapy patients is to decrease late cardiopulmonary toxicity without compromising the desired target coverage. The current study provides new evidence that the use passively scattered and intensity modulated proton therapy can significantly improve predicted normal tissue sparing while maintaining equal or better target coverage compared to volumetric modulated arc therapy for the treatment of left-sided post-mastectomy radiotherapy (PMRT). Thus, proton radiotherapy for PMRT can significantly reduce the calculated risk of radiation pneumonitis, cardiac mortality, and radiogenic second cancers of the heart and lungs compared to VMAT photon PMRT regardless of model and model parameters considered.

References

Abo-Madyan Y, Aziz M H, Aly M M, Schneider F, Sperk E, Clausen S, Giordano F A, Herskind C, Steil V, Wenz F and Glatting G 2014 Second cancer risk after 3D-CRT, IMRT and VMAT for breast cancer *Radiother Oncol*

Andratschke N, Maurer J, Molls M and Trott K R 2011 Late radiation-induced heart disease after radiotherapy. Clinical importance, radiobiological mechanisms and strategies of prevention *Radiother Oncol* **100** 160-6

Ares C, Khan S, Macartain A M, Heuberger J, Goitein G, Gruber G, Lutters G, Hug E B, Bodis S and Lomax A J 2010 Postoperative proton radiotherapy for localized and locoregional breast cancer: potential for clinically relevant improvements? *Int J Radiat Oncol Biol Phys* **76** 685-97

Ashenafi M, Boyd R A, Lee T K, Lo K K, Gibbons J P, Rosen, II, Fontenot J D and Hogstrom K R 2010 Feasibility of postmastectomy treatment with helical TomoTherapy *Int J Radiat Oncol Biol Phys* **77** 836-42

Boice J D, Jr., Harvey E B, Blettner M, Stovall M and Flannery J T 1992 Cancer in the contralateral breast after radiotherapy for breast cancer *N Engl J Med* **326** 781-5

Brenner D J 1993 Dose, volume, and tumor-control predictions in radiotherapy *Int J Radiat Oncol Biol Phys* **26** 171-9

Correa C R, Litt H I, Hwang W T, Ferrari V A, Solin L J and Harris E E 2007 Coronary artery findings after left-sided compared with right-sided radiation treatment for early-stage breast cancer *J Clin Oncol* **25** 3031-7

Darby S C, Ewertz M, McGale P, Bennet A M, Blom-Goldman U, Bronnum D, Correa C, Cutter D, Gagliardi G, Gigante B, Jensen M B, Nisbet A, Peto R, Rahimi K, Taylor C and Hall P 2013 Risk of ischemic heart disease in women after radiotherapy for breast cancer *N Engl J Med* **368** 987-98

Dillon D, Guidi A and Schnitt S 2010 *Disease of the Breast,* ed J Jonathan W. Pine (Philadelphia, PA: Lippincott Williams & Wilkins)

Eifel P, Axelson J A, Costa J, Crowley J, Curran W J, Jr., Deshler A, Fulton S, Hendricks C B, Kemeny M, Kornblith A B, Louis T A, Markman M, Mayer R and Roter D 2001 National Institutes of Health Consensus Development Conference Statement: adjuvant therapy for breast cancer, November 1-3, 2000 *J Natl Cancer Inst* **93** 979-89

Feuvret L, Noel G, Mazeron J J and Bey P 2006 Conformity index: a review *Int J Radiat Oncol Biol Phys* **64** 333-42

Gagliardi G, Lax I, Ottolenghi A and Rutqvist L E 1996 Long-term cardiac mortality after radiotherapy of breast cancer--application of the relative seriality model *Br J Radiol* **69** 839-46

Gagliardi G, Lax I and Rutqvist L E 2001 Partial irradiation of the heart *Semin Radiat Oncol* **11** 224-33

Gagliardi G, Lax I, Soderstrom S, Gyenes G and Rutqvist L E 1998 Prediction of excess risk of long-term cardiac mortality after radiotherapy of stage I breast cancer *Radiother Oncol* **46** 63-71

Gao X, Fisher S G and Emami B 2003 Risk of second primary cancer in the contralateral breast in women treated for early-stage breast cancer: a population-based study *Int J Radiat Oncol Biol Phys* **56** 1038-45

Giebeler A, Newhauser W D, Amos R A, Mahajan A, Homann K and Howell R M 2013 Standardized treatment planning methodology for passively scattered proton craniospinal irradiation *Radiat Oncol* **8** 32

Graham M V, Purdy J A, Emami B, Harms W, Bosch W, Lockett M A and Perez C A 1999 Clinical dose-volume histogram analysis for pneumonitis after 3D treatment for non-small cell lung cancer (NSCLC) *Int J Radiat Oncol Biol Phys* **45** 323-9

Hall E J 2006 Intensity-modulated radiation therapy, protons, and the risk of second cancers *Int J Radiat Oncol Biol Phys* **65** 1-7

Hojris I, Overgaard M, Christensen J J and Overgaard J 1999 Morbidity and mortality of ischaemic heart disease in high-risk breast-cancer patients after adjuvant postmastectomy systemic treatment with or without radiotherapy: analysis of DBCG 82b and 82c randomised trials. Radiotherapy Committee of the Danish Breast Cancer Cooperative Group *Lancet* **354** 1425-30

ICRU 2007 International Comission on Radiation Units and Measurements Report 78: Prescribing, recording, and reporting proton-beam therapy *ICRU* **7** 1-210

Inskip P D, Robison L L, Stovall M, Smith S A, Hammond S, Mertens A C, Whitton J A, Diller L, Kenney L, Donaldson S S, Meadows A T and Neglia J P 2009 Radiation dose and breast cancer risk in the childhood cancer survivor study *J Clin Oncol* **27** 3901-7

Jimenez R B, Goma C, Nyamwanda J, Kooy H M, Halabi T, Napolitano B N, McBride S M, Taghian A G, Lu H M and MacDonald S M 2013 Intensity modulated proton therapy for postmastectomy radiation of bilateral implant reconstructed breasts: a treatment planning study *Radiother Oncol* **107** 213-7

Johansson J, Isacsson U, Lindman H, Montelius A and Glimelius B 2002 Node-positive left-sided breast cancer patients after breast-conserving surgery: potential outcomes of radiotherapy modalities and techniques *Radiother Oncol* **65** 89-98

Kallman P, Agren A and Brahme A 1992 Tumour and normal tissue responses to fractionated non-uniform dose delivery *Int J Radiat Biol* **62** 249-62

Kutcher G J and Burman C 1989 Calculation of complication probability factors for non-uniform normal tissue irradiation: the effective volume method *Int J Radiat Oncol Biol Phys* **16** 1623-30

Li A X, Alber M, Deasy J, Jackson A and Kyung-Wook K J 2012 The use and QA of biologically related models for treatment planning: Report of AAPM Task Group 166 *Med Phys* **39**

Li Z 2012 Toward robust proton therapy planning and delivery *Translational Cancer Research*

Lomax A J, Boehringer T, Coray A, Egger E, Goitein G, Grossmann M, Juelke P, Lin S, Pedroni E, Rohrer B, Roser W, Rossi B, Siegenthaler B, Stadelmann O, Stauble H, Vetter C and Wisser L 2001 Intensity modulated proton therapy: A clinical example *Med Phys* **28** 317

Lomax A J, Cella L, Weber D, Kurtz J M and Miralbell R 2003 Potential role of intensity-modulated photons and protons in the treatment of the breast and regional nodes *Int J Radiat Oncol Biol Phys* **55** 785-92

Lyman J T 1985 Complication probability as assessed from dose-volume histograms *Radiat Res Suppl* **8** S13-9

Macdonald S M, Jimenez R, Paetzold P, Adams J, Beatty J, Delaney T F, Kooy H, Taghian A G and Lu H M 2013a Proton radiotherapy for chest wall and regional lymphatic radiation; dose comparisons and treatment delivery *Radiat Oncol* **8** 71

Macdonald S M, Patel S A, Hickey S, Specht M, Isakoff S J, Gadd M, Smith B L, Yeap B Y, Adams J, Delaney T F, Kooy H, Lu H M and Taghian A G 2013b Proton therapy for breast cancer after mastectomy: early outcomes of a prospective clinical trial *Int J Radiat Oncol Biol Phys* **86** 484-90

Marks L B, Bentzen S M, Deasy J O, Kong F M, Bradley J D, Vogelius I S, El Naqa I, Hubbs J L, Lebesque J V, Timmerman R D, Martel M K and Jackson A 2010 Radiation dose-volume effects in the lung *Int J Radiat Oncol Biol Phys* **76** S70-6

Mohan R, Gillin M T, Woo S Y and Lee A K 2010 *Leibel and Phillips Textbook of Radiaiton Oncology*: Elsevier Inc. pp 1493-510

Mohan R, Mageras G S, Baldwin B, Brewster L J, Kutcher G J, Leibel S, Burman C M, Ling C C and Fuks Z 1992 Clinically relevant optimization of 3-D conformal treatments *Med Phys* **19** 933-44

Moyers M F and Miller D W 2003 Range, range modulation, and field radius requirements for proton therapy of prostate cancer *Technol Cancer Res Treat* **2** 445-7

Moyers M F, Miller D W, Bush D A and Slater J D 2001 Methodologies and tools for proton beam design for lung tumors *Int J Radiat Oncol Biol Phys* **49** 1429-38

National Comprehensive Cancer Network 2014 Breast Cancer (Version 3.2014).

Nichols G P, Fontenot J D, Gibbons J P and Sanders M E 2014 Evaluation of volumetric modulated arc therapy for postmastectomy treatment *Radiat Oncol* **9** 66

Nixon A J, Manola J, Gelman R, Bornstein B, Abner A, Hetelekidis S, Recht A and Harris J R 1998 No long-term increase in cardiac-related mortality after breast-conserving surgery and radiation therapy using modern techniques *J Clin Oncol* **16** 1374-9

Obedian E, Fischer D B and Haffty B G 2000 Second malignancies after treatment of early-stage breast cancer: lumpectomy and radiation therapy versus mastectomy *J Clin Oncol* **18** 2406-12

Overgaard M, Hansen P S, Overgaard J, Rose C, Andersson M, Bach F, Kjaer M, Gadeberg C C, Mouridsen H T, Jensen M B and Zedeler K 1997 Postoperative radiotherapy in high-risk premenopausal women with breast cancer who receive adjuvant chemotherapy. Danish Breast Cancer Cooperative Group 82b Trial *N Engl J Med* **337** 949-55

Overgaard M, Jensen M B, Overgaard J, Hansen P S, Rose C, Andersson M, Kamby C, Kjaer M, Gadeberg C C, Rasmussen B B, Blichert-Toft M and Mouridsen H T 1999 Postoperative radiotherapy in high-risk postmenopausal breast-cancer patients given adjuvant tamoxifen: Danish Breast Cancer Cooperative Group DBCG 82c randomised trial *Lancet* **353** 1641-8

Pierce L J, Butler J B, Martel M K, Normolle D P, Koelling T, Marsh R B, Lichter A S and Fraass B A 2002 Postmastectomy radiotherapy of the chest wall: dosimetric comparison of common techniques *Int J Radiat Oncol Biol Phys* **52** 1220-30

Ragaz J, Jackson S M, Le N, Plenderleith I H, Spinelli J J, Basco V E, Wilson K S, Knowling M A, Coppin C M, Paradis M, Coldman A J and Olivotto I A 1997 Adjuvant radiotherapy and chemotherapy in node-positive premenopausal women with breast cancer *N Engl J Med* **337** 956-62

Rah J-E, Shin D, Park J-h, Hwang U-J, Oh D H and Park S Y 2013 Dosimetric verification of treatment planning system superficial dose calculations for proton beam *Radiation Measurements* **55** 60-3

Rechner L A, Howell R M, Zhang R, Etzel C, Lee A K and Newhauser W D 2012 Risk of radiogenic second cancers following volumetric modulated arc therapy and proton arc therapy for prostate cancer *Phys Med Biol* **57** 7117-32

Rutqvist L E, Rose C and Cavallin-ståhl E 2003 A Systematic Overview of Radiation Therapy Effects in Breast Cancer *Acta Oncol* **42** 532-45

Sandison G A, Papiez E, Bloch C and Morphis J 1997 Phantom assessment of lung dose from proton arc therapy *Int J Radiat Oncol Biol Phys* **38** 891-7

Schneider U and Kaser-Hotz B 2005a Radiation risk estimates after radiotherapy: application of the organ equivalent dose concept to plateau dose-response relationships *Radiat Environ Biophys* **44** 235-9

Schneider U and Kaser-Hotz B 2005b A simple dose-response relationship for modeling secondary cancer incidence after radiotherapy *Z Med Phys* **15** 31-7

Schneider U, Zwahlen D, Ross D and Kaser-Hotz B 2005 Estimation of radiation-induced cancer from three-dimensional dose distributions: Concept of organ equivalent dose *Int J Radiat Oncol Biol Phys* **61** 1510-5

Senkus-Konefka E and Jassem J 2007 Cardiovascular effects of breast cancer radiotherapy *Cancer Treat Rev* **33** 578-93

Seppenwoolde Y, Lebesque J V, de Jaeger K, Belderbos J S, Boersma L J, Schilstra C, Henning G T, Hayman J A, Martel M K and Ten Haken R K 2003 Comparing different NTCP models that predict the incidence of radiation pneumonitis. Normal tissue complication probability *Int J Radiat Oncol Biol Phys* **55** 724-35

Teoh M, Clark C H, Wood K, Whitaker S and Nisbet A 2011 Volumetric modulated arc therapy: a review of current literature and clinical use in practice *Br J Radiol* **84** 967-96

Travis L B, Hill D A, Dores G M, Gospodarowicz M, van Leeuwen F E, Holowaty E, Glimelius B, Andersson M, Wiklund T, Lynch C F, Van't Veer M B, Glimelius I, Storm H, Pukkala E, Stovall M, Curtis R, Boice J D, Jr. and Gilbert E 2003 Breast cancer following radiotherapy and chemotherapy among young women with Hodgkin disease *JAMA* **290** 465-75

Travis L B, Ng A K, Allan J M, Pui C H, Kennedy A R, Xu X G, Purdy J A, Applegate K, Yahalom J, Constine L S, Gilbert E S and Boice J D, Jr. 2011 Second malignant neoplasms and cardiovascular disease following radiotherapy *J Natl Cancer Inst* **104** 357-70

Wang X, Zhang X, Li X, Amos R A, Shaitelman S F, Hoffman K, Howell R, Salehpour M, Zhang S X, Sun T L, Smith B, Tereffe W, Perkins G H, Buchholz T A, Strom E A and Woodward W A 2013 Accelerated partial-breast irradiation using intensity-modulated proton radiotherapy: do uncertainties outweigh potential benefits? *Br J Radiol* **86** 20130176

Webb S and Nahum A E 1993 A model for calculating tumour control probability in radiotherapy including the effects of inhomogeneous distributions of dose and clonogenic cell density *Phys Med Biol* **38** 653-66

Weber D C, Ares C, Lomax A J and Kurtz J M 2006 Radiation therapy planning with photons and protons for early and advanced breast cancer: an overview *Radiat Oncol* **1** 22

Wigg D R 2001 Applied radiobiology and bioeffect planning *Med Phys* 489

Wu Q, Mohan R, Morris M, Lauve A and Schmidt-Ullrich R 2003 Simultaneous integrated boost intensity-modulated radiotherapy for locally advanced head-and-neck squamous cell carcinomas. I: dosimetric results *Int J Radiat Oncol Biol Phys* **56** 573-85

Zhang R, Howell R M, Homann K, Giebeler A, Taddei P J, Mahajan A and Newhauser W D 2013 Predicted risks of radiogenic cardiac toxicity in two pediatric patients undergoing photon or proton radiotherapy *Radiat Oncol* **8** 184

Appendix A: Isodose Distributions and Dose Volume Histograms

Isodose distributions along with the dose volume histograms for each patient within the sample population are displayed within this section. Color coding is consistent with methods listed in Table 3.1 and Table 3.2.

Patient CW-1

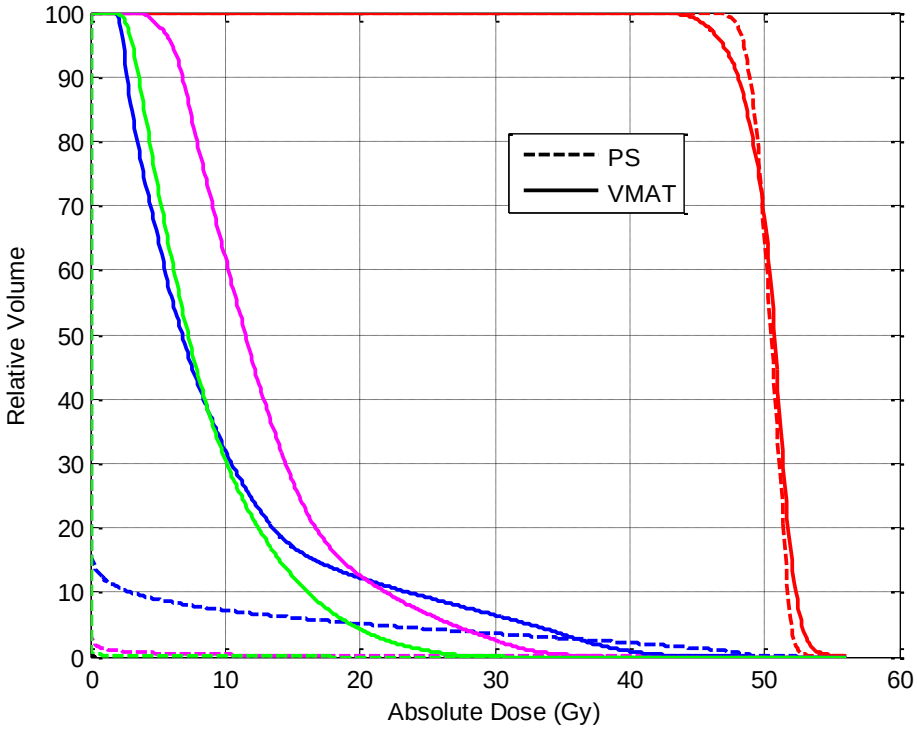

Figure A.1 DVH for patient CW-1 comparing PTV (red), lungs (blue), heart (magenta), and breast (green) for PS (dashed line) and VMAT (solid line)

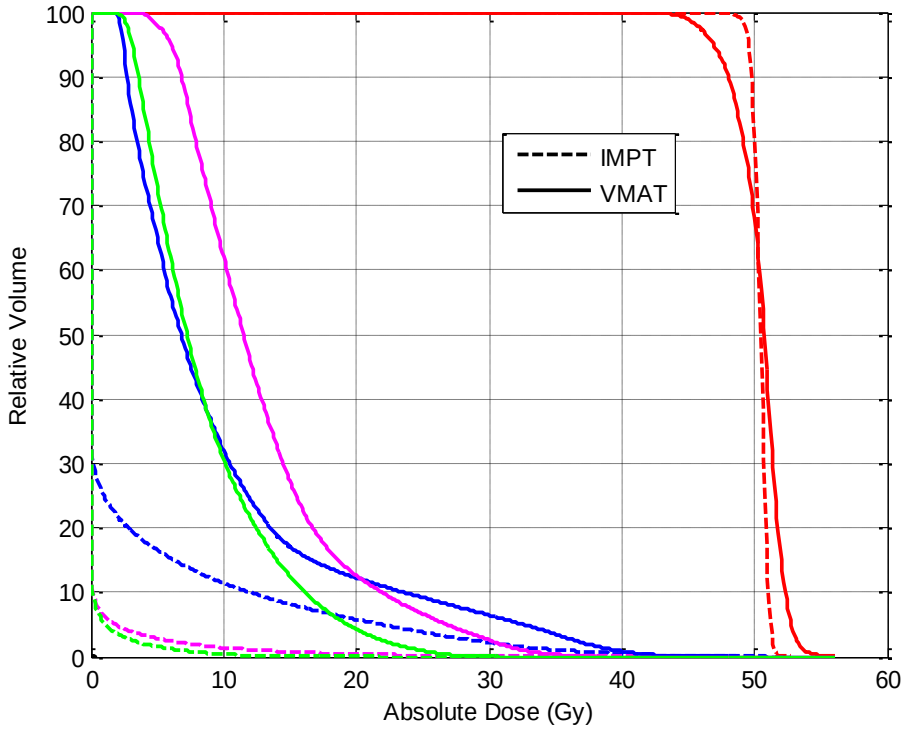

Figure A.2 DVH for patient CW-1 comparing PTV (red), lungs (blue), heart (magenta), and breast (green) for IMPT (dashed line) and VMAT (solid line)

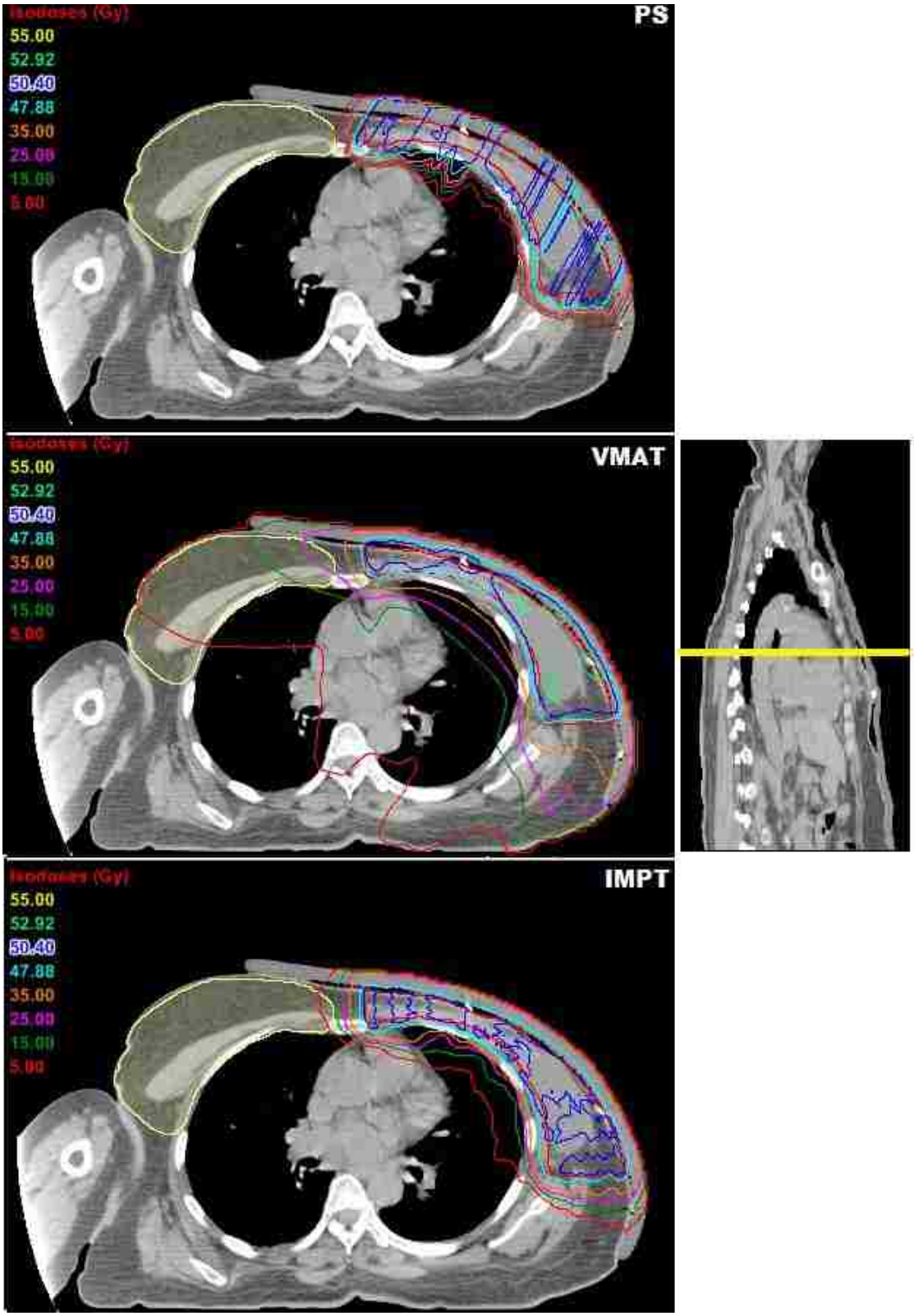

Figure A.3 Isodose distribution for patient CW-1 for PS (top), VMAT (middle), and IMPT (bottom) treatment plans in transverse slice- designated by yellow line in sagittal view- containing VMAT beam isocenter

Patient CW-2

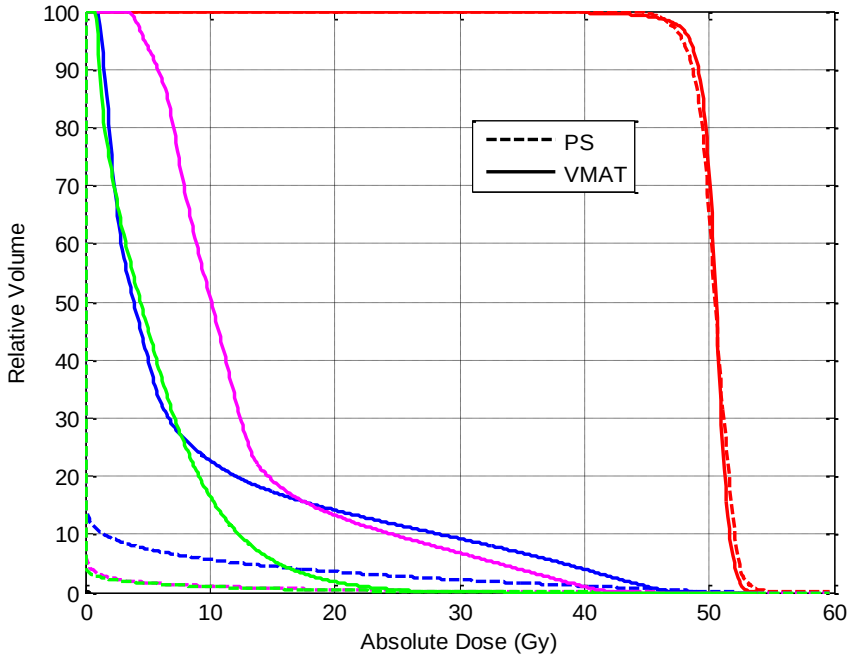

Figure A.4 DVH for patient CW-2 comparing PTV (red), lungs (blue), heart (magenta), and breast (green) for PS (dashed line) and VMAT (solid line)

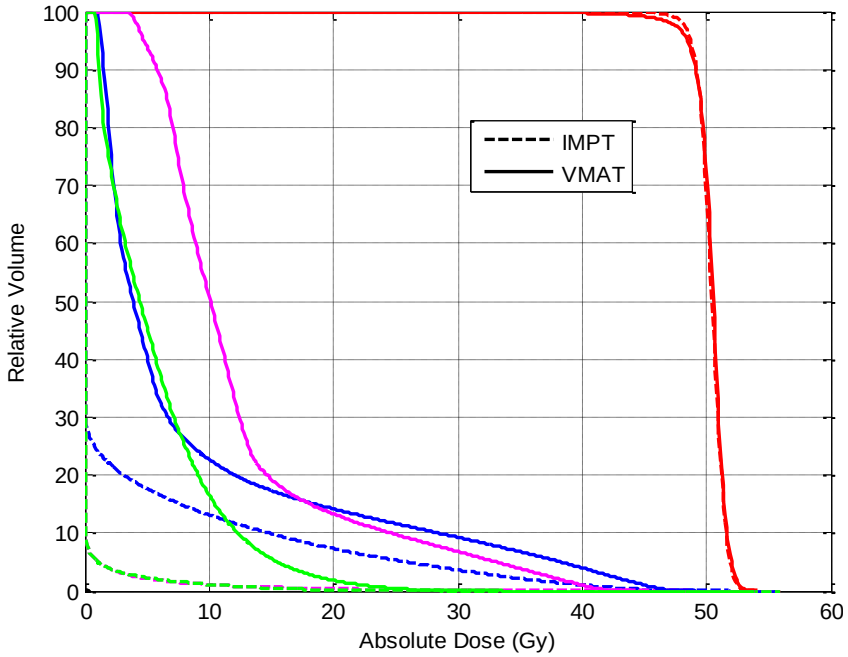

Figure A.5 DVH for patient CW-2 comparing PTV (red), lungs (blue), heart (magenta), and breast (green) for IMPT (dashed line) and VMAT (solid line)

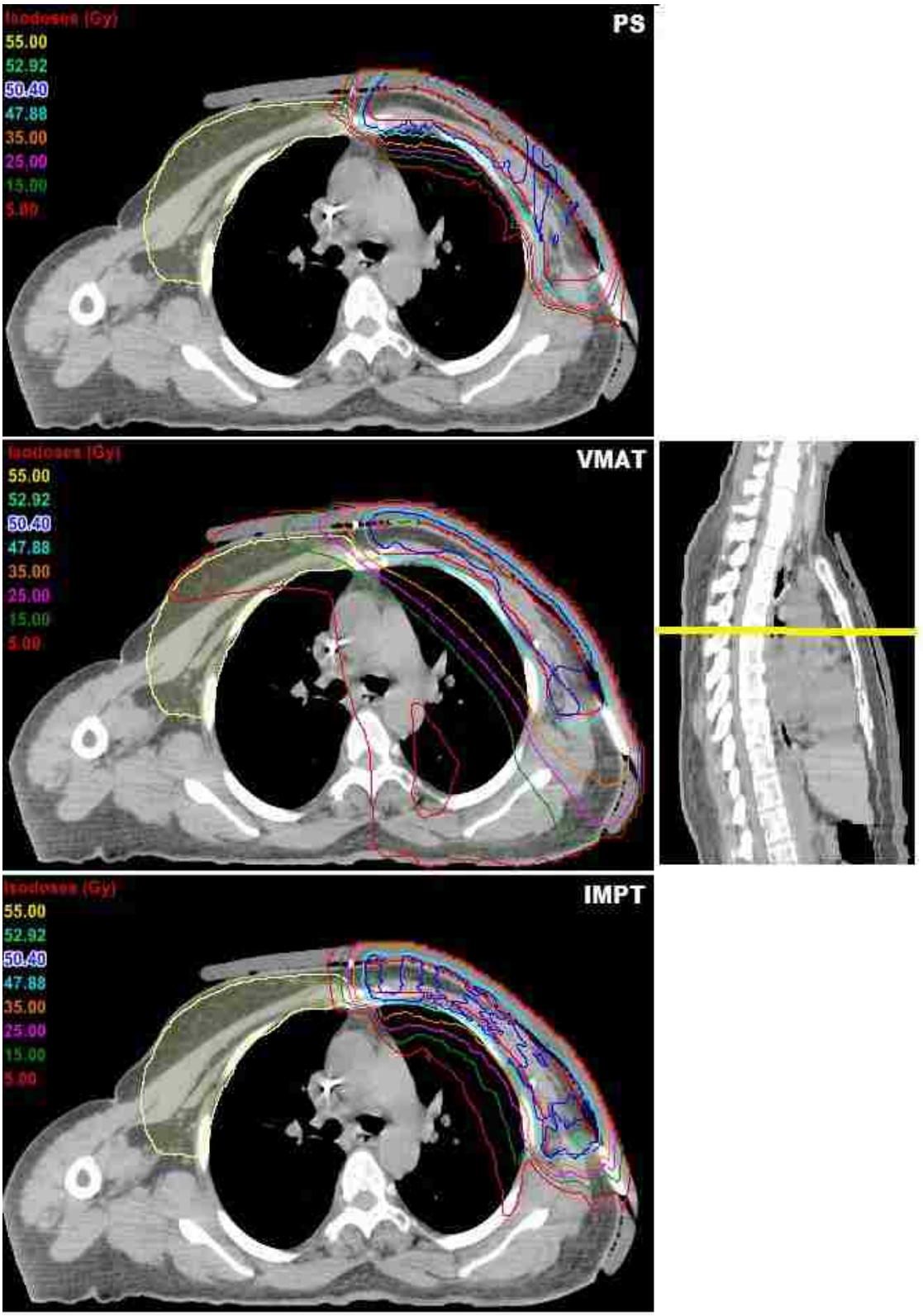

Figure A.6 Isodose distribution for patient CW-2 for PS (top), VMAT (middle), and IMPT (bottom) treatment plans in transverse slice- designated by yellow line in sagittal view- containing VMAT beam isocenter

Patient CW-4

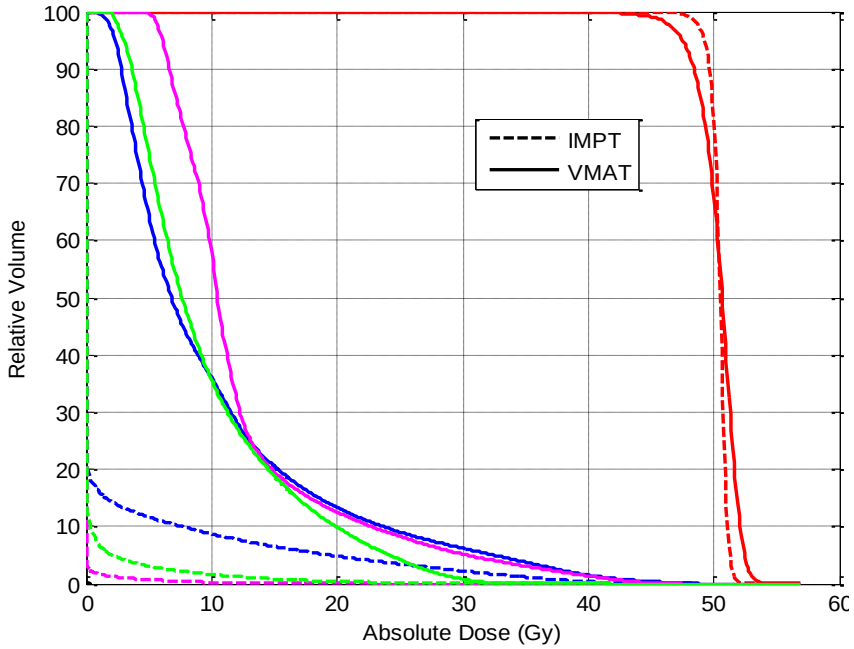

Figure A.7 DVH for patient CW-4 comparing PTV (red), lungs (blue), heart (magenta), and breast (green) for PS (dashed line) and VMAT (solid line)

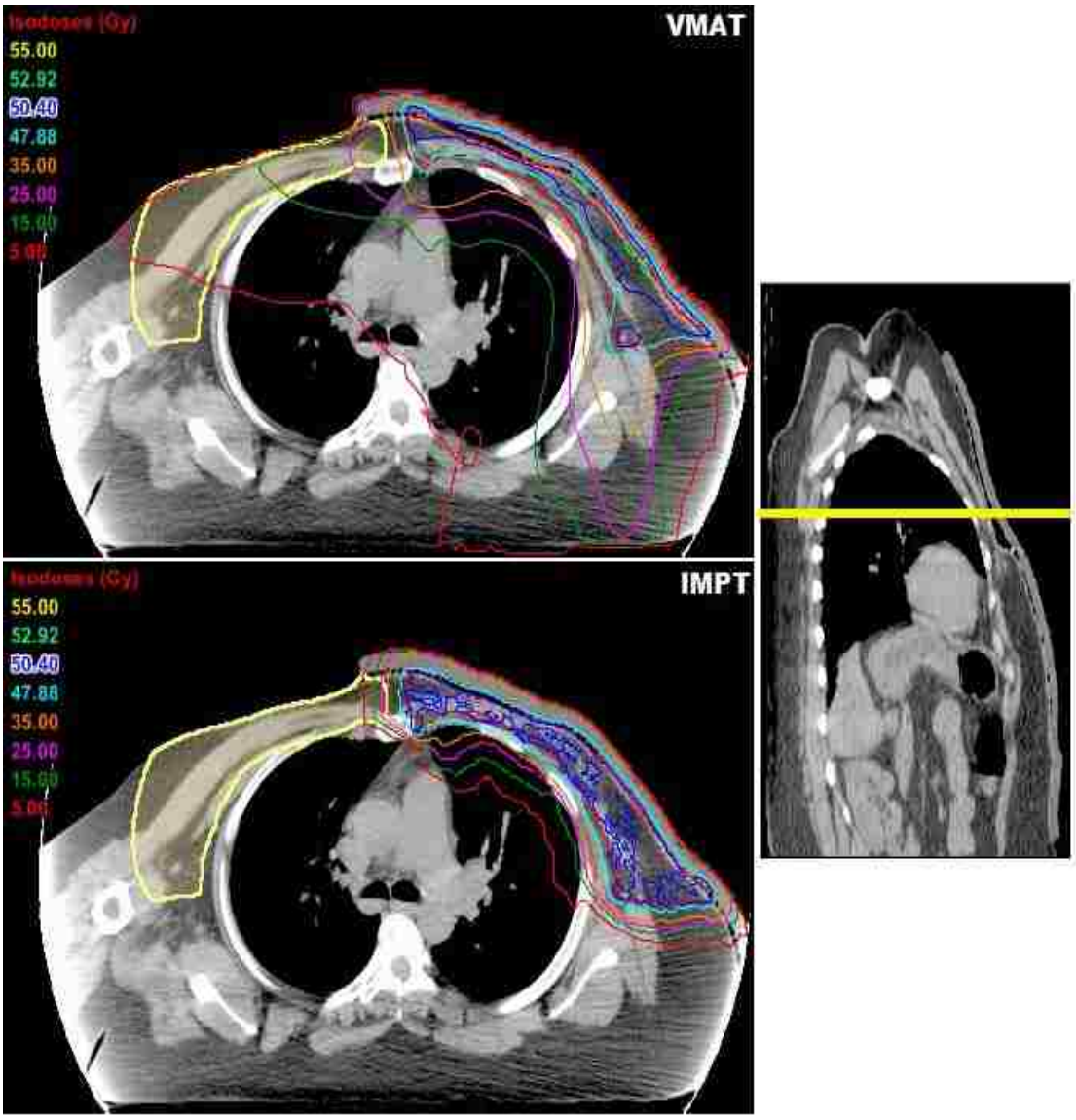

Figure A.8 Isodose distribution for patient CW-4 for VMAT (top), and IMPT (bottom) treatment plans in transverse slice- designated by yellow line in sagittal view- containing VMAT beam isocenter

Patient CW-5

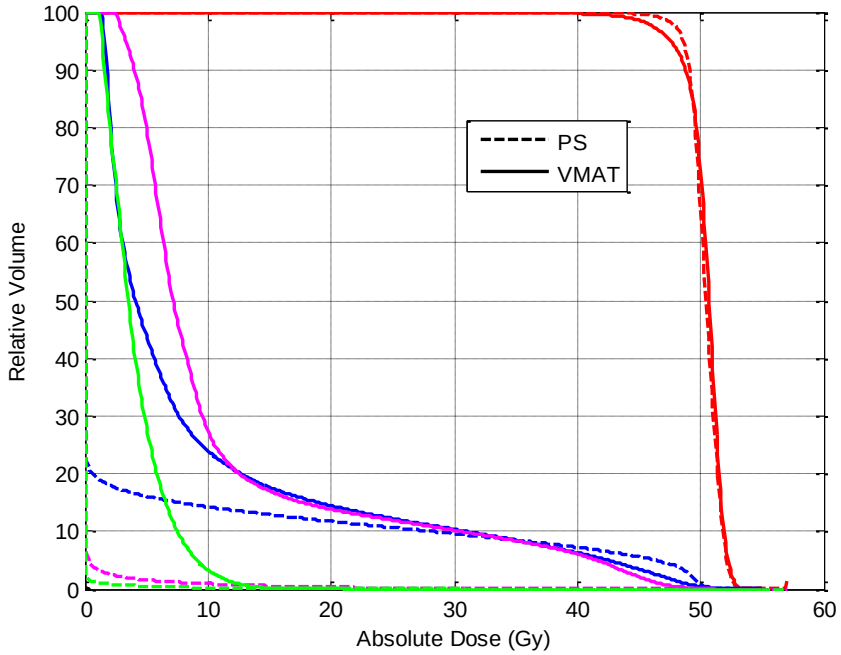

Figure A.9 DVH for patient CW-5 comparing PTV (red), lungs (blue), heart (magenta), and breast (green) for PS (dashed line) and VMAT (solid line)

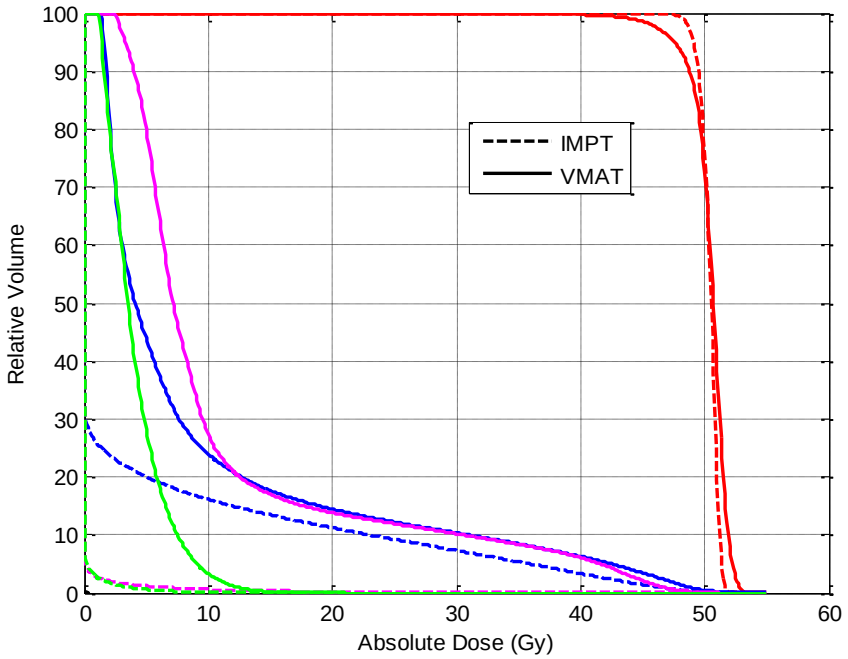

Figure A.10 DVH for patient CW-5 comparing PTV (red), lungs (blue), heart (magenta), and breast (green) for IMPT (dashed line) and VMAT (solid line)

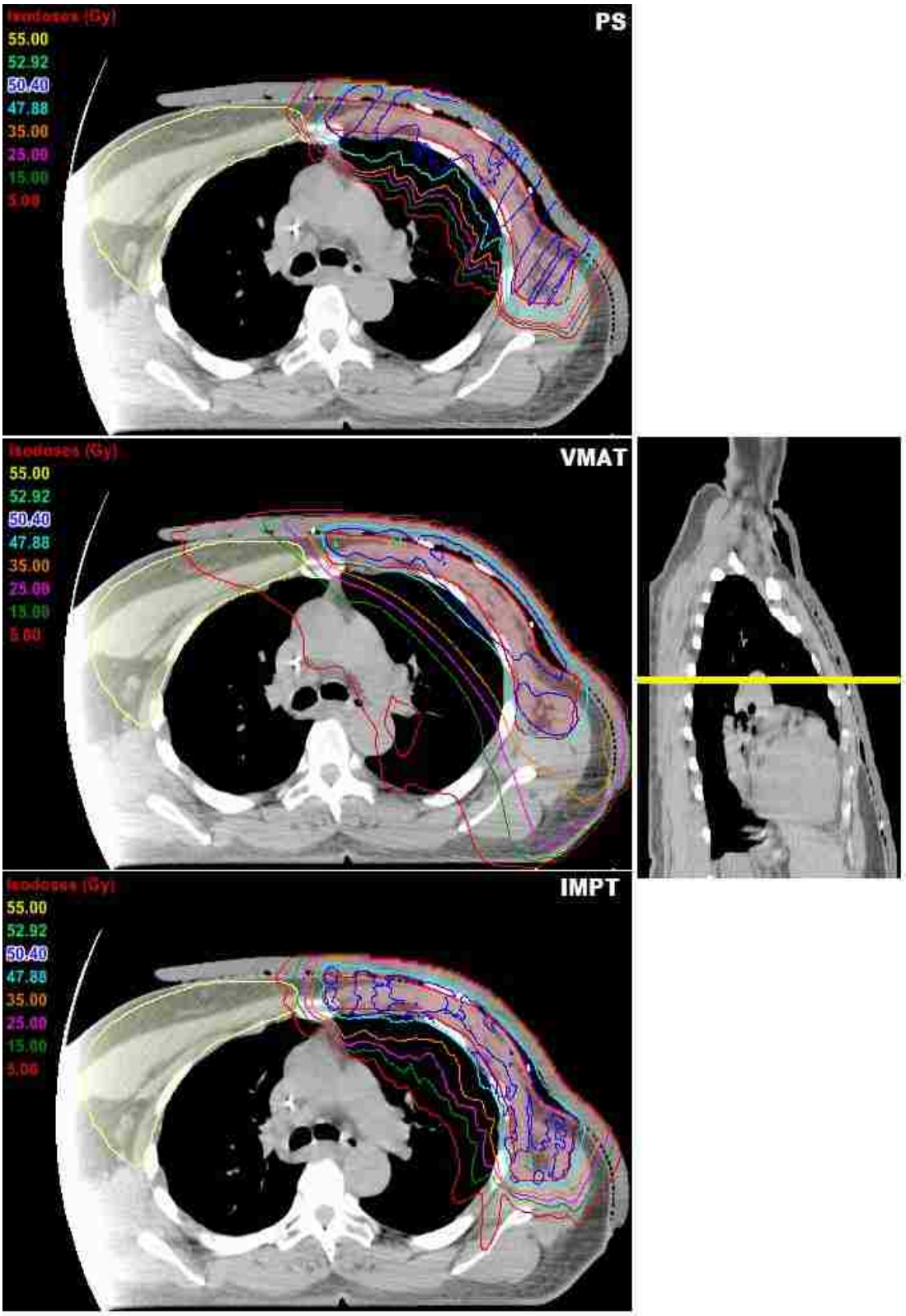

Figure A.11 Isodose distribution for patient CW-5 for PS (top), VMAT (middle), and IMPT (bottom) treatment plans in transverse slice- designated by yellow line in sagittal view- containing VMAT beam isocenter

Patient CW-6

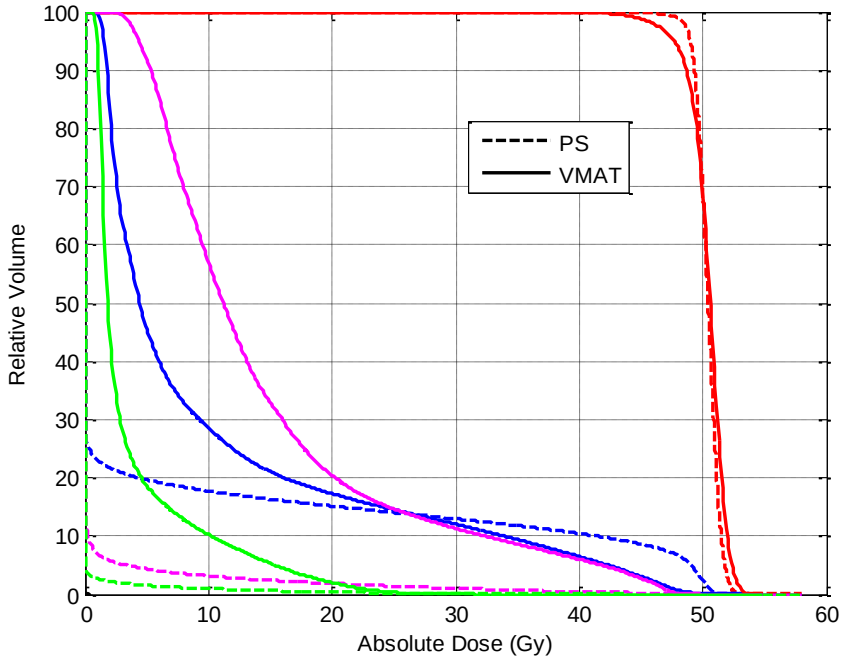

Figure A.12 DVH for patient CW-6 comparing PTV (red), lungs (blue), heart (magenta), and breast (green) for PS (dashed line) and VMAT (solid line)

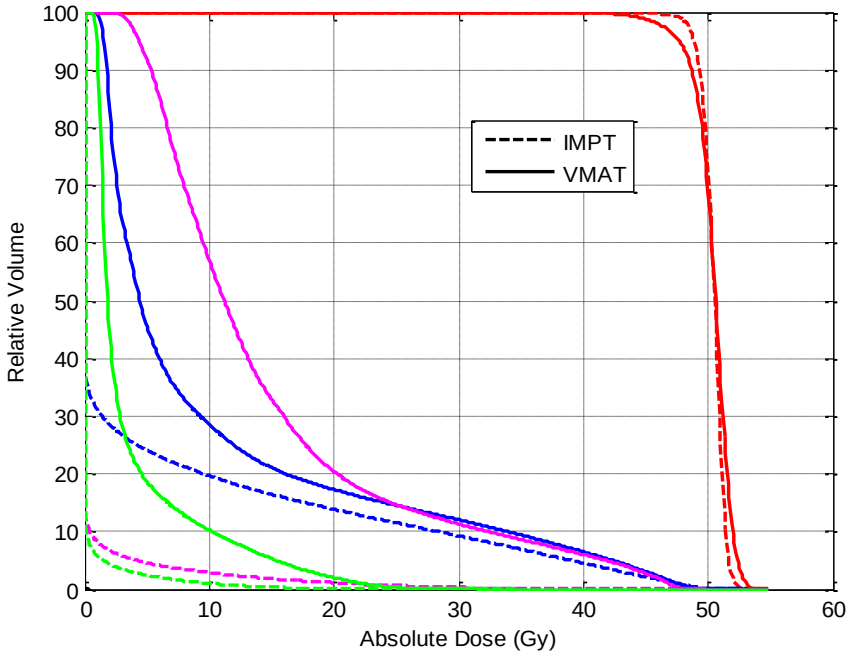

Figure A.13 DVH for patient CW-6 comparing PTV (red), lungs (blue), heart (magenta), and breast (green) for IMPT (dashed line) and VMAT (solid line)

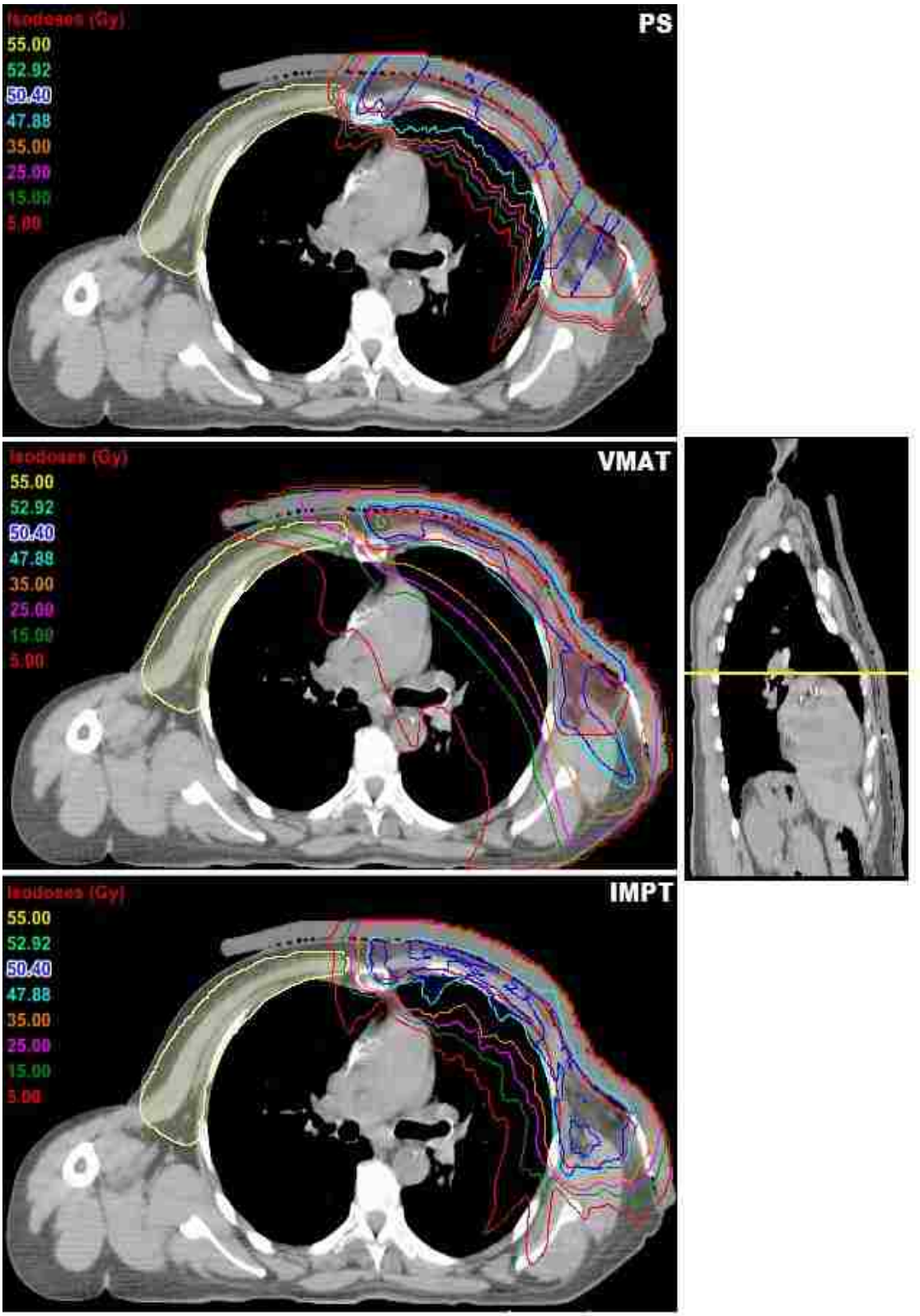

Figure A.14 Isodose distribution for patient CW-6 for PS (top), VMAT (middle), and IMPT (bottom) treatment plans in transverse slice- designated by yellow line in sagittal view- containing VMAT beam isocenter

Patient CW-7

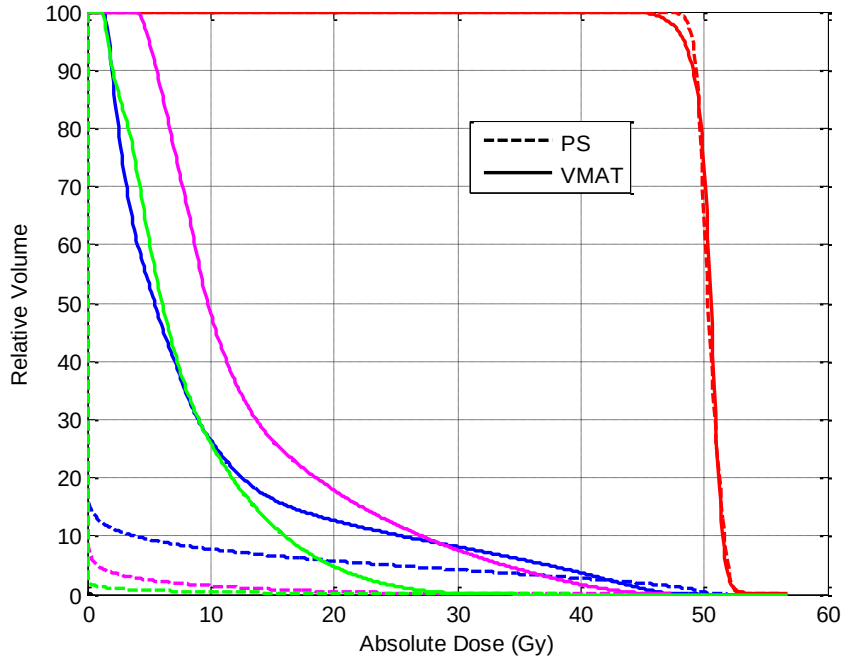

Figure A.15 DVH for patient CW-7 comparing PTV (red), lungs (blue), heart (magenta), and breast (green) for PS (dashed line) and VMAT (solid line)

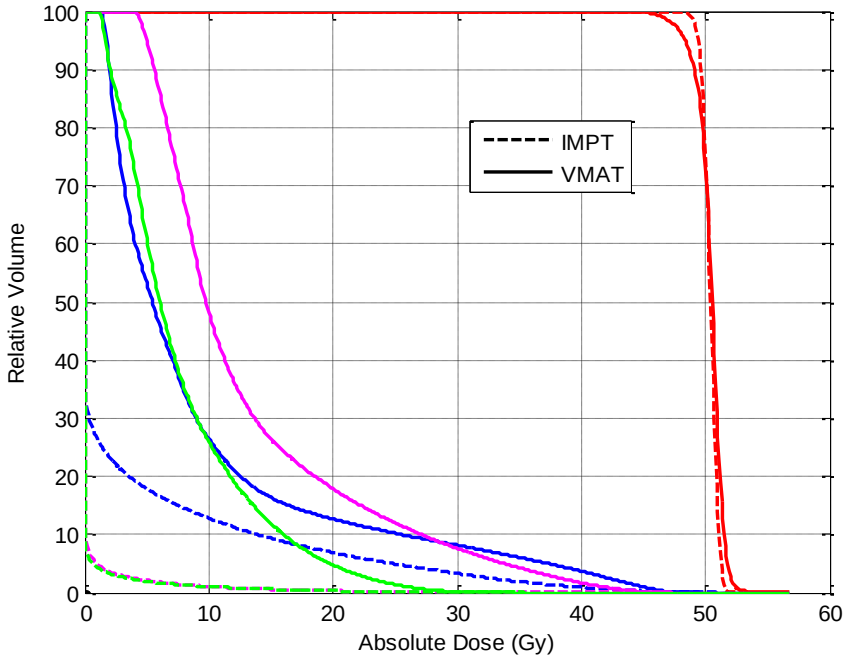

Figure A.16 DVH for patient CW-7 comparing PTV (red), lungs (blue), heart (magenta), and breast (green) for IMPT (dashed line) and VMAT (solid line)

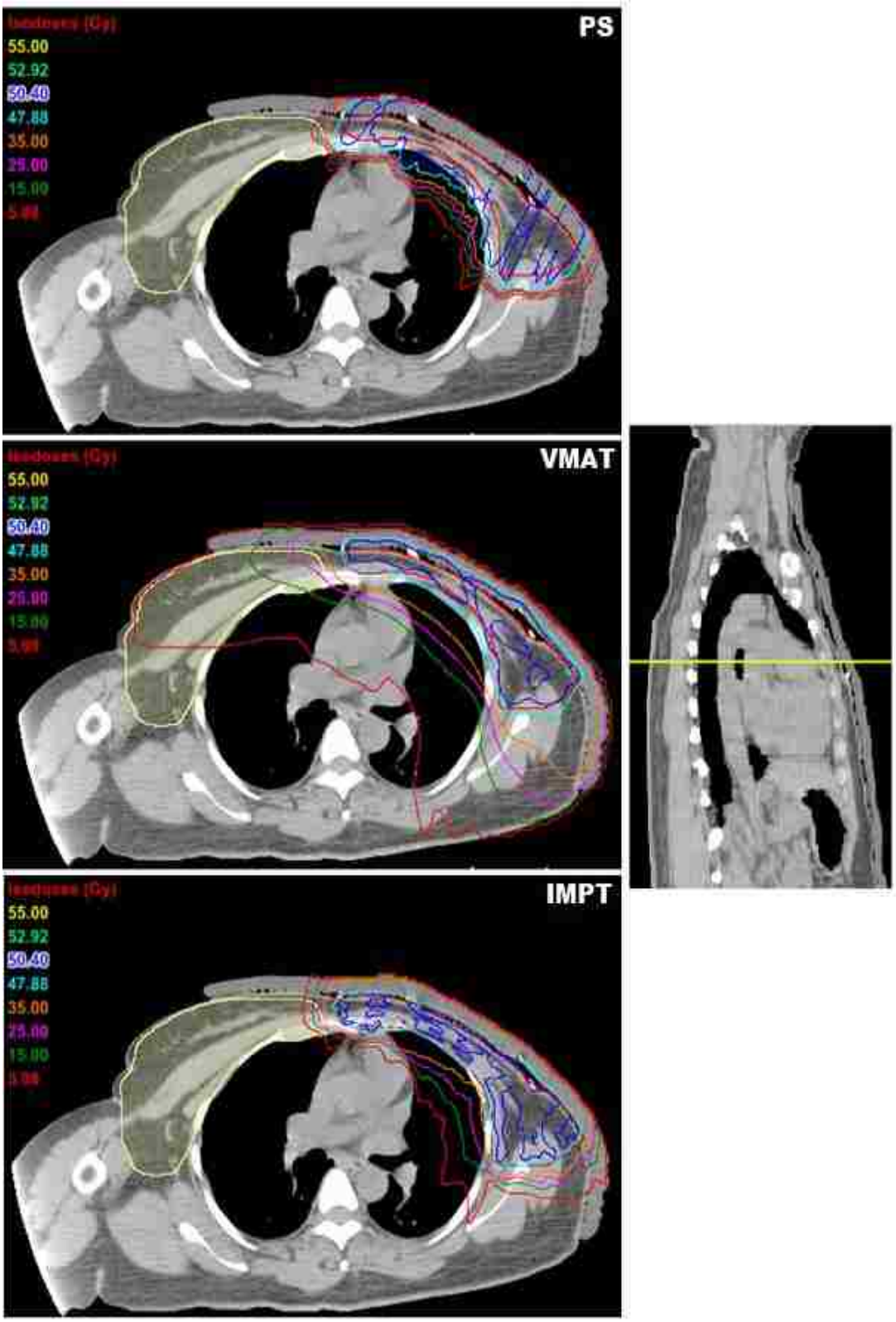

Figure A.17 Isodose distribution for patient CW-7 for PS (top), VMAT (middle), and IMPT (bottom) treatment plans in transverse slice- designated by yellow line in sagittal view- containing VMAT beam isocenter

Patient CW-8

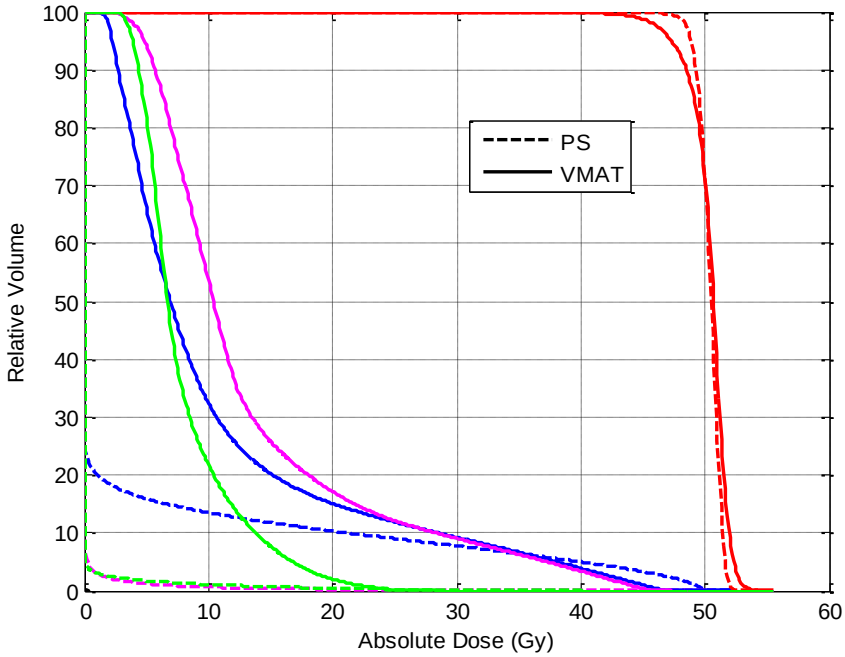

Figure A.18 DVH for patient CW-8 comparing PTV (red), lungs (blue), heart (magenta), and breast (green) for PS (dashed line) and VMAT (solid line)

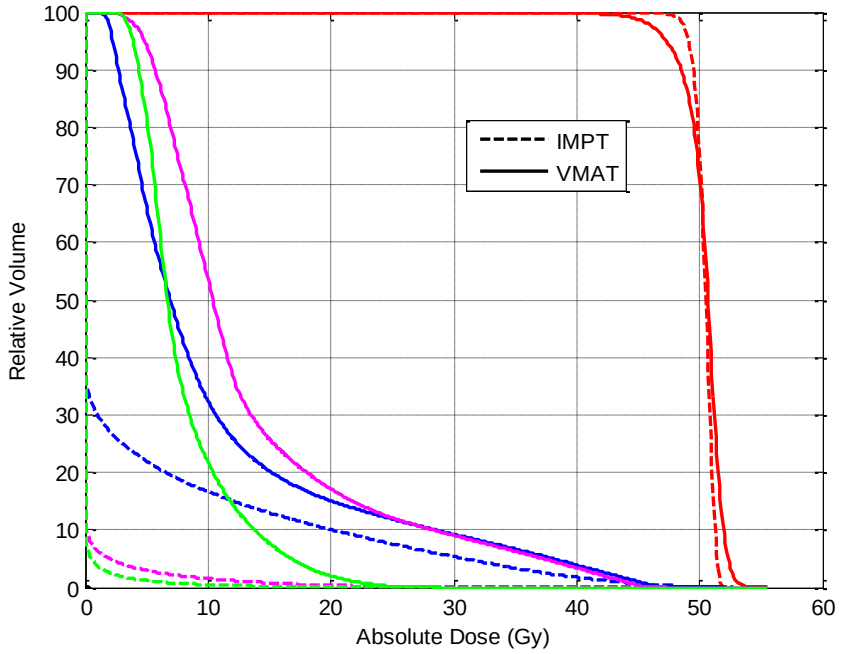

Figure A.19 DVH for patient CW-8 comparing PTV (red), lungs (blue), heart (magenta), and breast (green) for IMPT (dashed line) and VMAT (solid line)

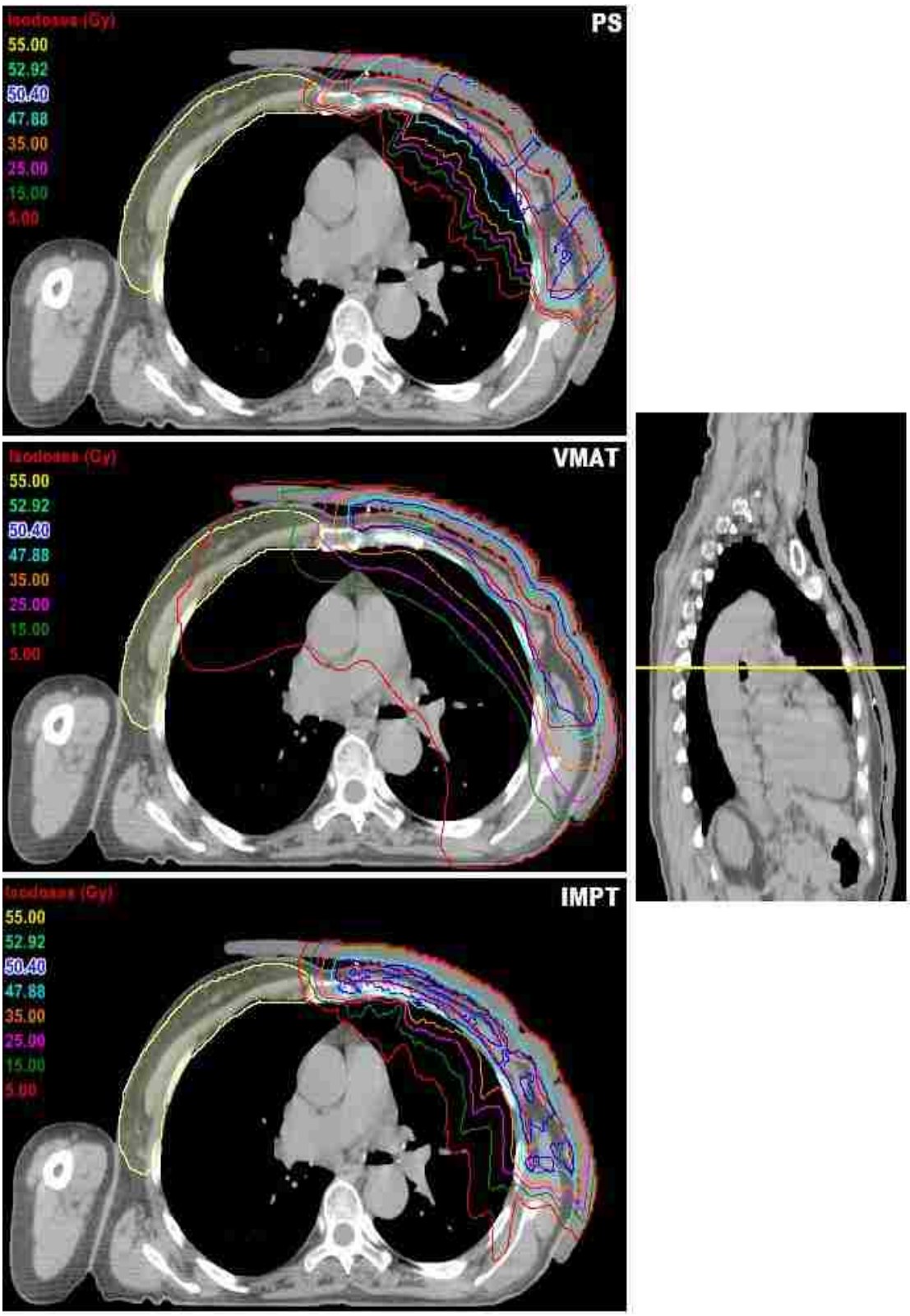

Figure A. 20 Isodose distribution for patient CW-8 for PS (top), VMAT (middle), and IMPT (bottom) treatment plans in transverse slice- designated by yellow line in sagittal view- containing VMAT beam isocenter

Vita

The daughter of Callie and Armando, Margaret was born in Prescott, Arizona, in June 1988. Following her graduation from a small ranching high school in Mayer, Arizona, in 2006, Margaret attended Oregon State University in Corvallis, Oregon, where she received a Bachelor of Science in Health Physics and a Minor in Physics. There she was a member of the Chi Omega Sorority and held multiple positions for the American Nuclear Society and Health Physics Society.

After graduating with honors in 2011, Margaret moved to Baton Rouge, Louisiana after accepting a graduate position within the medical physics program at Louisiana State University. She became involved with the Deep South Chapter of the Health Physics Society and has been its treasurer for the last two years. Margaret will begin the medical physics residency training program at Mary Bird Perkins Cancer Center in Baton Rouge, Louisiana, in 2014.